

MARCELO SALHAB BROGLIATO

ESSAYS IN  
COMPUTATIONAL MANAGEMENT SCIENCE



ESSAYS IN  
COMPUTATIONAL MANAGEMENT SCIENCE

MARCELO SALHAB BROGLIATO

Escola Brasileira de Administração Pública e de Empresas  
Fundação Getulio Vargas

June 2018

Marcelo Salhab Brogliato: *Essays in  
Computational Management Science*, © June 2018

**SUPERVISORS:**

Alexandre Linhares **LOCATION:**

Rio de Janeiro

## CONTENTS

---

i	AN INVITATION TO SPARSE DISTRIBUTED MEMORY: FROM THE THEORETICAL MODEL TO THE SYSTEM DYNAMICS	1
1	INTRODUCTION	3
1.1	Desiderata for a theory of memory	4
1.2	The wasted effort of duplicated, ad hoc, work	5
2	NOTATION	9
3	SPARSE DISTRIBUTED MEMORY	11
3.1	Neurons as pointers	17
3.2	Concepts	18
3.3	Read operation	18
3.3.1	Generalized read operation	19
3.4	Critical Distance	20
4	FRAMEWORK ARCHITECTURE	23
4.1	Bitstring	24
4.1.1	The distance between two bitstrings	24
4.2	Address space	25
4.2.1	Scanning for activated hard locations	25
4.2.2	OpenCL kernels	26
4.3	Counters	27
4.4	Read and write operations	36
5	RESULTS (I): PERFORMANCE	37
5.1	Kernels comparison	38
5.2	Scanners comparison	39
5.3	Read and write operations	39
5.3.1	Summary of results	39
6	RESULTS (II): FRAMEWORK VALIDATION	61
6.1	Distance between random bitstrings	61
6.2	Number of activated hard locations	62
6.3	Intersection of two circles	63
6.4	Storage and retrieval of sequences	64
6.4.1	k-fold memory using only one SDM	65
7	RESULTS (III): LOSS OF NEURONS	67
8	RESULTS (IV): CRITICAL DISTANCE	73
8.1	A deviation from the equator distance?	77
8.1.1	Bitmatches at i.	78
8.2	Counter bias	83
8.3	Read bias	86
8.4	Critical distance of 209	89
9	RESULTS (V): GENERALIZED READ OPERATION	91

10 RESULTS (VI): SUPERVISED CLASSIFICATION APPLICATION	95
11 RESULTS (VII): IMAGE NOISE FILTERING APPLICATION	105
12 RESULTS (VIII): THE POSSIBILITY OF UNSUPERVISED REINFORCEMENT LEARNING	111
12.1 Training	114
12.2 Results	114
13 RESULTS (IX): INFORMATION-THEORETICAL WRITE OPERATION	121
14 CONCLUSION	125
14.1 Another 'funny thing'...	125
14.2 Magic numbers	126
14.3 Symmetrical, rapidly accessible, hard locations	126
14.4 "i" versus "l"	127
14.5 Deep learning, multiple SDMs — and the incredible animal behavior of Dr. Linhares	127
14.6 Not a real Conclusion	133
15 APPENDIX	137
BIBLIOGRAPHY	141

## LIST OF FIGURES

---

- Figure 1 Here we have  $Q_n$ , for  $n \in \{3, 7, 10\}$ . Each node corresponds to a bitstring in  $\{0, 1\}^n$ , and two nodes are linked iff the bitstrings differ by a single dimension. A number of observations can be made here. First, the number of nodes grows as  $O(2^n)$ ; which makes the space rapidly intractable. Another interesting observation, better seen in the figures below, is that most of the space lies ‘at the center’, at a distance of around  $n/2$  from any given vantage point. [12](#)
- Figure 2 Activated addresses inside access radius  $r$  around the center address. [13](#)
- Figure 3 Shared addresses between the target datum  $\eta$  and the cue  $\eta_x$ . [14](#)
- Figure 4 Hard-locations randomly sampled from binary space. [15](#)
- Figure 5 In this example, four iterative readings were required to converge from  $\eta_x$  to  $\eta$ . [16](#)
- Figure 6 Hard-locations pointing, approximately, to the target bitstring. [17](#)

Figure 7

How far, in Hamming distance, is a read item from the original stored item? Kanerva demonstrated that, after a small number of iterative readings (6 here), a critical distance behavior emerges. Items read at close distance converge rapidly; whereas farther items do not converge. Most striking is the point in which the system displays the tip-of-tongue behavior. Described by psychological moments when some features of the item are prominent in one's thoughts, yet the item still cannot be recalled (but an additional cue makes convergence ‘immediate’). Mathematically, this is the precise distance in which, despite having a relatively high number of cues (correct bits) about the desired item, the time to convergence is infinite. Heatmap colors display the Hamming distance the associative memory is able to cleanly converge to—or not. In the x-axis, the distance from the desired item is displayed. In the y-axis, we display the read operation’s behavior as the number of items registered in the memory grows. These graphs are computing intensive, yet they can be easily tested by readers in our provided Jupyter notebooks. Note the different scales. [21](#)

Figure 8

Address space’s bitstrings are stored in a contiguous array. In a 64-bit computer, each bitstring is stored in a sub-array of 64-bit integers, with length  $8 \cdot \lceil n/64 \rceil$ . [25](#)

Figure 9

Kernel comparisons for MacBook Pro Retina 13-inch Late 2013 with a 2.6GHz Intel core i5 processor, 6GB DDR<sub>3</sub> RAM, and Intel Iris GPU. [41](#)

Figure 10

Scanner comparisons for MacBook Pro Retina 13-inch Late 2013 with a 2.6GHz Intel core i5 processor, 6GB DDR<sub>3</sub> RAM, and Intel Iris GPU. [42](#)

Figure 11

Read operation comparisons for MacBook Pro Retina 13-inch Late 2013 with a 2.6GHz Intel core i5 processor, 6GB DDR<sub>3</sub> RAM, and Intel Iris GPU. [43](#)

Figure 12	Write operation comparisons for MacBook Pro Retina 13-inch Late 2013 with a 2.6GHz Intel core i5 processor, 6GB DDR3 RAM, and Intel Iris GPU. <a href="#">44</a>
Figure 13	Kernel comparisons for iMac Retina 5K 27-inch 2017 with a 3.8GHz Intel core i5 processor, 8GB DDR4 RAM, and a Radeon Pro 580 8G GPU. <a href="#">46</a>
Figure 14	Scanner comparisons for iMac Retina 5K 27-inch 2017 with a 3.8GHz Intel core i5 processor, 8GB DDR4 RAM, and a Radeon Pro 580 8G GPU. <a href="#">47</a>
Figure 15	Read operation comparisons for iMac Retina 5K 27-inch 2017 with a 3.8GHz Intel core i5 processor, 8GB DDR4 RAM, and a Radeon Pro 580 8G GPU. <a href="#">48</a>
Figure 16	Write operation comparisons for iMac Retina 5K 27-inch 2017 with a 3.8GHz Intel core i5 processor, 8GB DDR4 RAM, and a Radeon Pro 580 8G GPU. <a href="#">49</a>
Figure 17	Kernel comparisons for Amazon EC2 p2.xlarge with Intel Xeon E5-2686v4 processor, 61GB DDR3 RAM, and NVIDIA K80 GPU. <a href="#">51</a>
Figure 18	Scanner comparisons for Amazon EC2 p2.xlarge with Intel Xeon E5-2686v4 processor, 61GB DDR3 RAM, and NVIDIA K80 GPU. <a href="#">52</a>
Figure 19	Read operation comparisons for Amazon EC2 p2.xlarge with Intel Xeon E5-2686v4 processor, 61GB DDR3 RAM, and NVIDIA K80 GPU. <a href="#">53</a>
Figure 20	Write operation comparisons for Amazon EC2 p2.xlarge with Intel Xeon E5-2686v4 processor, 61GB DDR3 RAM, and NVIDIA K80 GPU. <a href="#">54</a>
Figure 21	Kernel comparisons for Amazon EC2 p3.2xlarge with Intel Xeon E5-2686v4 processor, 488GB DDR3 RAM, and NVIDIA Tesla V100 GPU. <a href="#">56</a>
Figure 22	Scanner comparisons for Amazon EC2 p3.2xlarge with Intel Xeon E5-2686v4 processor, 488GB DDR3 RAM, and NVIDIA Tesla V100 GPU. <a href="#">57</a>

- Figure 23 Read operation comparisons for Amazon EC2 p3.2xlarge with Intel Xeon E5-2686v4 processor, 488GB DDR3 RAM, and NVIDIA Tesla V100 GPU. [58](#)
- Figure 24 Write operation comparisons for Amazon EC2 p3.2xlarge with Intel Xeon E5-2686v4 processor, 488GB DDR3 RAM, and NVIDIA Tesla V100 GPU. [59](#)
- Figure 25 Histogram of 10,000 distances between two random bitstrings with 1,000 bits. The curve in red is the theoretical normal distribution with  $\mu = 500$  and  $\sigma = \sqrt{500}/2$ . [61](#)
- Figure 26 Histogram of the number of activated hard locations in 10,000 scans from a random bitstring. The curve in red is the theoretical normal distribution with  $\mu = Hp$  and  $\sigma = p(p - 1)H$ . [62](#)
- Figure 27 Histogram of the distances of activated hard locations to the center of the circles. The curve in red is the theoretical distribution of Equation 2 [63](#)
- Figure 28 Number of hard locations in the intersection of circles around two bitstrings  $x$  bits away. [64](#)
- Figure 29 This graph shows the SDM's robustness against loss of neurons in a SDM with  $n = 1,000$  and  $H = 1,000,000$ . It shows that a loss of 200,000 neurons, 20% of the total, does not seem to affect SDM whatsoever. [68](#)
- Figure 30 This graph shows the SDM's robustness against loss of neurons in a SDM with  $n = 1,000$  and  $H = 1,000,000$ . The more neurons are lost, the smaller the critical distance, i.e., the worse the SDM recall. [68](#)
- Figure 31 This graph shows the SDM's robustness against loss of neurons in a SDM with  $n = 1,000$  and  $H = 1,000,000$ . Even when 50% of neurons are dead, SDM recall is barely affected, which is an impressive result and matches with some clinical results of children submitted to hemispherectomy. [70](#)
- Figure 32 This graph shows the SDM's robustness against loss of neurons in a SDM with  $n = 1,000$  and  $H = 1,000,000$ . [70](#)

Figure 33	This graph shows the SDM's robustness against loss of neurons in a SDM with $n = 256$ and $H = 1,000,000$ . <a href="#">71</a>
Figure 34	Kanerva's original Figure 7.3 (p. 70) predicting a $\sim 500$ -bit distance after a point. <a href="#">73</a>
Figure 35	Results generated by the framework diverging from Kanerva's original Figure 7.3. Here we had a 1,000 bit, 1,000,000 hard location SDM with 10,000 random bitstrings written into it, which was also Kanerva's configuration. <a href="#">74</a>
Figure 36	Results generated by the framework similar to Kanerva's original Figure 7.3. Here we have a 1,000 bit, 1,000,000 hard location SDM with (a) just 100 random bitstrings written into it and (b) steps of 1,000 random bitstrings written into it. <a href="#">75</a>
Figure 37	This graph shows the interaction effects more clearly. As we change the single read to a 6-iterative read, the effect has vanished, and all bitstrings above $x = 500$ have converged to 500-bit distance bitstrings. Here we have precisely the same configuration of Figure 35, except for the iterative read. <a href="#">76</a>
Figure 38	Kanerva's original Figure 7.3 generated using the equations from Brogliato et al. [9]. <a href="#">77</a>
Figure 39	The threshold size $r$ of hard-locations bring about the autocorrelation of Theorem 1. Consider, for instance, the extremes $\{0, n\}$ . Let us start with $n$ (in our case, $n = 1000$ dimensions): given the information that $d(x, y) \leq n$ , the probability of a bitmatch in dimension $i$ is $p = 1/2$ ; as $\forall x, y \in \{0, 1\}^N, d(x, y) \leq n$ . At the other extreme, consider that we have the information that $d(x, y) \leq 0$ : in this case $x = y$ and the probability of a bitmatch, in any dimension, is $p = 1$ . The autocorrelation hence drops monotonically until convergence at $p = 1/2$ as the distance grows. <a href="#">80</a>
Figure 40	The same setup as in Figure 35, but for $n = 10,000$ . It shows that the interference has almost gone away when $n$ is sufficiently large. <a href="#">82</a>

- Figure 41 Given an address  $x$  and a dimension  $i$ , how many hard locations with bitmatches in  $i$  are activated by reading at  $x$ ? The histogram was obtained through numerical simulation. The red curve is the theoretical normal distribution found in Theorem 5. 83
- Figure 42 The value of the counters after  $s = 10,000$  writes shows the autocorrelation in the counters in autoassociative memories ("x at x"). The histogram was obtained through simulation. The red curve is the theoretical normal distribution found in equations (20) and (21). 85
- Figure 43 Autocorrelation in the counters in autoassociative memories ("x written at x"). The histogram was obtained through simulation. The red curve is the theoretical distribution. 86
- Figure 44 The histogram was obtained through simulation. The red curve is the theoretical normal distribution. 87
- Figure 45 The histogram was obtained through simulation. The red curve is the theoretical normal distribution. 88
- Figure 46 The histogram was obtained through simulation. The red curve is the theoretical normal distribution. 89
- Figure 47 New distance after a single read operation in a bitstring  $\eta_d$ , which is  $d$  bits away from  $\eta$ . The new distance was calculated between  $\eta_d$  and  $\text{read}(\eta_d)$ . Notice that when  $d \geq 520$ , the intersection between  $\eta$  and  $\eta_d$  is zero, which means there is only random bitstrings written into the activated hard locations. The distance 220 equals  $1000 \cdot 0.220$  which is the probability found in Figure 46. 89
- Figure 48 Zoom-in around  $d = 209$  of Figure 38. 90
- Figure 49 Zoom-in around  $d = 209$  of Figure 35. 90

Figure 50	(a) and (b) show the behavior of a single read. As stated previously, we can see a deterioration of convergence, with lower critical distance as $z > 1$ . Another observation can be made here, concerning the discrepancy of Kanerva's Fig 7.3 and our data. It seems that Kanerva may not have considered that a single read would only 'clean' a small number of dimensions <i>after the critical distance</i> . What we observe clearly is that with a single read, as the distance grows, the system only 'cleans' towards the orthogonal distance 500 after a number of iterative readings. <a href="#">92</a>
Figure 51	(a) and (b) show the behavior of Figure 50, now executed with 6-iterative reads. What we observe clearly is that with a single read, as the distance grows, the system only 'cleans' towards the orthogonal distance 500 after a number of iterative readings. <a href="#">93</a>
Figure 52	Examples of noisy images with uppercase letters, lowercase letters, and numbers. <a href="#">95</a>
Figure 53	One noisy image for each of the 62 classification groups. <a href="#">96</a>
Figure 54	100 noisy images generated to train label A. <a href="#">97</a>
Figure 55	Images generated using a 20% noise for the high noise scenario. <a href="#">97</a>
Figure 56	Images generated for the no noise scenario. <a href="#">98</a>
Figure 57	Images of different characters which may be confusing depending on the noise level. <a href="#">99</a>
Figure 58	Characters in the low noise scenario in which the classifier has made at least one mistake. In all the other cases, it correctly classified the images. We may notice that the groups of "i" and "l" have been completely merged by the classifier, because it cannot distinguish them, not even with no noise. <a href="#">100</a>
Figure 57	Characters in the high noise scenario in which the classifier has made at least one mistake. In all the other cases, it correctly classified the images. <a href="#">103</a>
Figure 58	Progressive noise into letter "A", from 0% to 45% in steps of 5%. <a href="#">105</a>

- Figure 59 Training images written into the SDM. They were written in their own addresses — write(address=bs\_image, datum=bs\_image). [106](#)
- Figure 60 In order to test the SDM as a noise filter, we read from noisy images expecting to get a clean image. It is interesting to highlight that SDM has never seen a clean version letters "T" and "I". [106](#)
- Figure 61 Probability of getting the right pixel when reading from an image with noise  $p$ . It assumes that SDM was trained with 200 images with 15% noise. [107](#)
- Figure 62 Training images in which the intersection between images is too high. They were written in their own addresses — write(address=bs\_image, datum=bs\_image). [108](#)
- Figure 63 When the intersection between images becomes too high, there appears some interference in the resulting image. All cases have 10% noise. We can notice that the empty space on the right side of the "C" letter generates some white pixels on the right side of both "B" and "D" letters. [108](#)
- Figure 64 Using labels solves the interference problem when the intersection between images becomes too high. All cases have 20% noise. [109](#)
- Figure 65 Each action is a cell in the TicTacToe board and is mapped to slice of the bitstring. [112](#)
- Figure 66 Example of a game with 7 movements in which X wins. [112](#)
- Figure 67 Positive reward bitstrings used in our reinforcement learning algorithm. [113](#)
- Figure 68 Results playing against the random player. Each cycle was made of 100 games for training, and then 100 games for measuring statistics. [116](#)
- Figure 69 Results playing against the smart player. Each cycle was made of 100 games for training, and then 100 games for measuring statistics. [117](#)

Figure 70	Results playing against another SDM player. Each cycle was made of 100 games for training, and then 100 games for measuring statistics. <a href="#">118</a>
Figure 71	Results playing against a randomly chosen player between random player, smart player, and another SDM player. Each cycle was made of 100 games for training, and then 100 games for measuring statistics. <a href="#">119</a>
Figure 72	Shannon write operation: Computing the amount of information of a signal to each hard location in its access radius. (a) entirety of the space; (b) region of interest; (c) Fast integer computation is possible through a stepwise function. <a href="#">123</a>
Figure 73	Behavior of the critical distance under the information-theoretic weighted write operation when $n = 1,000$ , $H = 1,000,000$ and $r = 451$ . <a href="#">124</a>
Figure 74	Bongard problems 71 - 73, courtesy of noted Bongardologist, Dr. Harry Foundalis. What distinguishes the boxes on the left hand side to those on the right hand side? <a href="#">129</a>

## LIST OF TABLES

---

Table 1	Write operation example in a 7-dimensional memory of data $\eta$ being written to $\xi$ , one of the activated addresses. <a href="#">17</a>
Table 2	Comparison of Kanerva's read and Chada's read. Each $\xi_i$ is an activated hard location and the values come from their counters. Gray cells' value is obtained randomly with probability 50%. <a href="#">20</a>

Table 3

MacBook Pro Retina 13-inch Late 2013 with a 2.6GHz Intel core i5 processor, 6GB DDR3 RAM, and Intel Iris GPU. The SDM settings were: (i)  $n = 256$ ,  $r = 103$ , and  $H = 1,000,000$ ; (ii)  $n = 1,000$ ,  $r = 451$ , and  $H = 1,000,000$ ; and (iii)  $n = 10,000$ ,  $r = 4850$ , and  $H = 1,000,000$ . There is no benchmark for  $n = 10,000$  because memory is not enough on either RAM or GPU—it would consume 37.25 GB of RAM and 1.2GB of memory in the GPU. For the histogram of durations, see Figures 9, 10, 11, and 12. 40

Table 4

iMac Retina 5K 27-inch 2017 with a 3.8GHz Intel core i5 processor, 8GB DDR4 RAM, and a Radeon Pro 580 8G GPU. The SDM settings were: (i)  $n = 256$ ,  $r = 103$ , and  $H = 1,000,000$ ; (ii)  $n = 1,000$ ,  $r = 451$ , and  $H = 1,000,000$ ; and (iii)  $n = 10,000$ ,  $r = 4850$ , and  $H = 1,000,000$ . There is no benchmark for read and write operations with  $n = 10,000$  because RAM is not enough to allocate the counters—it would consume 37.25 GB of RAM. For the histogram of durations, see Figures 13, 14, 15, and 16. 45

Table 5

Amazon EC2 p2.xlarge with Intel Xeon E5-2686v4 processor, 61GB DDR3 RAM, and NVIDIA K80 GPU. Running an SDM with  $n = 256$  bits,  $H = 1,000,000$ , and  $r = 103$ . The SDM settings were: (i)  $n = 256$ ,  $r = 103$ , and  $H = 1,000,000$ ; (ii)  $n = 1,000$ ,  $r = 451$ , and  $H = 1,000,000$ ; and (iii)  $n = 10,000$ ,  $r = 4850$ , and  $H = 1,000,000$ . There is no benchmark for kernel `single_scan5_unroll` because it returns the wrong result in this GPU. The problem is related to the premises of the optimization used by this kernel, which are not true for this GPU. For the histogram of durations, see Figures 17, 14, 15, and 16. 50

Table 6	Amazon EC2 p3.2xlarge with Intel Xeon E5-2686v4 processor, 488GB DDR3 RAM, and NVIDIA Tesla V100 GPU. The SDM settings were: (i) $n = 256$ , $r = 103$ , and $H = 1,000,000$ ; (ii) $n = 1,000$ , $r = 451$ , and $H = 1,000,000$ ; and (iii) $n = 10,000$ , $r = 4850$ , and $H = 1,000,000$ . There is no benchmark for kernel <code>single_scan5_unroll</code> because it returns the wrong result in this GPU. The problem is related with the premises of the optimization used by this kernel, which are not true for this GPU. For the histogram of durations, see Figures 21, 22, 23, and 24. 55
Table 7	Dual process theories. 128
Table 8	Desiderata of open-source, creative-common deliverables, longer-term. Some of these items are mature for wide dissemination, whereas others are in planning phase. For an online SDM course, for instance, we might partner with a Ph.D. program in the Teaching of Mathematics and Physics, such as IM/UFRJ [38], who are intent on developing and measuring the effects of new educational tools. 133



## Part I

### AN INVITATION TO SPARSE DISTRIBUTED MEMORY: FROM THE THEORETICAL MODEL TO THE SYSTEM DYNAMICS



# 1

## INTRODUCTION

---

*How is memory gradually built up during one's conscious, or even unconscious, life and thought? My guess is that everything we experience is classified and registered on very many parallel channels in different locations*

— Stanislaw Ulam

*Pentti Kanerva's memory model was a revelation for me: it was the very first piece of research I had ever come across that made me feel I could glimpse the distant goal of understanding how the brain works as a whole. It gave me a concrete sense for how familiar mental phenomena could be thought of as distributed patterns of micro-events, thanks to beautiful mathematics.*

— Douglas Hofstadter

Suddenly, you feel the danger. You tighten your grip on the child's hand and step up your walking. In these large cities, walking on a dark alley was never recommended, but somehow that's what you have done — and now everything you can think of is to get back to safety. You are afraid of something, but you cannot explain — in rigorous detail, at least — what exactly is causing your fear. One just feels it.

We may interpret this situation as clues of the present — a dark alley; a giant metropolitan area; people going on about their lives mostly indifferent from each other; constrained routes ahead and behind; a general lack of activity; that very feeling that something isn't right... without knowing precisely what isn't right, or even what 'right' means — recalling past experiences from memory and thus generating the feeling. Our memory is able to make a parallel between previous experiences and the clues. Although one has never been in the exactly same situation, one's brain involuntarily, through analogy with previous experiences, recognizes the possibility of danger. The whole process happens so fast it feels like it only took a single indivisible unit of psychological time. A single cycle, to use the computing word.

As much as we can rationalize our ability to understand the why of a feeling like this, it seems unlikely that we will be able to nail all reasons down into rules. Let us compare this to what a child might

do. While an adult may respond by discreetly stepping up the walking speed, a child might open her eyes and be surprised and ask, indiscretely, questions about the walking speed... Because children do not have the accumulated experience of adults in dealing with large metropolian areas, their behavior differs markedly from ours.

Sparse Distributed Memory (SDM) [41] (see also [24, 28, 43–48, 52, 78, 91]) is a mathematical model of long-term memory that has a number of neuroscientific and psychologically plausible dynamics. This model is used in all sort of applications due to its incredible ability to closely reflect the human capacity to remember past experiences from the subtlest of clues. Applications range from call admission control [54, 55], to behavior-based robotics [39, 64, 75], to noise filtering [66], etc.

This flexibility into mapping one situation in another is an essential human feature which is hard to replicate in computers.

### 1.1 DESIDERATA FOR A THEORY OF MEMORY

Sparse Distributed Memory reads like a *desiderata* of a theory for human long-term memory. To understand the breadth of topics that SDM encompasses, consider the following questions:

1. Why are most concepts orthogonal, unrelated to each other?
2. Why is there Miller's magic number, i.e., we can't hold too many things in mind at once?
3. Why do we at times instantly recall an experience; other times we can't recall anything at all; and still other times we get into this strange tip-of-the-tongue situation... it is clearly 'there'... but where? (and 'what' is 'there'?<sup>1</sup>.)
4. How does this recall process work? What is remembering?
5. Why do neurons die and we still remember most everything?
6. What do neurons actually do? What is their primary function?

These are some of the questions touched by SDM. It is a theory of long-term memory that constructs the process of recall from a very microscopic level of neuron-firings. While there are numerous groups working on related research, it seems that most are simply bypassing each other; starting from scratch instead of building on top of what already exists.

---

<sup>1</sup> Psychologists have documented interesting properties about this state: it happens, for instance, around every 1-week cycle; and it happens mostly over proper names, subjects have access to the first letter and to the number of syllables better than chance, etc. Also interesting is their clever way of triggering the state: through definitions of rarely-used words. For some psychological studies about the tip-of-tongue, see Brown [10], Brown and McNeill [11], Meyer and Bock [67].

## 1.2 THE WASTED EFFORT OF DUPLICATED, AD HOC, WORK

As expected for such an important theory, SDM has been applied in many different fields, like pattern recognition [72, 76], noise reduction [65], handwriting recognition [26], robot automation [64, 75], and so forth. Linhares et al. [62] has argued that SDM respects the limits of short-term memory [19, 68]. Kanerva's book has over 1,000 citations in Google Scholar. Despite this, there is not a reference implementation which would allow one to replicate the results published in a paper, to check the source code for details, and to improve it. Thus, even though intriguing results have been achieved using SDM, it requires counter-productive, duplicate effort from researchers to build on top of previous work.

Our motivation is our own effort to run our models. As there is no reference implementation, we had to develop our own and run several simulations to ensure that our implementation was correct and bug-free. Thus, we had to deviate from our primary goal — which was to test our hypothesis and explore the 'ideas space' — and to focus on the implementation itself. Furthermore, new members of our research group had to go through different source code developed by former members, in different languages. Consider the implementations of SDM present — as of this writing — on its wikipedia entry[1]<sup>2</sup>:

1. The original 1989 hardware implementation developed in NASA by Flynn et al. [28];
2. a 1995 LISP implementation for the Connection Machine by Turk and Gorz [90];
3. a 1992 APL implementation by Surkan [88];
4. a 2004 FPGA implementation by Silva et al. [81];
5. a 2005 C++ implementation by Berchtold [5] from Lancaster University, in the 'CommonSense ToolKit' (CSTK) [20] for realtime sensor data includes SDM as one of its classification algorithms;
6. a 2015 'C Binary Vector Symbols (CBVS)': includes SDM implementation as a part of vector symbolic architecture developed by Emruli et al. [25] from EISLAB at Luleå University of Technology <sup>3</sup>;

---

<sup>2</sup> There has recently been a plethora of hardware implementations to minimize energy expenditure and parallelize processes [49, 50, 59, 70, 79]. While these implementations are extremely interesting, they do not afford the flexibility to experiment that software does.

<sup>3</sup> The code is available at <http://pendicular.net/cbvs.php>

7. a 2013 Java implementation ‘Learning Intelligent Distribution Agent’ (LIDA) developed by [31, 86, 87] Stan Franklin’s group from the University of Memphis includes implementation.<sup>4</sup>;

Let us analyze these. The Connection Machine is obsolete. The NASA implementation is hardware-based and obsolete. APL, while reasonably influential, is not a mainstream language in science.

The FPGA implementation by Silva et al. [81] has yielded a fast scan of hard locations at low energy costs, provided one has access to the proper hardware. Their article claims a four-fold speedup over assembly language; but it does not deal with parallel processing details. For example, it is unclear whether there was more than a single thread running on the software implementation. Note that the framework presented here is also able to reconfigure field-programmable gate arrays, through the OpenCL heterogeneous computing platform ability to interface with Hardware Description Language and hence, reconfigure FPGAs [21, 94] for our tasks.

Then there is LIDA — a whole cognitive architecture based on Hofstadter’s Fluid Concepts, Kanerva’s SDM, and other ideas [4, 31, 86, 87]. It is developed in Java; which makes it difficult to connect to the lowest levels of hardware; to connect to GPUs or FPGAs, and to other languages — at least in comparison to the combination Python and OpenCL proposed here<sup>5</sup>. It has a non-standard license, strange to the open-source community, *the LIDA Framework Software NonExclusive, Non-Commercial Use License*. We have not found any parallelism in their code [12], which may make simulations slow or unfeasible. Moreover, potential contributors must sign an “Agreement Regarding Contributory Code for the LIDA Framework Software”... ‘before Memphis can accept it’<sup>6</sup>.

The closest implementations to ours, in philosophy at least, is the one in ‘the common sense toolkit’. It is executed in C++, with a normal open-source license, and hosted on an open-source code repository. It is, however, strikingly dissimilar to ours on the following aspects:

---

<sup>4</sup> <http://ccrg.cs.memphis.edu/framework.html>; see also <http://ccrg.cs.memphis.edu/projects.html> where they link to a github repository.

<sup>5</sup> Python is sometimes called a ‘glue language’. That is, in my opinion, not the best metaphor. A glue connects two things leaving an inflexible structure. Python is perhaps best described as the interstate highway system of Programming; if something is out there, there is a way to reach it with Python. In the comparison with Java, for instance, take the `popcnt(xor(bi, bj))` operation, executed billions of times in SDM. How easy is it to program that for a particular GPU or FPGA with Java?

<sup>6</sup> What they are attempting to do with this bureaucracy remains unclear, the history of computing has not been kind to those who favored centralization [27]. We certainly refrain from contributing given the legal uncertainties of non-standard licenses and dubious processes — even as we would like to link these libraries

1. SDM is but a part of the system; the description of the system reads that cstk is ‘A toolkit for processing and visualising sensor data in real time with support for use with embedded platforms.’
2. The whole SDM code is composed of 143 *lines* of C++ in the cstk/cstk – devonly/sdm folder.
3. There is no work on making the system parallel.
4. There is strong coupling between location address and location data, which makes experimentation hard.
5. There are no tests or examples to be found instantly.
6. Finally, the last commit to this repository seems to have been made in 2005?
7. There are no publishable or published scientific applications or experiments available to be reproduced at installation time.
8. there is no tutorial, installation instructions, performance benchmarks, framework validation or SDM Documentation.

Note that all these criticisms apply to the implementations in both the ‘common sense toolkit’ and the ‘C Binary Vector Symbols’ [5, 20, 25]. While these implementations have around 150 lines of C++; at last count, the *documentation of our implementation* had over 100 pages [61]: they have aimed at running code, and we aim at improving a community and industry standard.

There is obviously a demand for use of SDM; but each group has been tied to their own *ad-hoc* needs, and there has not been the emergence of a community centered on a tool. It is our belief that a tool such as standard open-source framework could bring orders of magnitude more researchers and attention if they were able to use the model, at zero cost, with an easy to use high-level language such as Python, in an intuitive platform such as Jupyter notebooks. Neuroscientists interested in long-term memory storage should not have to worry about high-bandwidth vector parallel computation. This new tool would provide a ready to use system in which experiments could be executed almost as soon as designed — and provide the needed replication of studies [80].

The main contribution of this work is a reference implementation which yields (i) orders of magnitude gains in performance, (ii) has several backends<sup>7</sup> and operations, (iii) is fully validated against the mathematical model, (iv) is cross-platform<sup>8</sup>, and (v) is easily extensible to test new research ideas — and to let others replicate the studies.

---

<sup>7</sup> CPUs, GPUs, FPGAs

<sup>8</sup> Unix, Linux, MacOs, Windows, Amazon Web Services, etc.

Another issue is *extensibility*: Extensions of SDM have been used in many applications. For example, Snaider and Franklin [85] extended SDM to store sequences of vectors and trees efficiently. Rao and Fuentes [75] used a modified SDM in an autonomous robot. Meng et al. [65] modified SDM to clean patterns from noisy inputs. Fan and Wang [26] extended SDM with genetic algorithms. Chada [13] extended SDM creating the Rotational Sparse Distributed Memory (RSDM), which models network motifs, dynamic flexibility, and hierarchical organization — reflecting results from the neuroscience literature.

Our reference implementation may, hopefully, accelerate research into the model’s dynamics and make it easier for readers to replicate any previous results and easily understand the source-code of the model. Moreover, it is compatible with Jupyter notebook and researchers may share their notebooks possibly accelerating the advances in their fields [80].

Other contributions have also been introduced, which include (i) a noise filtering approach, (ii) a supervised classification algorithm, (iii) and a reinforcement learning algorithm, all of them using only the original SDM proposed by Kanerva, i.e., with no additional mechanisms, algorithms, data structures, etc. Although some of these applications have already been explored in previous work [26, 65, 76], all of them have adapted SDM to fit their problems, and none of them have used just the ideas introduced by Kanerva. We have presented different approaches with no adaptations whatsoever.

Finally, I have striven to provide a visual tour of the theory and application of SDM: whenever possible, detailed figures should tell the story — or at least do the heavy lifting. In this study, we will see an anomaly in one of Kanerva’s predictions, which I believe is related to SDM capacity. We will see tests of a generalized reading operation proposed by Physics Professor Paulo Murilo (personal communication). We will see what happens when neurons — and all their information — is simply and suddenly lost. We will see whether information-theory can improve some of Kanerva’s ideas. From (basic) noise filtering to learning to play tic-tac-toe, we will review the entirety of Dr. Pentti Kanerva’s proposal.

This time, however, it will be running on a computer: anomalies between expected theory and numerical results will appear; implicit, hidden, assumptions will emerge; and reproducible experiments will be conducted.

# 2

## NOTATION

---

$n$	Number of dimensions, i.e., $n = 1,000$ .
$N$	Size of the binary space, $ \{0, 1\}^n  = 2^n$ .
$N'$	Number of hard locations samples from $\{0, 1\}^n$ . Its typical value is 1,000,000, as suggested by Kanerva [41].
$H$	Same as $N'$ .
$r$	Access radius, i.e., when $n = 1,000$ and $N' = 1,000,000$ , its typical value is 451. This value is calculated to activate, on average, one-thousandth of $N'$ .
$\eta$	A bitstring, usually a datum.
$\eta_x$	A clue $x$ bits away from $\eta$ , i.e., $\text{dist}(\eta, \eta_x) = x$ .
$\xi$	A bitstring, usually an address.
$\text{dist}(x, y)$	Hamming distance between $x$ and $y$ .
$d(x, y)$	Same as $\text{dist}(x, y)$ .



# 3

## SPARSE DISTRIBUTED MEMORY

---

Sparse Distributed Memory (SDM) is a mathematical model developed and suggested as a theory of human memory by Finnish Scientist Penti Kanerva [41]. It introduces many interesting mathematical properties of  $n$ -dimensional binary space that, in a memory model, seem to be remarkably psychologically plausible. Most notable among these are the tip-of-the-tongue phenomenon, conformity to Miller's magic number [62], and robustness against loss of neurons.

The data — and address space on which it is stored — are represented by large sequences of bits, called *bitstrings*. The *Hamming distance* provides comparisons between bitstrings and is used as a metric for the system. The Hamming distance is defined for two bitstrings of equal length as the number of positions in which bits differ. For example,  $00110_b$  and  $01100_b$  are bitstrings of length 5 and their Hamming distance is 2.

The space studied by Kanerva is also called the *hypercube graph*, or  $Q_n$ , as in Figure 1. For a fixed  $n \in \mathbb{Z}$ , the graph  $G = (V, E)$ , in which  $v \in V$  iff there is a bijective function  $b : V \rightarrow \{0, 1\}^n$  and  $(v_i, v_j) \in E$  iff  $H(b(v_i), b(v_j)) = 1$ , where  $H$  is the Hamming distance. That is,  $n$ -sized bitstrings correspond to nodes, and edges exist between nodes iff they flip a single bit. Though Kanerva has derived many combinatorial properties of the space, additional results have been found by the graph-theoretical community: it is a bipartite graph with chromatic number 2, and it is planar only if  $n \leq 3$ . The proofs, though elementary, illuminate some of its properties: vertices connect bitstrings with an even number of 1's with bitstrings with an odd number of 1's, therefore (i) it is *bipartite* and (ii) it *may be colored with two colors*. As for planarity, the case  $n = 3$  is the largest planar one. A good survey is provided by Harary et al. [33] — and some interesting results may be found in [29, 56, 77, 93].

One has to be careful when thinking intuitively about distance in SDM because the Hamming distance does not have the same properties of, say, our 3-dimensional space.

A major difference is that in the 3-d world, there exist very far points, while in  $Q_n$  the largest possible distance is  $n$ . Another one is that the number of directions in  $Q_n$  is enormous: at *every point* there are  $n$  directions to choose from.

Though both follow the triangle inequality ( $d(A, C) \leq d(A, B) + d(B, C)$ ), which in 3-d Euclidean distance may be loosely interpreted as “if A is close to B, and B is close to C, then A is also close to C” —

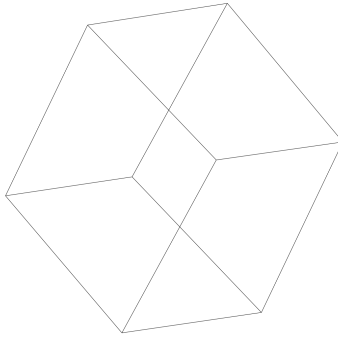
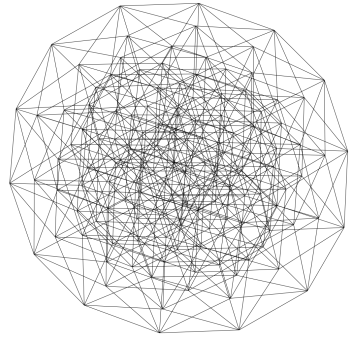
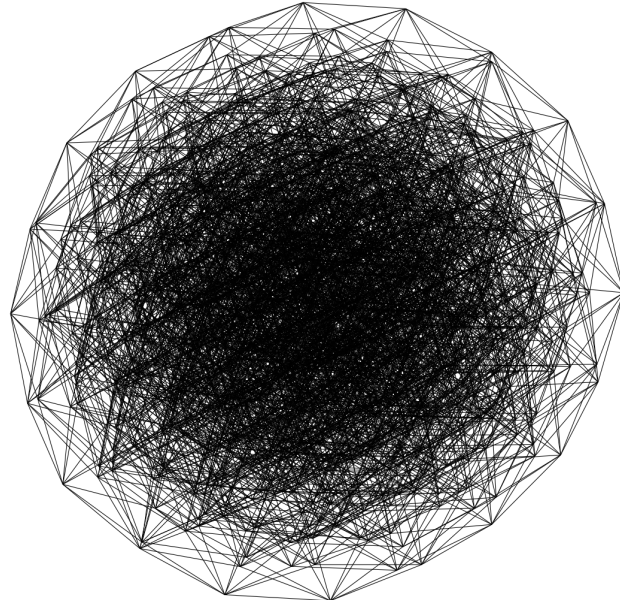
(a)  $Q_3$ (b)  $Q_7$ (c)  $Q_{10}$ 

Figure 1: Here we have  $Q_n$ , for  $n \in \{3, 7, 10\}$ . Each node corresponds to a bitstring in  $\{0, 1\}^n$ , and two nodes are linked iff the bitstrings differ by a single dimension. A number of observations can be made here. First, the number of nodes grows as  $O(2^n)$ ; which makes the space rapidly intractable. Another interesting observation, better seen in the figures below, is that most of the space lies ‘at the center’, at a distance of around  $n/2$  from any given vantage point.

$d(A, B) \leq r$  and  $d(B, C) \leq r \Rightarrow d(A, C) \leq 2r$  —, but in SDM, although the inequality is also valid, two bitstrings would be close when, for instance,  $r = 430$ , so  $2r = 860$  would cover all other bitstrings. Hence, it makes no sense to say that A is also close to C.

There are numerous, beautiful, counter-intuitive notions involved in this space. This difference in intuition may trick even experienced researchers when analyzing some situations.

Unlike traditional memory used by computers, SDM performs read and write operations in a multitude of addresses, also called neurons. That is, the data is not written, or it is not read in a single address spot, but in many addresses. These are called activated addresses, or activated neurons.

The activation of addresses takes place according to their distances from the datum. Suppose one is writing datum  $\eta$  at address  $\xi$ , then all addresses inside a circle with center  $\xi$  and radius  $r$  are activated. So,  $\eta$  will be stored in all these activated addresses, which are around address  $\xi$ , such as in Figure 2. An address  $\xi'$  is inside the circle if its Hamming distance to the center  $\xi$  is less than or equal to the radius  $r$ , i.e.  $\text{distance}(\xi, \xi') \leq r$ .

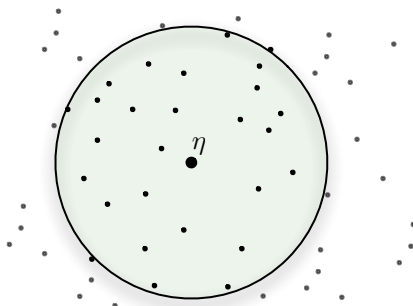


Figure 2: Activated addresses inside access radius  $r$  around the center address.

Every write or read in SDM memory activates a number of addresses with close distance. The data is written in these activated addresses or read from them. These issues will be addressed in due detail further on, but a major difference from a traditional computer memory is that the data are always stored and retrieved in a multitude of addresses. This way SDM memory has robustness against loss of addresses (e.g., death of a neuron).

In traditional memory, each datum is stored in an address and every lookup of a specific datum requires a search through the memory. In spite of computer scientists having developed beautiful algorithms to perform fast searches, almost all of them do a precise search. That is, if you have an imprecise clue of what you need, these algorithms will simply fail.

In SDM, the data space is the same as the address space, which amounts to a vectorial, binary space, that is, a  $\{0, 1\}^n$  space. This way, the addresses where the data will be written are the same as the data themselves. For example, the datum  $\eta = 00101_b \in \{0, 1\}^5$  will be written to the address  $\xi = \eta = 00101_b$ . If one chooses a radius of 1, the SDM will activate all addresses one bit away or less from the center address. So, the datum  $00101_b$  will be written to the addresses  $00101_b, 10101_b, 01101_b, 00001_b, 00111_b$ , and  $00100_b$ .

In this case, when one needs to retrieve the data, one could have an imprecise cue at most one bit away from  $\eta$ , since all addresses one bit away have  $\eta$  stored in themselves. Extending this train of thought for larger dimensions and radius, exponential numbers of addresses are activated and one can see why SDM is a distributed memory.

When reading a cue  $\eta_x$  that is  $x$  bits away from  $\eta$ , the cue shares many addresses with  $\eta$ . The number of shared addresses decreases as the cue's distance to  $\eta$  increases, in other words, as  $x$  increases. This is shown in Figure 3. The target datum  $\eta$  was written in all shared addresses, thus they will bias the read output in the direction of  $\eta$ . If the cue is sufficiently near the target datum  $\eta$ , the read output will be closer to  $\eta$  than  $\eta_x$  was. Repeating the read operation increasingly gets results closer to  $\eta$ , until it is precisely the same. So, it may be necessary to perform more than one read operation to converge to the target data  $\eta$ .

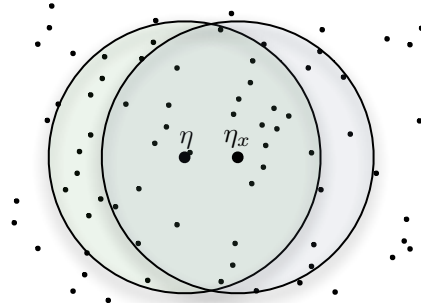


Figure 3: Shared addresses between the target datum  $\eta$  and the cue  $\eta_x$ .

The addresses of the  $\{0, 1\}^n$  space grow exponentially with the number of dimensions  $n$ , i.e.,  $N = 2^n$ . For  $n = 100$  we have  $N \approx 10^{30}$ , which is incredibly large when related to computer memory. Furthermore, Kanerva [41] suggests  $n$  between 100 and 10,000. Recently he has postulated 10,000 as a desirable minimum  $N$  (personal communication). To solve the feasibility problem of implementing this memory, Kanerva made a random sample of  $\{0, 1\}^n$ , in his work, having  $N'$  elements. All these addresses in the sample are called hard locations. Other elements of  $\{0, 1\}^n$ , not in  $N'$ , are called virtual neurons. This is represented in Figure 4. All

properties of reading and write operations presented before remain valid but limited to hard locations. Kanerva suggests taking a sample of about one million hard locations.

Using this sample of binary space, our data space does not exist completely. That is, the binary space has  $2^n$  addresses, but the memory is far away from having these addresses available. In fact, only a fraction of this vectorial space is actually instantiated. Following Kanerva's suggestion of one million hard locations, for  $n = 100$ , only  $100 \cdot 10^6 / 2^{100} = 7 \cdot 10^{-23}$  percent of the whole space exists, and for  $n = 1,000$  only  $100 \cdot 10^6 / 2^{1000} = 7 \cdot 10^{-294}$  percent.

Kanerva also suggests the selection of a radius that will activate, on average, one-thousandth of the sample, which is 1,000 hard locations for a sample of one million addresses. In order to achieve his suggestion, a 1,000-dimension memory uses an access radius  $r = 451$ , and a 256-dimensional memory,  $r = 103$ . We think that a 256-dimensional memory may be important because it presents conformity to Miller's magic number [62].

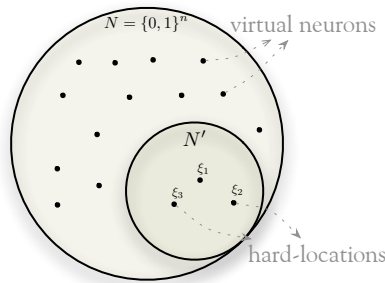


Figure 4: Hard-locations randomly sampled from binary space.

Since a cue  $\eta_x$  near the target bitstring  $\eta$  shares many hard locations with  $\eta$ , SDM can retrieve data from imprecise cues. Despite this feature, it is very important to know how imprecise this cue could be while still giving accurate results. What is the maximum distance from our cue to the original data that still retrieves the right answer? An interesting approach is to perform a read operation with a cue  $\eta_x$ , that is  $x$  bits away from the target  $\eta$ . Then measure the distance from the read output and  $\eta$ . If this distance is smaller than  $x$  we are converging. Convergence is simple to handle, just read again and again, until it converges to the target  $\eta$ . If this distance is greater than  $x$  we are diverging. Finally, if this distance equals  $x$  we are in a tip-of-the-tongue process. A tip-of-the-tongue psychologically happens when you know that you know, but you can't say what exactly it is. In SDM mathematical model, a tip-of-the-tongue process takes infinite time to converge. Kanerva [41] called this  $x$  distance, where the read's output averages  $x$ , the critical distance. Intuitively, it is the distance from which smaller distances converge

and greater distances diverge. In Figure 5, the circle has radius equal to the critical distance and every  $\eta_x$  inside the circle should converge. The figure also shows convergence in four readings.

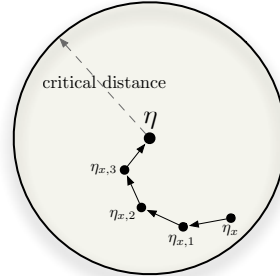


Figure 5: In this example, four iterative readings were required to converge from  $\eta_x$  to  $\eta$ .

The  $\{0, 1\}^n$  space has  $N = 2^n$  locations from which we instantiate  $N'$  samples. Each location in our sample is called a hard location. On these hard locations, we do operations of read and write. One of the insights of SDM is exactly the way we read and write: using data as addresses in a distributed fashion. Each datum  $\eta$  is written in every activated hard location inside the access radius centered on the address, that equals datum,  $\xi = \eta$ . Kanerva suggested using an access radius  $r$  having about one-thousandth of  $N'$ . As an imprecise cue  $\eta_x$  shares hard locations with the target bitstring  $\eta$ , it is possible to retrieve  $\eta$  correctly. (Actually, probably more than one read is necessary to retrieve exactly  $\eta$ ). Moreover, if some neurons are lost, only a fraction of the datum is lost and it is possible that the memory can still retrieve the right datum.

A random bitstring is generated with equal probability of 0's and 1's for each bit. One can readily see that the average distance between two random bitstrings follows the binomial distribution with mean  $n/2$  and standard deviation  $\sqrt{n/4}$ . For a large  $n$ , most of the space lies close to the mean and has fewer shared hard locations. As two bitstrings with distance far from  $n/2$  are very improbable, Kanerva [41] defined that two bitstrings are orthogonal when their distance is  $n/2$ .

The write operation needs to store, for each dimension bit which happened more (0's or 1's). This way, each hard location has  $n$  counters, one for each dimension. The counter is incremented for each bit 1 and decremented for each bit 0. Thus, if the counter is positive, there have been more 1's than 0's, if the counter is negative, there have been more 0's than 1's, and if the counter is zero, there have been an equal number of 1's and 0's. Table 1 shows an example of a write operation being performed in a 7-dimensional memory.

$\eta$	0	1	1	0	1	0	0
$\xi_{before}$	6	-3	12	-1	0	2	4
$\xi_{after}$	5	-2	13	-2	1	1	3

$\Downarrow -1 \quad \Downarrow +1 \quad \Downarrow +1 \quad \Downarrow -1 \quad \Downarrow +1 \quad \Downarrow -1 \quad \Downarrow -1$

Table 1: Write operation example in a 7-dimensional memory of data  $\eta$  being written to  $\xi$ , one of the activated addresses.

The read is performed polling each activated hard location and statistically choosing the most written bit for each dimension. It consists of adding all  $n$  counters from the activated hard locations and, for each bit, choosing bit 1 if the counter is positive, choosing bit 0 if the counter is negative, and randomly choose bit 0 or 1 if the counter is zero.

### 3.1 NEURONS AS POINTERS

One interesting view is that neurons in SDM work like pointers. As we write bitstrings in memory, the hard locations' counters are updated and some bits are flipped. Thus, the activated hard locations do not necessarily point individually to the bitstring that activated it, but together they point correctly. In other words, the read operation depends on many hard locations to be successful. This effect is represented in Figure 6: where all hard locations inside the circle are activated and they, individually, do not point to  $\eta$ . But, like vectors, adding them up points to  $\eta$ . If another datum  $v$  is written into the memory near  $\eta$ , the shared hard locations will have information from both of them and would not point to either. All hard locations outside of the circle are also pointing somewhere (possibly other data points). This is not shown, however, in order to keep the picture clean and easily understandable.

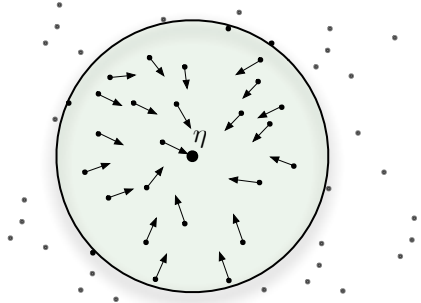


Figure 6: Hard-locations pointing, approximately, to the target bitstring.

### 3.2 CONCEPTS

Although Kanerva does not mention concepts directly in his book [41], the author's interpretation is that each bitstring may be mapped to a concept. Thus, unrelated concepts are orthogonal and concepts could be linked through a bitstring near both of them. For example, "beauty" and "woman" have distance  $n/2$ , but a bitstring that means "beautiful woman" could have distance  $n/4$  to both of them. As a bitstring with distance  $n/4$  is very improbable, it is linking those concepts together. Linhares et al. [62] approached this concept via "chunking through averaging".

Due to the distribution of hard locations between two random bitstrings, the vast majority of concepts is orthogonal to all others. Consider a non-scientific survey during a cognitive science seminar, where students asked to mention ideas unrelated to the course brought up terms like birthdays, boots, dinosaurs, fever, executive order, x-rays, and so on. Not only are the items unrelated to cognitive science, the topic of the seminar, but they are also unrelated to each other.

For any two memory items, one can readily find a stream of thought relating two such items ("Darwin gave dinosaurs the boot"; "she ran a fever on her birthday"; "isn't it time for the Supreme Court to x-ray that executive order?", ... and so forth). Robert French presents an intriguing example in which one suddenly creates a representation linking the otherwise unrelated concepts of "coffee cups" and "old elephants" [32].

This mapping from concepts to bitstrings brings us two central questions: (i) Suppose we have a bitstring that is linking two major concepts. How do we know which concepts are linked together? (ii) From a concept bitstring, how can we list all concepts that are somehow linked to it? This second question is called the problem of spreading activation.

### 3.3 READ OPERATION

In his work, Kanerva proposed and analyzed a read algorithm called here Kanerva's read. His read takes all activated hard locations counters and sum them. The resulting bitstring has bit 1 where the result is positive, bit 0 where the result is negative, and a random bit where the result is zero. In a word, each bit is chosen according to all written bitstrings in all hard locations, being equal to the bit more appeared. Table 2a shows an example of Kanerva's read result bitstring.

Daniel Chada, one member of our research group, proposed another way to read in SDM, in this work called Chada's read. Instead of summing all hard location counters, each hard location

evaluates its resulting bitstring individually. Then, all resulting bitstrings are summed again, and the same rule as Kanerva applies. Table 2b shows an example of Chada's read result bitstring. The counter's values are normalized to 1, for positive ones, or -1, for negative ones, and the original values are the same as in Table 2a.

The main difference between Kanerva's read and Chada's is that, in the former, a hard location that has more bitstrings written has a greater weight in the decision of each bit. In the latter, all hard locations have the same weight, because they can contribute to the sum with only one bitstring.

It is important to say that Chada's read came from Anwar and Franklin [4] which gave a misguided description of the read operation. The original description is the following:

With our datum distributively stored, the next question is how to retrieve it. With this in mind, let us ask first how one reads from a single hard location,  $x$ . Compute  $\zeta$ , the bit vector read at  $x$ , by assigning its  $i$ th bit the value 1 or 0 according to the  $i$ th counter at  $x$  is positive or negative. Thus, each bit of  $\zeta$  results from a majority rule decision of all the data that have been written at  $x$ . [...] Knowing how to read from a hard location allows us to read from any of the  $2^{1000}$  arbitrary locations. Suppose  $\zeta$  is any location. The bit vector,  $\xi$ , to be read at  $\zeta$ , [...] Put another way, pool the bit vectors read from hard locations accessible from  $\zeta$ , and let each of their  $i$ th bits vote on the  $i$ th bit of  $\xi$ .

— Anwar and Franklin [4, p.342]

This fact just highlights how important it is to have a reference implementation that one may read the code to clarify one's understanding about the details of each operation.

### 3.3.1 Generalized read operation

A member of my Master's committee, Prof. Paulo Murilo<sup>1</sup>, has proposed a generalized reading operation (personal communication), which covers both Kanerva's and Chada's read — and opens a new venue of potential discoveries. He proposed summing all hard location counters raised to the power of  $z$  while holding the original sign of the counter (positive or negative). Thus, Kanerva's read would be the same as  $z = 1$ , while Chada's would be the same as  $z = 0$ . Hence, we will here explore how SDM would behave with other values of  $z$ , such as 0.5, 2, and 3. Mathematically, let  $A$  be the set of the counters of the activated hard location, and  $c_i$  be the counter of the  $i$ th bit. Then,

---

<sup>1</sup> Universidade Federal Fluminense's Physics Professor Paulo Murilo

$\xi_1$	-2	12	4	0	-3
$\xi_2$	-5	-4	2	8	-2
$\xi_3$	-1	0	-1	-2	-1
$\xi_4$	3	2	-1	3	1
$\sum$	<b>-5</b>	<b>10</b>	<b>4</b>	<b>3</b>	<b>-5</b>
	↓	↓	↓	↓	↓
	0	1	1	1	0

$\xi_1$	-1	1	1	1	-3
$\xi_2$	-1	-1	1	1	-1
$\xi_3$	-1	1	-1	-1	-1
$\xi_4$	1	1	-1	-1	1
$\sum$	<b>-2</b>	<b>1</b>	<b>0</b>	<b>0</b>	<b>-2</b>
	↓	↓	↓	↓	↓
	0	1	1	1	0

(a) Kanerva's read example

(b) Chada's read example

Table 2: Comparison of Kanerva's read and Chada's read. Each  $\xi_i$  is an activated hard location and the values come from their counters. Gray cells' value is obtained randomly with probability 50%.

$$s_i = \sum_{c \in A} \frac{c_i}{|c_i|} |c_i|^z$$

Finally, the  $i$ th bit of the resulting bitstring is 1 if  $s_i > 0$ , or 0 if  $s_i < 0$ , or random if  $s_i = 0$ . Notice that when  $z = 1$ , then  $s_i = \sum_{c \in A} c_i$ , which is the Kanerva's read; and when  $z = 0$ , then  $s_i = \frac{c_i}{|c_i|} = \text{sign}(c_i)$ , which is the Chada's read.

### 3.4 CRITICAL DISTANCE

Kanerva describes the critical distance as the threshold of convergence of a sequence of read words. It is “the distance beyond which divergence is more likely than convergence”[41]. Furthermore, Kanerva explains that “a very good estimate of the critical distance can be obtained by finding the distance at which the arithmetic mean of the new distance to the target equals the old distance to the target”[41]. In other words, the critical distance can be equated as the edge to our memory, the limit of human recollection.

In his book, Kanerva analyzed a specific situation with  $n = 1000$  ( $N = 2^{1000}$ ), 1 million hard locations ( $N' = 1,000,000$ ), an access-radius of 451 (within 1,000 hard locations in each circle), and 10 thousand writes of random bitstrings in the memory. As computer resources were very poor those days, Kanerva couldn't make a more generic analysis.

Starting from the premise of SDM as a faithful model of human short-term memory, a better understanding of the critical distance may shed light on our understanding of the thresholds that bind our own memory.

Figure 7 compares the critical distance behavior under different scenarios. This replicates our previous results [7, 9] and is a first part of the process of framework validation, to which we throw our attention next.

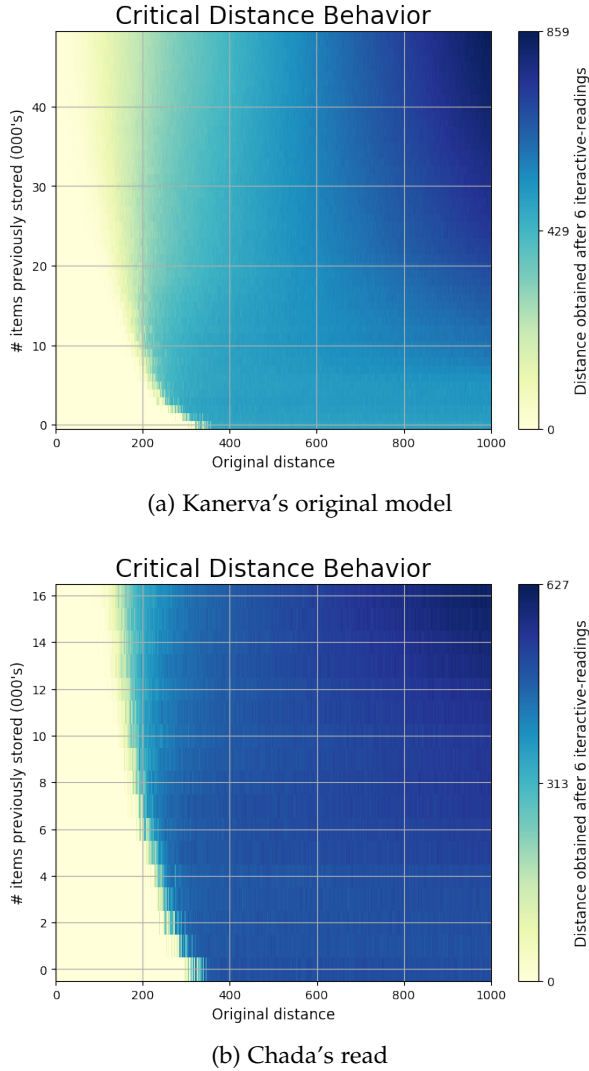


Figure 7: How far, in Hamming distance, is a read item from the original stored item? Kanerva demonstrated that, after a small number of iterative readings (6 here), a critical distance behavior emerges. Items read at close distance converge rapidly; whereas farther items do not converge. Most striking is the point in which the system displays the tip-of-tongue behavior. Described by psychological moments when some features of the item are prominent in one’s thoughts, yet the item still cannot be recalled (but an additional cue makes convergence ‘immediate’). Mathematically, this is the precise distance in which, despite having a relatively high number of cues (correct bits) about the desired item, the time to convergence is infinite. Heatmap colors display the Hamming distance the associative memory is able to cleanly converge to—or not. In the x-axis, the distance from the desired item is displayed. In the y-axis, we display the read operation’s behavior as the number of items registered in the memory grows. These graphs are computing intensive, yet they can be easily tested by readers in our provided Jupyter notebooks. Note the different scales.



# 4

## FRAMEWORK ARCHITECTURE

---

The framework implements the basic operations in a Sparse Distributed Memory which may be used to create more complex operations. It is developed in C language and the OpenCL parallel framework — which may be loaded in many platforms and programming languages — with a wrapper in Python. The Python module makes it easy to create and execute simulations in a Sparse Distributed Memory and works properly in Jupyter Notebook [53]. It works in both Python 2 and Python 3.

The SDM memory has been split into two parts: the hard location addresses and the hard location counters. Thus, the addresses (bitstrings) of the hard locations are stored in one array, while their counters in another. This makes possible to create multiple SDMs using the same address space, which would save computational effort to scan a bitstring in all the SDMs — since they share the same address space, the activated hard locations will be the same in all of them. As the slowest part of reading and writing operations is scanning the address space, the performance benefits are significant.

Each part may be stored either in the RAM memory or in a file. The RAM memory is interesting for quick experiments, automated tests, and others scenarios in which the SDM may be lost, while the file is interesting for a long-term SDM, like creating an SDM file with 10,000 random writes, which will be copied over and over to run multiple experiments. The file may also be sent to another researcher or may be published within the paper to let others run their own checks and verify the results. In summary, the framework fits many different uses and necessities.

Let a SDM memory with  $n$  dimensions and  $H$  hard locations. Then, in a 64-bit computer, the array of hard location addresses will use  $H \cdot 8 \cdot \lceil n/64 \rceil$  bytes of memory, and there will be  $H \cdot n$  hard location counters. For example, in a SDM memory with 1,000 dimensions and 1,000,000 hard locations, using 32-bit integers for the counters, the array of addresses will use 122MB of memory and the counters will use 3.8 GB of memory.

Basic operations were grouped into four sets: (i) for bitstrings, (ii) for addresses, (iii) for counters, and (iv) for memories (SDMs). Operations include creating new bitstrings, flipping bits, generating a bitstring with a specific distance from a given bitstring, scanning the address space using different algorithms, writing a bitstring to a counter, writing in an SDM, reading from an SDM, and iteratively reading from an SDM until convergence.

#### 4.1 BITSTRING

Bitstrings are the main structure of SDM. The addresses are represented in bitstrings, as well as the data. A bitstring is stored as an array of integers. Each integer may be 16-bit, 32-bit, or 64-bit long, depending on the configuration. By default, each integer is 64-bit long.

For instance, a 1,000-bit bitstring will have  $\lceil 1000/64 \rceil = 16$  integers. These integers will have a total of  $16 \cdot 64 = 1,024$  bits. The remaining 24 bits are always zero, so they do not affect the result of any operation. The memory usage efficiency is  $1 - 24/1024 = 97.65\%$ . Bitstrings store neither how many bits they have nor the array length. These pieces of information are only stored in the address space.

##### 4.1.1 *The distance between two bitstrings*

The distance between two bitstrings is calculated by the Hamming distance, which is the number of different bits between them. It is calculated counting the number of ones in the exclusive or (xor) between the bitstrings, i.e.,  $d(x, y) = \text{number of ones in } x \oplus y$ .

There are several algorithms to calculate the number of ones [95], but the performance depends on the processor. So, we have implemented three different algorithms and one may be selected through compiling flags. The default algorithm is to use a built-in `_popcnt()` instruction from the compiler.

There is also the naive algorithm, which really counts the number of ones checking bit by bit. It is available only for testing purposes and should never be used.

The other algorithm available is the lookup. It pre-calculates a table with the number of ones of all possible 16-bit integers. This table is accessed a few times to calculate the number of ones of a 64-bit integer, i.e., to calculate the distance between two bitstrings, it sums the distance of each 16-bit part of the bitstrings, i.e.,  $d(x[0 : 63], y[0 : 63]) = d(x[0 : 15], y[0 : 15]) + d(x[16 : 31], y[16 : 31]) + d(x[32 : 47], y[32 : 47]) + d(x[48 : 63], y[48 : 63])$  where  $x[i : i + 15]$  and  $y[i : i + 15]$  are the 16-bit integers formed by the bits between  $i$  and  $i + 15$  of  $x$  and  $y$ , respectively. Each 16-bit distance is calculated through a single table access. As each distance is calculated in  $O(1)$ , this algorithm runs in  $O(\lceil \text{bits}/16 \rceil)$ . This table uses 65MB of RAM. One may change the table from 16-bit integers to 32-bit integers, which would halve the number of accesses at the expense of 4GB of RAM (instead of 65MB).

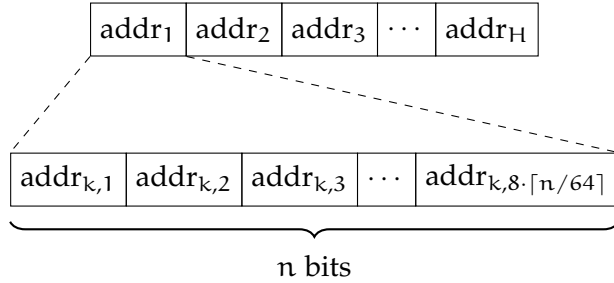


Figure 8: Address space's bitstrings are stored in a contiguous array. In a 64-bit computer, each bitstring is stored in a sub-array of 64-bit integers, with length  $8 \cdot \lceil n/64 \rceil$ .

## 4.2 ADDRESS SPACE

An address space is a fixed collection of bitstrings, and each bitstring represents a hard location address. They store the number of bitstrings, as well as the number of bits, number of integers per bitstring, and the number of remaining bits.

Bitstrings are stored in a contiguous array of 64-bit integers, as shown in Figure 8. Hence, basic pointer arithmetic provides us with performance improvements in their access, as processors realize fetches of contiguous chunks of memory [74].

The scan for activated hard locations is performed in an address space. It returns the indexes of the bitstrings which were inside the circle (and their distances). Then, each operation uses these pieces of information in a different way.

### 4.2.1 Scanning for activated hard locations

Scanning for the activated hard locations is a problem similar to well-known problems in computational geometry called “range reporting in higher dimensions”. In this case, none of the known algorithms is able to solve our problem faster than  $O(H)$ . The algorithm which seems to best fit in our problem consumes  $O(H)$  space and runs in  $O(\log^n(H))$  [15], which is significantly slower than  $O(H)$  when, for instance,  $H = 1,000,000$  and  $n = 1,000$ . For a review of the range reporting algorithms, see Chan et al. [14].

In 2014, Norouzi et al. [73] published a solution to fast search in hamming space which seems applicable to our problem. It provides a fast search when  $r/n < 0.11$  or  $r/n < 0.06$ , where  $r$  is the radius and  $n$  is the number of bits. But, in our case, for a 1,000 bits SDM,  $r/n = 0.451$ , which changes the runtime to  $O(H^{0.993})$ . This is very close to  $O(H)$ , but with a larger constant. Unfortunately,  $O(H)$  is still faster.

It is intriguing that none of those algorithms is able to solve our scanning problem. The roughly idea behind those computational

geometry algorithms is to split the search space in half each step, which would take  $O(\log(H))$  to go through the whole space. But this approach does not work because of the high number of dimensions (i.e., 1,000) and because the hard locations' addresses are randomly sampled from the  $\{0, 1\}^n$  space. Although each addresses' bit itself splits the hard locations in half, it does not split the search space in half since both halves still must be covered by the algorithm. For instance, let's say we have  $n = 1,000$  dimensions with  $H = 1,000,000$  hard locations, and we are scanning within a circle with radius  $r = 451$ , then after checking the first bit we have two cases: (i) for the half with the same first bit, we must keep scanning with radius 451; and (ii) for the half with a different first bit, we must keep scanning with radius 450. Hence, the search space has not been split in half because both halves have been covered (and one of them should have been skipped).

Finally, as our best approach is to scan through all hard locations, we may distribute the scan into many tasks which will be executed independently. The tasks may be executed in different processes, threads, or even computers. They may also run in the CPU or in the GPU. In this case, we may take into account both the time required to distribute the tasks and the time to receive their results.

The framework implements three main scanner algorithms: linear scanner, thread scanner, and OpenCL scanner. The linear scanner runs in a single core, is the slowest one, and was developed only for testing purposes; the thread scanner runs at the CPU in multiple threads sharing memory (and our recommendation is to use the number of threads equals to twice the number of CPU cores); and the OpenCL scanner runs in multiple GPU cores and support multiple devices. The speed of a scan depends on the CPU and GPU devices, thus the best approach to choose which scanner is best for one's setup is to run a benchmark.

The OpenCL must be initialized, which basically copies the address space's bitstrings to the GPU's memory. Then, many scans may be executed with no necessity to upload the bitstrings again. The OpenCL scanner supports running on multiple devices.

#### 4.2.2 *OpenCL kernels*

There are eight OpenCL kernels which differently explore the GPU architecture to improve performance. It is necessary because there are several GPU microarchitectures and a single kernel will never be optimal for all of them. In simplified form, OpenCL splits the tasks into workgroups which, in turn, split their part of the task into workers. The works are like threads in a computer. OpenCL specifies four levels of memory hierarchy for the GPUs: global memory, read-only memory, local memory, and private memory. The global memory

and read-only memory are accessible by all workgroups, while each workgroup has its own local memory, shared by its workers. Finally, each worker has its own private memory. The number of workers per workgroup is defined by user and must be multiple of the number of tasks.

All eight kernels do the same thing: calculate the exclusive OR (XOR) between two 64-bit integers and count the number of bits one in the result. They just do it with different approaches. For instance, `single_scan0` calculates one distance between bitstrings per worker (Listing 1); while `single_scan2` uses a whole workgroup to calculate each distance, distributing each element of the 64-bit integer array per worker (Listing 3).

The OpenCL kernels `single_scan3` (Listing 4), `single_scan4` (Listing 5), `single_scan5` (Listing 6), `single_scan5_unroll` (Listing 7), `single_scan6` (Listing 8) explore the GPU architecture to improve the sum of the partial distances. Each workgroup calculates the distance of several bitstrings. During the distance calculation, each worker calculates the exclusive OR (XOR) between two 64-bit integers and use the built-in `popcount` function to count the number of ones. Then, they update an array of partial distances with their results. This array is stored in the local memory and is shared between all workers of the same workgroup. This whole step happens simultaneously in the GPU. Then, a reduction algorithm is used to sum the partial distances array in order to calculate the total distance. This reduction algorithm is also distributed among the workers and runs in  $O(\log_2(\text{bs\_step}))$ . Finally, the first worker of each workgroup checks whether the distance is less than or equal to the radius to include the bitstring index into the resulting array.

Some of the optimizations may not work in some GPUs because not all their premises are valid. Before choosing a kernel, one should check whether it works properly for one's specific GPU device.

#### 4.3 COUNTERS

A counter is an array of integers which stores the data of all hard locations. Each hard location has one integer of data per bit. For instance, each hard location of a 1,000 bits SDM has 1,000 integers, totaling 1,000,000 integers. Those integers are stored in a counter. So, the counter's array has  $n \cdot H$  integers.

When two counters are added in a third counter, there may occur an overflow. It is not supposed to be a problem because, by default, each counter is a signed 32-bit integer that can store any number between -2,147,483,648 and 2,147,483,647, which means they will not overflow with fewer writes than  $2^{31} - 1$  divided by the average number of activated hard locations. For instance, when  $n = 1,000$ ,  $H = 1,000,000$ , and  $r = 451$ , the average number of activated hard

```

1 __kernel
2 void single_scan0(
3             _constant const uchar *bitcount_table,
4             _global const ulong *bitstrings,
5             const uint bs_len,
6             const uint sample,
7             _constant const ulong *bs,
8             const uint radius,
9             _global uint *counter,
10            _global uint *selected,
11            _local uint *partial_dist)
12 {
13     uint id = get_global_id(0);
14
15     if (id < sample) {
16         ulong a;
17         uint dist;
18
19         const __global ulong *row = bitstrings + id*bs_len;
20
21         dist = 0;
22         for(uint j=0; j<bs_len; j++) {
23             a = row[j] ^ bs[j];
24             dist += popcount(a);
25         }
26         if (dist <= radius) {
27             selected[atomic_inc(counter)] = id;
28         }
29     }
30 }
```

Listing 1: OpenCL kernel `single_scan0`. It calculates one distance per worker and lets the GPU decide how to distribute this task between workgroups and workers. It is the most straightforward kernel and does not explore any details of the GPU architecture.

```

1 --kernel
2 void single_scan1(
3     --constant const uchar *bitcount_table,
4     --global const ulong *bitstrings,
5     const uint bs_len,
6     const uint sample,
7     --constant const ulong *bs,
8     const uint radius,
9     --global uint *counter,
10    --global uint *selected,
11    --local uint *partial_dist)
12 {
13     uint id;
14     ulong a;
15     uint dist;
16     const --global ulong *row;
17
18     for (id=get_global_id(0); id < sample; id += get_global_size(0)) {
19
20         row = bitstrings + id*bs_len;
21
22         dist = 0;
23         for(uint j=0; j<bs_len; j++) {
24             a = row[j] ^ bs[j];
25             dist += __popcount(a);
26         }
27         if (dist <= radius) {
28             selected[atomic_inc(counter)] = id;
29         }
30     }
31 }
32 }
```

Listing 2: OpenCL kernel `single_scan1`. It is just like `single_scan0`, but it distributes several distances per workgroup, which, in turn, distributes the distances among their workers.

```

1 __kernel
2 void single_scan2(
3     __constant const uchar *bitcount_table,
4     __global const ulong *bitstrings,
5     const uint bs_len,
6     const uint sample,
7     __constant const ulong *bs,
8     const uint radius,
9     __global uint *counter,
10    __global uint *selected,
11    __local uint *partial_dist)
12 {
13     uint dist;
14     ulong a;
15     uint j;
16
17     for (uint id = get_group_id(0); id < sample; id += get_num_groups(0)) {
18
19         const __global ulong *row = bitstrings + id*bs_len;
20
21         dist = 0;
22         j = get_local_id(0);
23         if (j < bs_len) {
24             a = row[j] ^ bs[j];
25             dist += popcount(a);
26         }
27         partial_dist[get_local_id(0)] = dist;
28
29         barrier(CLK_LOCAL_MEM_FENCE);
30
31         if (get_local_id(0) == 0) {
32             dist = 0;
33             for(uint t = 0; t < bs_len; t++) {
34                 dist += partial_dist[t];
35             }
36             if (dist <= radius) {
37                 selected[atomic_inc(counter)] = id;
38             }
39         }
40
41         barrier(CLK_LOCAL_MEM_FENCE);
42     }
43 }
```

Listing 3: OpenCL kernel `single_scan2`. It calculates one distance per workgroup, distributing each 64-bit integer operation per worker, and then summing the results obtained by the workers. The sum algorithm is done by only the first worker of each workgroup.

```

1 __kernel
2 void single_scan3(
3     __constant const uchar *bitcount_table,
4     __global const ulong *bitstrings,
5     const uint bs_len,
6     const uint sample,
7     __constant const ulong *bs,
8     const uint radius,
9     __global uint *counter,
10    __global uint *selected,
11    __local uint *partial_dist)
12 {
13     uint dist;
14     ulong a;
15     uint j;
16
17     for (uint id = get_group_id(0); id < sample; id += get_num_groups(0)) {
18
19         const __global ulong *row = bitstrings + id*bs_len;
20
21         dist = 0;
22         j = get_local_id(0);
23         if (j < bs_len) {
24             a = row[j] ^ bs[j];
25             dist = popcount(a);
26         }
27         partial_dist[get_local_id(0)] = dist;
28
29         // Parallel reduction to sum all partial_dist array.
30         for(uint stride = get_local_size(0)/2; stride > 0; stride /= 2) {
31             barrier(CLK_LOCAL_MEM_FENCE);
32             if (get_local_id(0) < stride) {
33                 partial_dist[get_local_id(0)] +=
34                     partial_dist[get_local_id(0) + stride];
35             }
36         }
37
38         if (get_local_id(0) == 0) {
39             if (partial_dist[0] <= radius) {
40                 selected[atomic_inc(counter)] = id;
41             }
42         }
43
44         barrier(CLK_LOCAL_MEM_FENCE);
45     }
46 }
```

Listing 4: OpenCL kernel `single_scan3`. It calculates one distance per workgroup, distributing each 64-bit integer operation per worker, and then summing the results obtained by the workers. The sum algorithm is a parallel reduction, in which the workers split the array into two parts and sum the second part in the first part every loop. So, the sum is calculated in  $O(\log_2(\text{number of workers per workgroup}))$ . This kernel only works when the number of workers per workgroup is a power-of-2.

```

1  __kernel
2  void single_scan4(
3      __constant const uchar *bitcount_table,
4      __global const ulong *bitstrings,
5      const uint bs_len,
6      const uint sample,
7      __constant const ulong *bs,
8      const uint radius,
9      __global uint *counter,
10     __global uint *selected,
11     __local uint *partial_dist)
12 {
13     uint dist;
14     ulong a;
15     uint j;
16
17     for (uint id = get_group_id(0); id < sample; id += get_num_groups(0)) {
18
19         const __global ulong *row = bitstrings + id*bs_len;
20
21         dist = 0;
22         j = get_local_id(0);
23         if (j < bs_len) {
24             a = row[j] ^ bs[j];
25             dist = popcount(a);
26         }
27         partial_dist[get_local_id(0)] = dist;
28
29         uint old_stride = get_local_size(0);
30         __local uint extra;
31         extra = 0;
32         for(uint stride = get_local_size(0)/2; stride > 0; stride /= 2) {
33             barrier(CLK_LOCAL_MEM_FENCE);
34             if ((old_stride&1) == 1 && get_local_id(0) == old_stride-1) {
35                 extra += partial_dist[get_local_id(0)];
36             }
37             if (get_local_id(0) < stride) {
38                 partial_dist[get_local_id(0)] +=
39                     partial_dist[get_local_id(0) + stride];
40             }
41             old_stride = stride;
42         }
43
44         if (get_local_id(0) == 0) {
45             if (partial_dist[0] + extra <= radius) {
46                 selected[atomic_inc(counter)] = id;
47             }
48         }
49
50         barrier(CLK_LOCAL_MEM_FENCE);
51     }
52 }
```

Listing 5: OpenCL kernel `single_scan4`. This kernel is just like `single_scan3`, but it works with any number of workers per workgroup. The tradeoff is that it includes an additional step in the parallel reduction algorithm.

```

1 __kernel
2 void single_scan5(
3     __constant const uchar *bitcount_table,
4     __global const ulong *bitstrings,
5     const uint bs_len,
6     const uint sample,
7     __constant const ulong *bs,
8     const uint radius,
9     __global uint *counter,
10    __global uint *selected,
11    __local uint *partial_dist)
12 {
13     uint dist;
14     ulong a;
15     uint j;
16
17     for (uint id = get_group_id(0); id < sample; id += get_num_groups(0)) {
18         const __global ulong *row = bitstrings + id*bs_len;
19
20         dist = 0;
21         j = get_local_id(0);
22         if (j < bs_len) {
23             a = row[j] ^ bs[j];
24             dist = popcount(a);
25         }
26         partial_dist[get_local_id(0)] = dist;
27
28         uint stride;
29         for(stride = get_local_size(0)/2; stride > 32; stride /= 2) {
30             barrier(CLK_LOCAL_MEM_FENCE);
31             if (get_local_id(0) < stride) {
32                 partial_dist[get_local_id(0)] +=
33                     partial_dist[get_local_id(0) + stride];
34             }
35         }
36         barrier(CLK_LOCAL_MEM_FENCE);
37         for/**; stride > 0; stride /= 2) {
38             if (get_local_id(0) < stride) {
39                 partial_dist[get_local_id(0)] +=
40                     partial_dist[get_local_id(0) + stride];
41             }
42         }
43
44         if (get_local_id(0) == 0) {
45             if (partial_dist[0] <= radius) {
46                 selected[atomic_inc(counter)] = id;
47             }
48         }
49         barrier(CLK_LOCAL_MEM_FENCE);
50     }
51 }
```

Listing 6: OpenCL kernel `single_scan5`. This kernel is just like `single_scan3`, but it explores one more detail of many GPU microarchitecture: the size of the warp. As the workers in the same warp are always synchronized, there is no need to sync them using a barrier. This specific kernel only works when the number of workers per workgroup is a power-of-2.

```

1  __kernel
2  void single_scan5_unroll(
3      __constant const uchar *bitcount_table,
4      __global const ulong *bitstrings,
5      const uint bs_len,
6      const uint sample,
7      __constant const ulong *bs,
8      const uint radius,
9      __global uint *counter,
10     __global uint *selected,
11     __local uint *partial_dist)
12  {
13      uint dist;
14      ulong a;
15      uint j;
16
17      for (uint id = get_group_id(0); id < sample; id += get_num_groups(0)) {
18          const __global ulong *row = bitstrings + id*bs_len;
19
20          dist = 0;
21          j = get_local_id(0);
22          if (j < bs_len) {
23              a = row[j] ^ bs[j];
24              dist = popcount(a);
25          }
26          partial_dist[get_local_id(0)] = dist;
27
28          for(uint stride = get_local_size(0)/2; stride > 32; stride /= 2) {
29              barrier(CLK_LOCAL_MEM_FENCE);
30              if (get_local_id(0) < stride) {
31                  partial_dist[get_local_id(0)] += partial_dist[get_local_id(0) + stride];
32              }
33          }
34
35          // We do not need to sync because they all run in the same warp.
36          if (get_local_id(0) < 32 && get_local_size(0) >= 64) {
37              partial_dist[get_local_id(0)] += partial_dist[get_local_id(0) + 32];
38          }
39          if (get_local_id(0) < 16 && get_local_size(0) >= 32) {
40              partial_dist[get_local_id(0)] += partial_dist[get_local_id(0) + 16];
41          }
42          if (get_local_id(0) < 8 && get_local_size(0) >= 16) {
43              partial_dist[get_local_id(0)] += partial_dist[get_local_id(0) + 8];
44          }
45          if (get_local_id(0) < 4 && get_local_size(0) >= 8) {
46              partial_dist[get_local_id(0)] += partial_dist[get_local_id(0) + 4];
47          }
48          if (get_local_id(0) < 2 && get_local_size(0) >= 4) {
49              partial_dist[get_local_id(0)] += partial_dist[get_local_id(0) + 2];
50          }
51
52          if (get_local_id(0) == 0) {
53              partial_dist[0] += partial_dist[1];
54              if (partial_dist[0] <= radius) {
55                  selected[atomic_inc(counter)] = id;
56              }
57          }
58          barrier(CLK_LOCAL_MEM_FENCE);
59      }
60  }

```

Listing 7: OpenCL kernel `single_scan5_unroll`. This kernel is exactly like `single_scan5`, but it unrolls the last `for` since it has at most 5 loops.

```

1  __kernel
2  void single_scan6(
3      __constant const uchar *bitcount_table,
4      __global const ulong *bitstrings,
5      const uint bs_len,
6      const uint sample,
7      __constant const ulong *bs,
8      const uint radius,
9      __global uint *counter,
10     __global uint *selected,
11     __local uint *partial_dist)
12 {
13     uint dist;
14     ulong a;
15     uint j;
16
17     for (uint id = get_group_id(0); id < sample; id += get_num_groups(0)) {
18         const __global ulong *row = bitstrings + id*bs_len;
19
20         dist = 0;
21         j = get_local_id(0);
22         if (j < bs_len) {
23             a = row[j] ^ bs[j];
24             dist = popcount(a);
25         }
26         partial_dist[get_local_id(0)] = dist;
27
28         uint old_stride = get_local_size(0);
29         uint stride;
30         __local uint extra;
31         extra = 0;
32         for(stride = get_local_size(0)/2; stride > 32; stride /= 2) {
33             barrier(CLK_LOCAL_MEM_FENCE);
34             if ((old_stride&1) == 1 && get_local_id(0) == old_stride-1) {
35                 extra += partial_dist[get_local_id(0)];
36             }
37             if (get_local_id(0) < stride) {
38                 partial_dist[get_local_id(0)] +=
39                     partial_dist[get_local_id(0) + stride];
40             }
41             old_stride = stride;
42         }
43         barrier(CLK_LOCAL_MEM_FENCE);
44         for/**/; stride > 0; stride /= 2) {
45             if ((old_stride&1) == 1 && get_local_id(0) == old_stride-1) {
46                 extra += partial_dist[get_local_id(0)];
47             }
48             if (get_local_id(0) < stride) {
49                 partial_dist[get_local_id(0)] +=
50                     partial_dist[get_local_id(0) + stride];
51             }
52             old_stride = stride;
53         }
54
55         if (get_local_id(0) == 0) {
56             if (partial_dist[0] + extra <= radius) {
57                 selected[atomic_inc(counter)] = id;
58             }
59         }
60         barrier(CLK_LOCAL_MEM_FENCE);
61     }
62 }
```

Listing 8: OpenCL kernel `single_scan6`. This kernel is just like `single_scan5`, but it works with any number of workers per work. The tradeoff is an additional step in the parallel reduction algorithm.

locations is 1,000 and it would require at least one million writes before any overflow is possible. Note also that it would be more likely to saturate the memory before any overflow.

Anyway, counters may have overflow protection depending on compiling options. By default, there is no overflow check for performance reasons (and because it does not seem necessary).

#### 4.4 READ AND WRITE OPERATIONS

The reading and writing operations are executed in two steps: first, the address space is swept looking for the activated addresses; then, the operation is performed in the counters. Reading operation assembles the bitstring according to the counters of the activated addresses, while the writing operation changes the counters.

The iterated reading keeps reading until it gets exactly the same bitstring (or the number of maximum interactions has been reached), i.e., it performs  $\eta_{i+1} = \text{read}(\eta_i)$  and stops when  $\eta_{k+1} = \eta_k$ . If the initial bitstring is inside the critical distance of  $\eta$ , it will converge to  $\eta$ , but, if it is not, it will diverge and reach the maximum number of iterations.

The framework has both Kanerva's read and Murilo's generalized read. The generalization brings a parameter  $z$ , which is the exponent. In this case, the results are floating points instead of integers, which considerably reduces performance. When  $z = 1$ , it is precisely as the Kanerva's read. When  $z = 0$ , it is the Chada's read. We also explored how SDM would behave for different values of  $z$ .

There is another particular read operation: the weighted reading. In the weighted reading, the value of the counters is multiplied by a weight which depends only on the distance between the reading address and the hard location address. The weight is retrieved from a lookup table of integers indexed by the distance. The remaining of the read operation is just the same.

There is also a weighted writing operation. In this case, the weight is applied when the counters are updated, i.e., if the weight is 2, the counters are increased twice when bits are 1, and decreased twice when bits are 0. Just as in the weighted reading, the weights depend only on the distance between the writing address and the hard location address. The weights are retrieved from a lookup table of integers indexed by the distance.

# 5

## RESULTS (I): PERFORMANCE

---

Performance matters. A framework that does not offer cutting-edge performance is not valuable. If an experiment takes a few seconds, there is no point arguing whether we should try it. If it takes a few hours, maybe we should think first. If it takes a few days — or more —, it is important to devise a good plan. As SDM consumes large processor and memory resources, some experiments may take a long time.

Each scan on a 1,000-bits SDM with 1,000,000 hard locations executes  $10^9$  bit compares through  $10^9/64 = 15,625,000$  XORs and calls to the built-in `popcount`. So, 10,000 writes execute  $10^{13}$  bit compares, while a 6-iterative reading executes  $6 \cdot 10^{12}$  bit compares. The heatmap of Figure 7a executed  $3.05 \cdot 10^{15}$  bit compares. For comparison, the number of seconds since Jesus's birth is  $63,639,648,000 = 6.36 \cdot 10^{10}$ . The number of people who have ever lived on earth is estimated to be  $1,08 \cdot 10^{11}$ . There are approximately  $1.8 \cdot 10^9$  websites on the internet. A modern laptop can increment a counter  $5 \cdot 10^8$  times per second. Hence, a naive implementation of SDM may take several hours — or days — to simply write 10,000 random bitstrings.

Amazon EC2 p3.2xlarge has generated the heatmap of Figure 7a in 15 minutes and 3 seconds. It has compared  $3.37 \cdot 10^{12}$  bits per second through  $52.6 \cdot 10^9 = 52.6$  billion XORs and `popcounts` per second. It is a 60-fold improvement over the first versions of the code which took 16 hours to generate the same heatmap (and its memory use was already optimized and the computations were distributed in threads).

We have created a benchmark to be able to compare the performance of different devices. So, the same performance test was executable in our devices, with results reported in tables and figures. The benchmark has 3 parts: (i) the first part consists of comparing the available OpenCL kernels to find which works best for that device; than (ii) the second part consists of comparing the linear scanner, the thread scanner, and the OpenCL scanners with the best kernel found in part one; finally, (iii) the third part consists of comparing read and write operations using the thread scanner and the OpenCL scanner with the best kernel. Each part was run for three SDM setups: (i)  $n = 1,000$ ,  $r = 451$ , and  $H = 1,000,000$ ; (ii)  $n = 256$ ,  $r = 103$ , and  $H = 1,000,000$ ; and (iii)  $n = 10,000$ ,  $r = 4850$ , and  $H = 1,000,000$ . The whole source code is available in the “Performance test” notebook [8]. We would like to invite the reader to run this benchmark and, if possible, share the results.

Our first device was a personal MacBook Pro Retina 13-inch Late 2013 with a 2.6GHz Intel core i5 processor, 6GB DDR3 RAM, and Intel Iris GPU. It was not possible to run the 10,000-bits on this device because there was no memory available — it needs 37.25 GB of memory. For its results, see Table 3

Our second device was an iMac Retina 5K 27-inch 2017 with a 3.8GHz Intel core i5 processor, 8GB DDR4 RAM, and a Radeon Pro 580 8G GPU. For its results, see Table 4.

Beyond that, we were also running in state-of-the-art devices: (i) an Amazon EC2 p2.xlarge with Intel Xeon E5-2686v4 processor, 61GB DDR3 RAM, and NVIDIA K80 GPU (see Table 5), and (ii) an Amazon EC2 p3.2xlarge with Intel Xeon E5-2686v4 processor, 488GB DDR3 RAM, and NVIDIA Tesla V100 GPU (see Table 6).

### 5.1 KERNELS COMPARISON

OpenCL is a framework for writing software that executes in *heterogeneous* devices [71], like CPUs, GPUs, FPGA and other co-processors for hardware acceleration. Because they are heterogeneous, they may differ a lot in architecture and performance, which means there is no one-size-fits-all kernel. A *kernel* is generally a small function on the code that runs in thousands of parallel threads, executing the same steps on different parts of a large vector or matrix. The slower kernel for one device may be the fastest for another device, as we will see happening in our case.

A total of 8 kernels have been developed for benchmarking in our framework: `single_scan0`, `single_scan1`, `single_scan2`, `single_scan3`, `single_scan4`, `single_scan5`, `single_scan5_unroll`, and `single_scan6`. Each scan uses a different algorithm to do exactly the same thing: calculate which hard locations are inside the circle of the given bitstring. They differ in how they split the work between work-groups and how they explore the GPU architecture to obtain performance gains.

The difference in which kernel is the best also depends on the SDM setup. The best kernel for the 1,000-bits SDM in the iMac 2017 was `single_scan5_unroll` with average scan time of 3.61ms; but, for the 256-bits SDM in the same device, it was `single_scan0` with average scan time of 3.03ms; while, for the 10,000-bits SDM in the same device, it was `single_scan6` with 10.96ms (see Table 4).

We recommend users to run a specific kernel comparison test for their own GPU and SDM settings. This is available in the Jupyter notebooks.

## 5.2 SCANNERS COMPARISON

In this section, we are comparing the OpenCL scanner (with the best kernel) with the linear scanner and the threads scanner. Again, which one is faster depends on the SDM settings. In the iMac 2017, the fastest scanner for a 1,000-bits SDM was the OpenCL scanner with `single_scan5_unroll`, but, for a 256-bit SDM, it was the threads scanner.

What happened here is that the OpenCL kernel chosen was a generic one which performs the scan for any SDM. It is always possible to optimize the OpenCL kernel to a specific setting, and it would be faster than the threads. By default, the framework chooses a generic kernel which we believe would be reasonable for the most common setups.

We can notice that Amazon EC2 p3.2xlarge and p2.xlarge's linear and thread scanners, both running on CPU, were much slower than the CPU of both the personal MacBook Pro and the iMac 2017. As Amazon EC2 are virtual machines with GPU devices, their CPU is shared with other virtual machines which significantly reduces CPU power. Hence, for both virtual machines we have tested, using the GPU seriously boosts performance, but using the CPU should be avoided (see Table 4)

## 5.3 READ AND WRITE OPERATIONS

Even though scanning is an important part of the operations, we are really interested in the performance of the entirety of operations themselves. Comparing the times of the thread and OpenCL scanners with the times of their respective operations (either read or write), we can notice that their difference remains almost constant, which means the operation time itself is negligible when compared to the scan time. In other words, in order to gain even more performance, we have to pursue ways to improve the scan.

### 5.3.1 *Summary of results*

The results, beyond showing the obvious fact that consumer grade hardware is not comparable to the Amazon instances, indicate a non-trivial issue: The chosen kernel for scanning the memory is of crucial importance to performance, and this kernel speed is a function of both the hardware used and the particular parameters used in the SDM settings.

It is reasonable to consider that the performance results obtained are of particular merit, and one particular fact stands out: The scanning of 1,000,000 hard locations has become, in the desired

	<b>256 bits</b>	<b>1,000 bits</b>	<b>10,000 bits</b>
Kernel	Duration (ms)	Duration (ms)	Duration (ms)
single_scan0	8.36	23.60	
single_scan1	10.43	13.22	
single_scan2	23.48	47.28	
single_scan3	25.51	33.06	
single_scan4	42.39	40.32	
single_scan5	24.42	31.51	
single_scan5_unroll	22.77	27.55	
single_scan6	42.18	39.48	
Scanner	Duration (ms)	Duration (ms)	Duration (ms)
Linear scan	9.07	17.98	
Thread scan	5.14	10.17	
OpenCL scan	8.05	12.35	
Operation	Duration (ms)	Duration (ms)	Duration (ms)
Thread write	6.72	14.13	
Thread single read	5.88	11.12	
OpenCL write	6.39	18.55	
OpenCL single read	5.26	13.06	

Table 3: MacBook Pro Retina 13-inch Late 2013 with a 2.6GHz Intel core i5 processor, 6GB DDR3 RAM, and Intel Iris GPU. The SDM settings were: (i)  $n = 256$ ,  $r = 103$ , and  $H = 1,000,000$ ; (ii)  $n = 1,000$ ,  $r = 451$ , and  $H = 1,000,000$ ; and (iii)  $n = 10,000$ ,  $r = 4850$ , and  $H = 1,000,000$ . There is no benchmark for  $n = 10,000$  because memory is not enough on either RAM or GPU—it would consume 37.25 GB of RAM and 1.2GB of memory in the GPU. For the histogram of durations, see Figures 9, 10, 11, and 12.

professional-grade machines, *faster* than the updating of the 1,000 active locations.

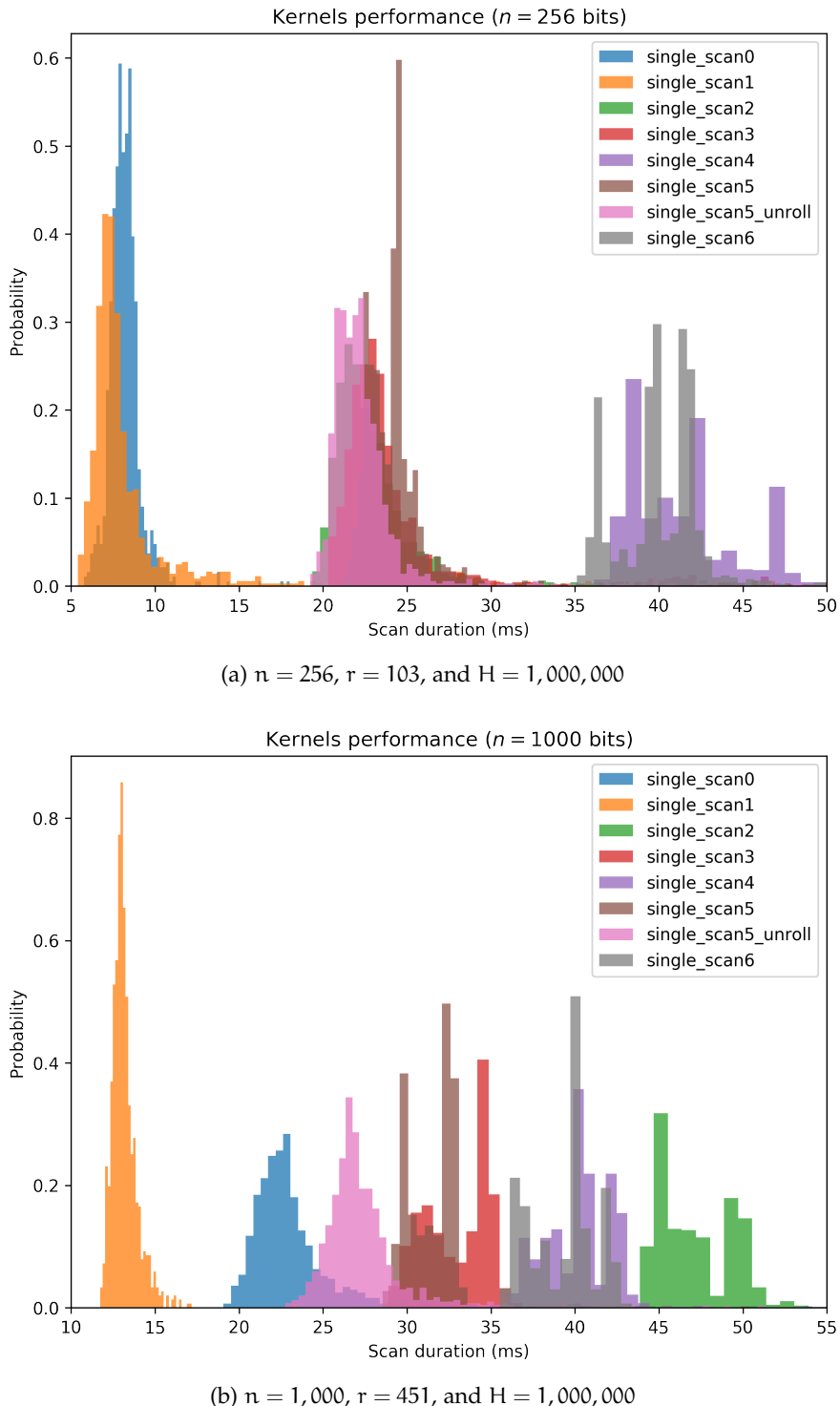


Figure 9: Kernel comparisons for MacBook Pro Retina 13-inch Late 2013 with a 2.6GHz Intel core i5 processor, 6GB DDR3 RAM, and Intel Iris GPU.

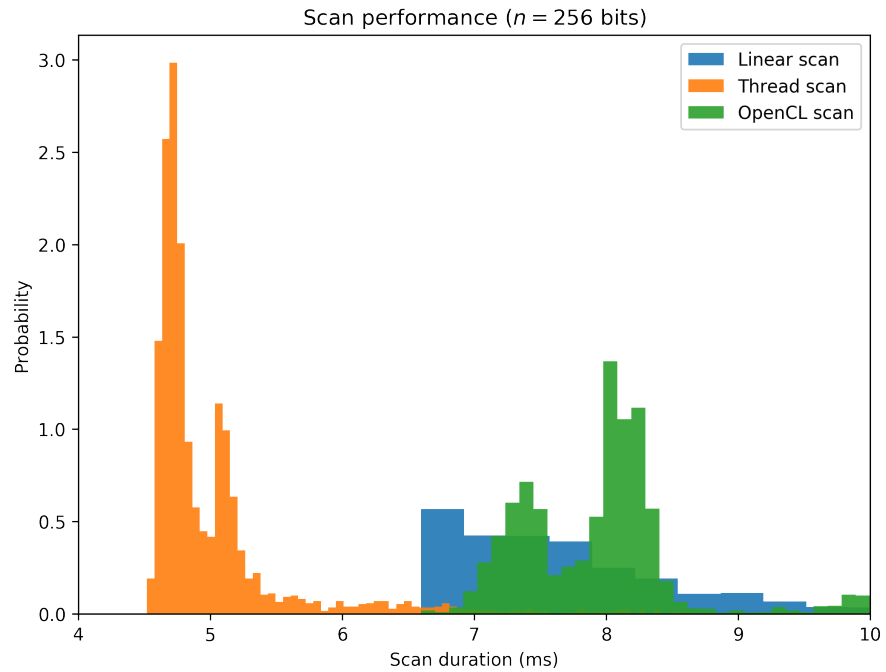
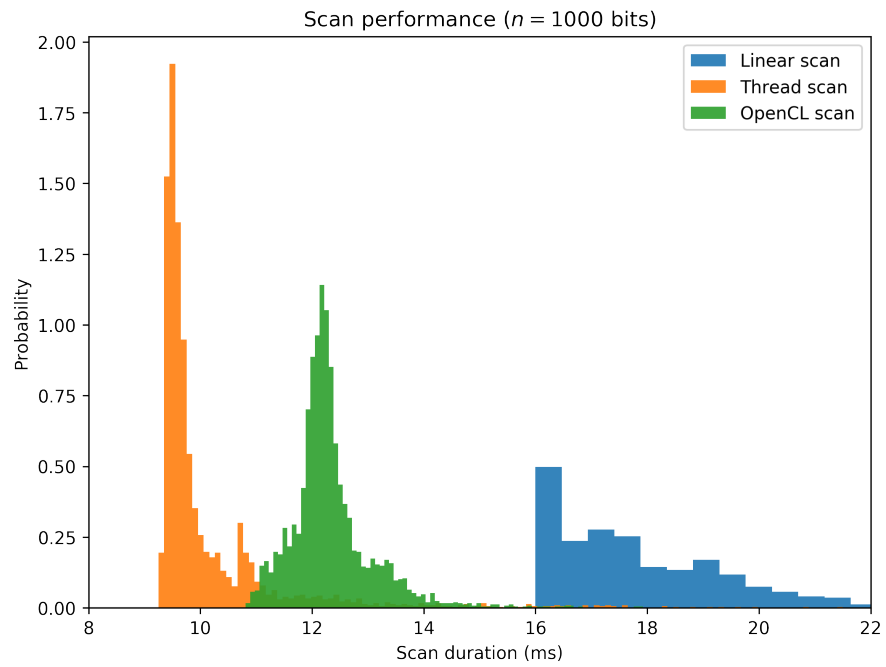
(a)  $n = 1,000$ ,  $r = 451$ , and  $H = 1,000,000$ (b)  $n = 1,000$ ,  $r = 451$ , and  $H = 1,000,000$ 

Figure 10: Scanner comparisons for MacBook Pro Retina 13-inch Late 2013 with a 2.6GHz Intel core i5 processor, 6GB DDR3 RAM, and Intel Iris GPU.

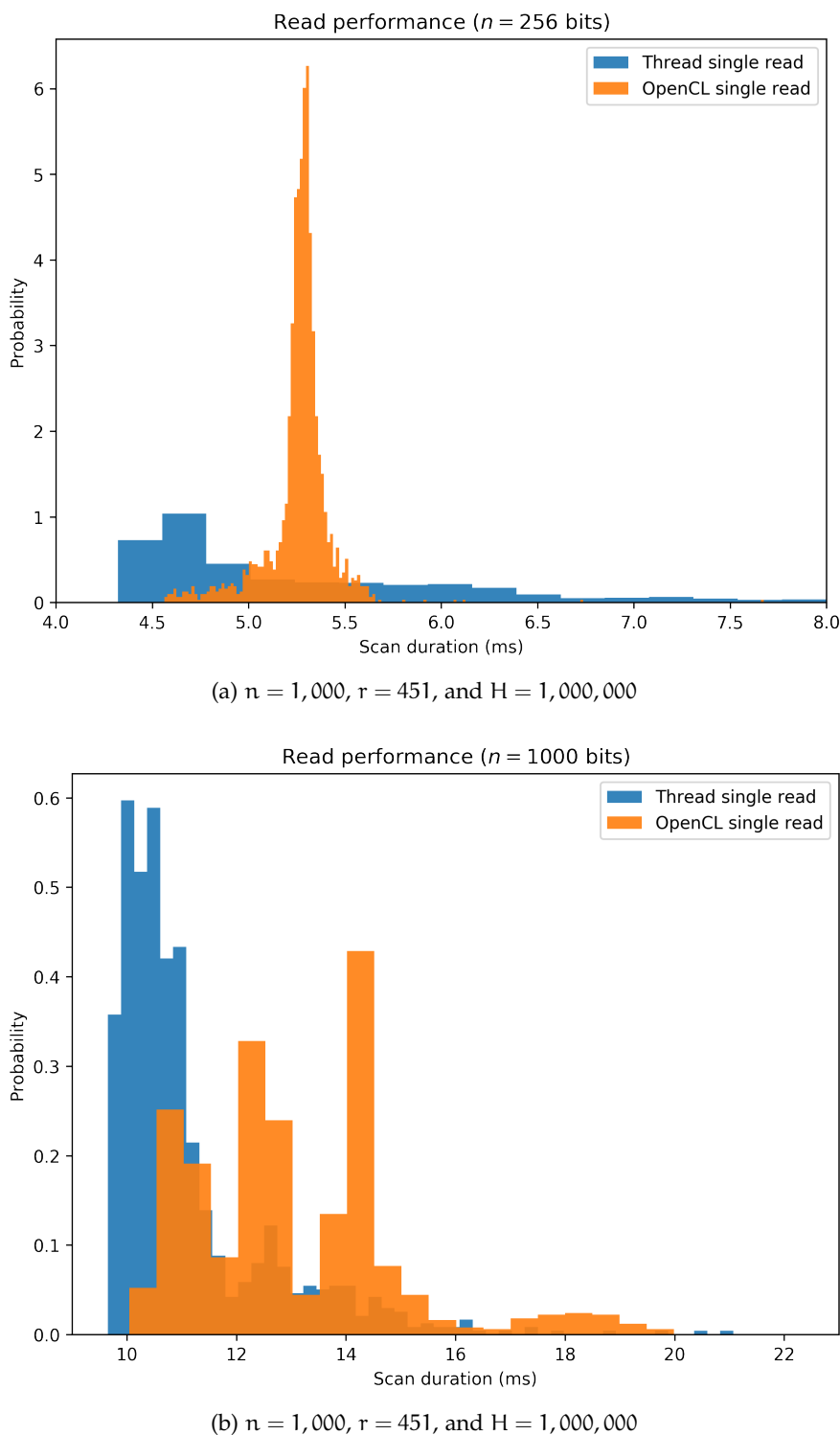


Figure 11: Read operation comparisons for MacBook Pro Retina 13-inch Late 2013 with a 2.6GHz Intel core i5 processor, 6GB DDR3 RAM, and Intel Iris GPU.

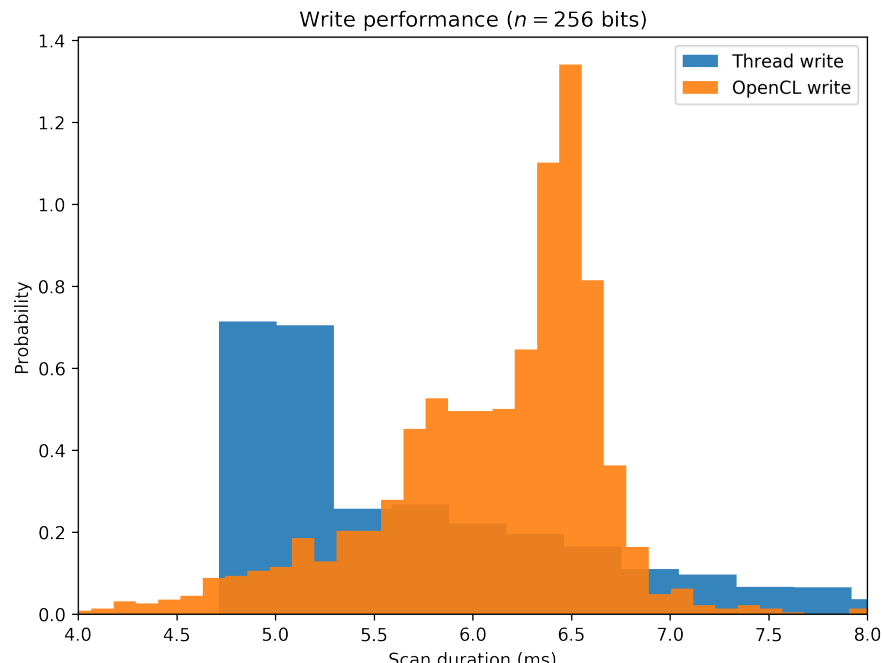
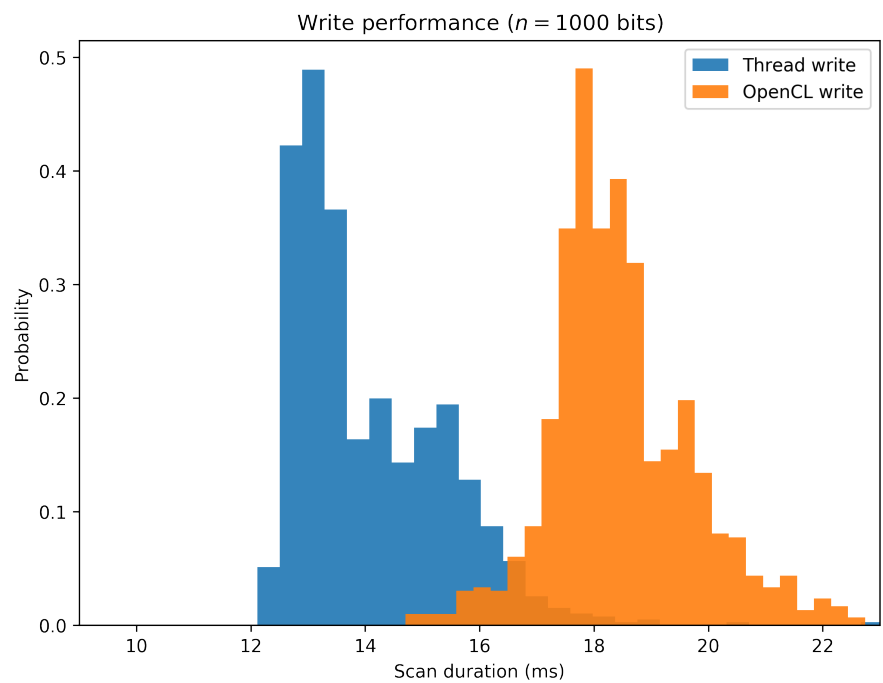
(a)  $n = 1,000$ ,  $r = 451$ , and  $H = 1,000,000$ (b)  $n = 1,000$ ,  $r = 451$ , and  $H = 1,000,000$ 

Figure 12: Write operation comparisons for MacBook Pro Retina 13-inch Late 2013 with a 2.6GHz Intel core i5 processor, 6GB DDR3 RAM, and Intel Iris GPU.

	<b>256 bits</b>	<b>1,000 bits</b>	<b>10,000 bits</b>
Kernel	Duration (ms)	Duration (ms)	Duration (ms)
single_scan0	3.03	5.00	61.06
single_scan1	2.87	3.95	44.96
single_scan2	3.82	4.57	44.98
single_scan3	3.72	3.68	12.67
single_scan4	4.48	4.04	11.45
single_scan5	3.76	3.72	12.58
single_scan5_unroll	3.79	3.61	11.37
single_scan6	4.36	4.02	10.96
Scanner	Duration (ms)	Duration (ms)	Duration (ms)
Linear scan	5.04	12.25	116.38
Thread scan	2.92	6.95	53.56
OpenCL scan	2.81	4.20	12.95
Operation	Duration (ms)	Duration (ms)	Duration (ms)
Thread write	3.28	13.34	
Thread single read	2.55	10.39	
OpenCL write	2.64	7.90	
OpenCL single read	2.14	5.25	

Table 4: iMac Retina 5K 27-inch 2017 with a 3.8GHz Intel core i5 processor, 8GB DDR4 RAM, and a Radeon Pro 580 8G GPU. The SDM settings were: (i)  $n = 256$ ,  $r = 103$ , and  $H = 1,000,000$ ; (ii)  $n = 1,000$ ,  $r = 451$ , and  $H = 1,000,000$ ; and (iii)  $n = 10,000$ ,  $r = 4850$ , and  $H = 1,000,000$ . There is no benchmark for read and write operations with  $n = 10,000$  because RAM is not enough to allocate the counters—it would consume 37.25 GB of RAM. For the histogram of durations, see Figures 13, 14, 15, and 16.

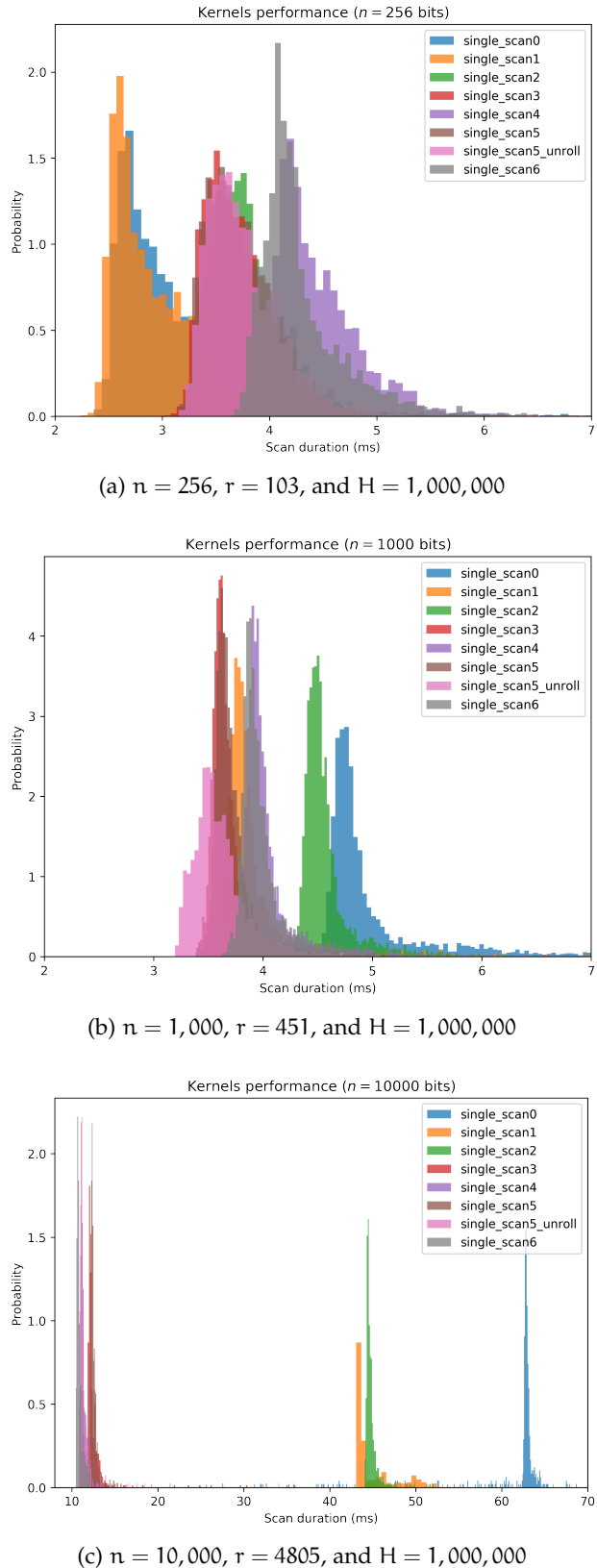


Figure 13: Kernel comparisons for iMac Retina 5K 27-inch 2017 with a 3.8GHz Intel core i5 processor, 8GB DDR4 RAM, and a Radeon Pro 580 8G GPU.

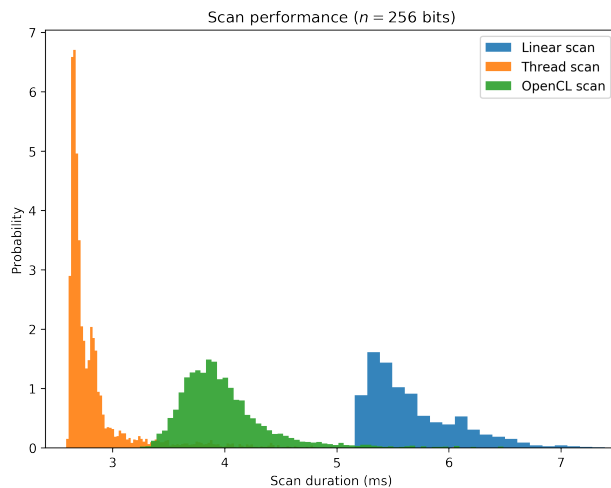
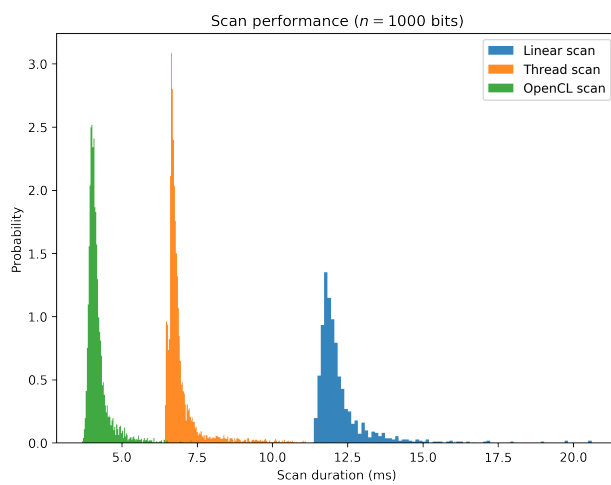
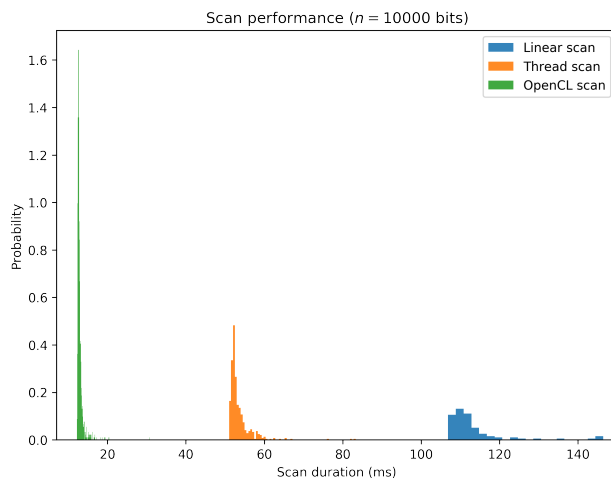
(a)  $n = 1,000$ ,  $r = 451$ , and  $H = 1,000,000$ (b)  $n = 1,000$ ,  $r = 451$ , and  $H = 1,000,000$ (c)  $n = 10,000$ ,  $r = 4805$ , and  $H = 1,000,000$ 

Figure 14: Scanner comparisons for iMac Retina 5K 27-inch 2017 with a 3.8GHz Intel core i5 processor, 8GB DDR4 RAM, and a Radeon Pro 580 8G GPU.

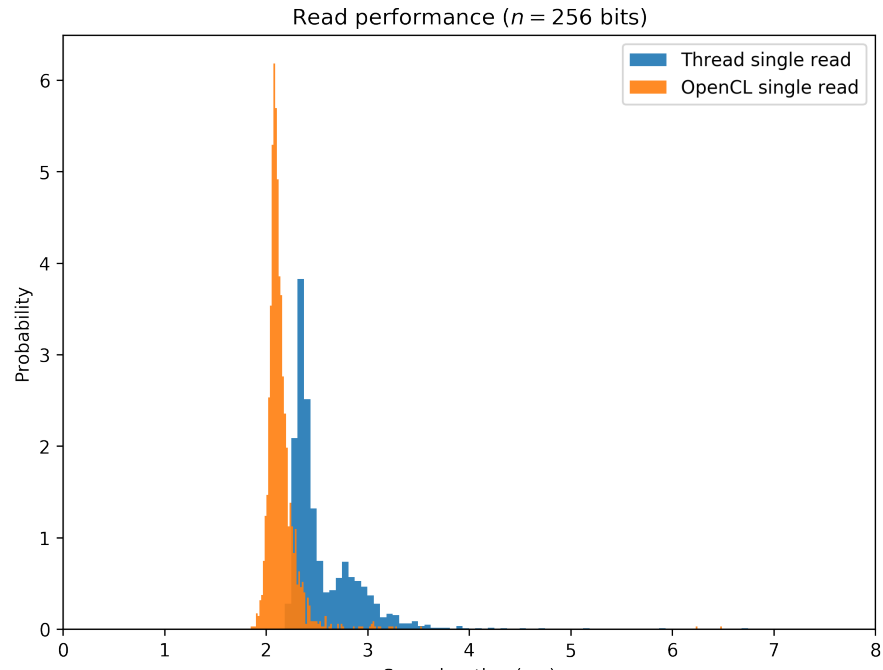
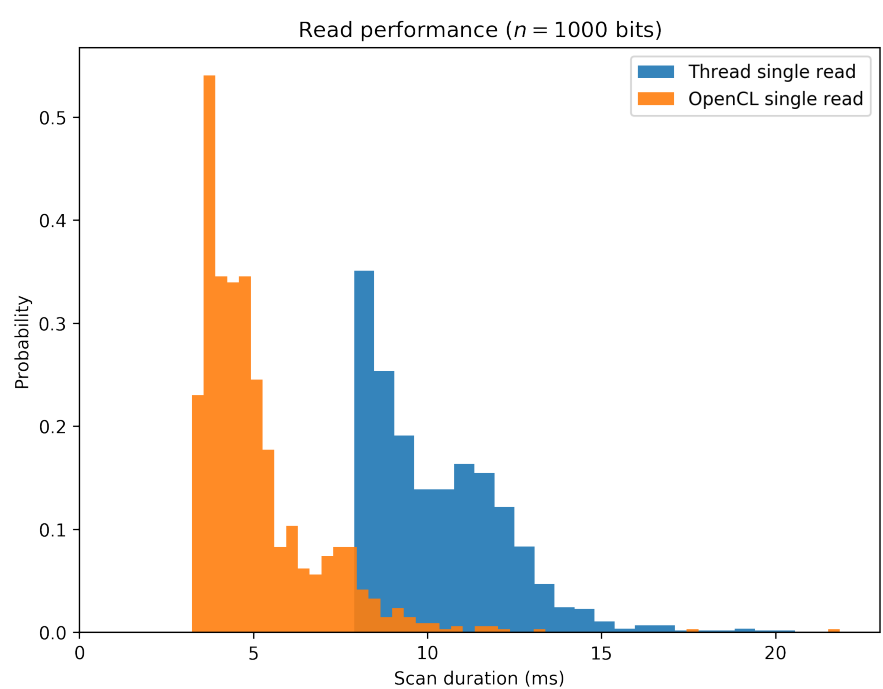
(a)  $n = 1,000$ ,  $r = 451$ , and  $H = 1,000,000$ (b)  $n = 1,000$ ,  $r = 451$ , and  $H = 1,000,000$ 

Figure 15: Read operation comparisons for iMac Retina 5K 27-inch 2017 with a 3.8GHz Intel core i5 processor, 8GB DDR4 RAM, and a Radeon Pro 580 8G GPU.

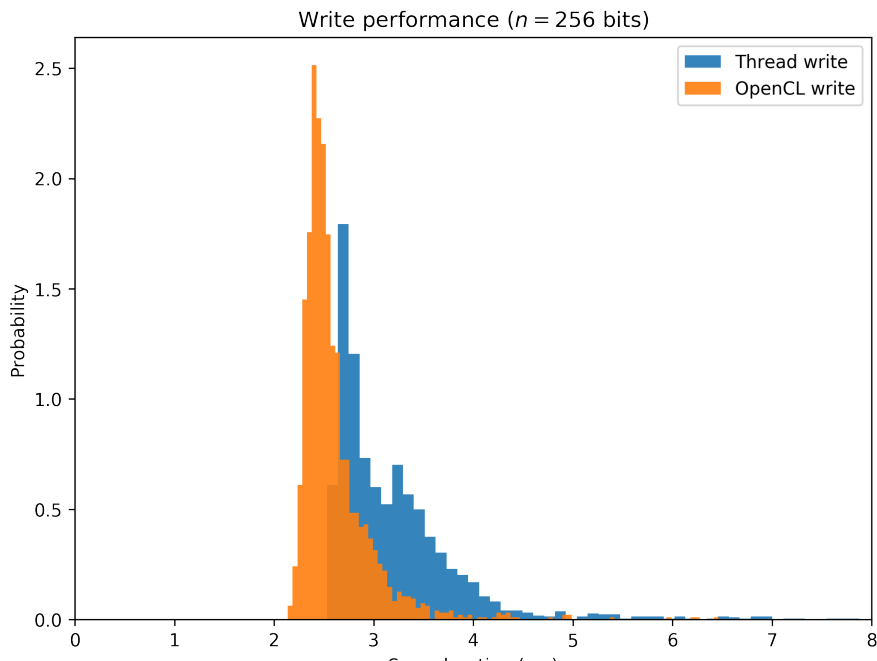
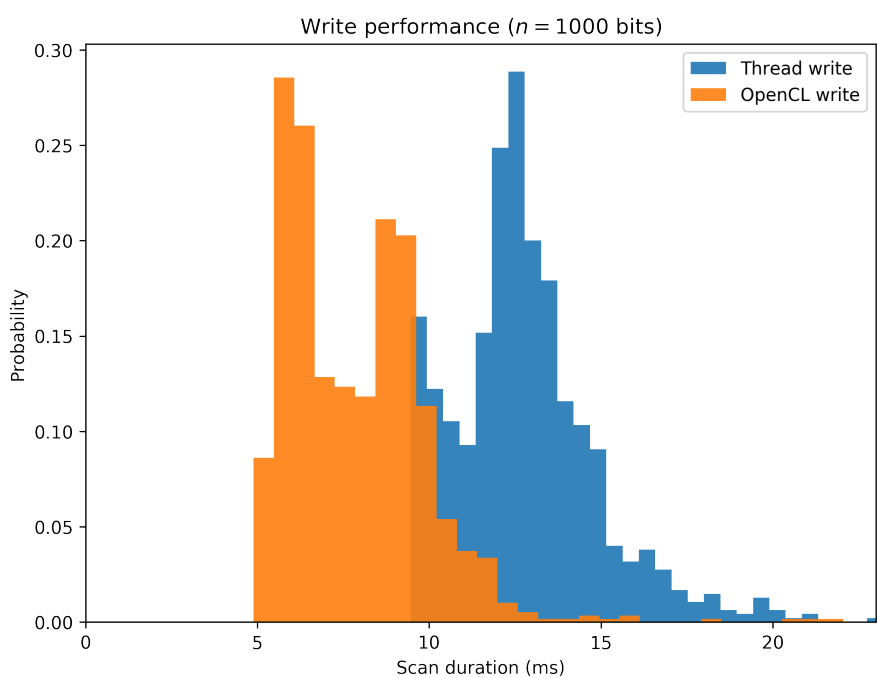
(a)  $n = 1,000$ ,  $r = 451$ , and  $H = 1,000,000$ (b)  $n = 1,000$ ,  $r = 451$ , and  $H = 1,000,000$ 

Figure 16: Write operation comparisons for iMac Retina 5K 27-inch 2017 with a 3.8GHz Intel core i5 processor, 8GB DDR4 RAM, and a Radeon Pro 580 8G GPU.

	<b>256 bits</b>	<b>1,000 bits</b>	<b>10,000 bits</b>
<b>Kernels</b>			
single_scano	0.76	3.79	35.45
single_scan1	0.80	3.94	57.80
single_scan2	5.59	8.54	63.71
single_scan3	6.31	9.73	39.92
single_scan4	10.29	11.38	45.49
single_scan5	6.69	9.95	43.51
single_scan5_unroll			
single_scan6	10.29	11.33	41.42
<b>Scanners</b>			
Linear scan	19.09	64.73	600.75
Thread scan	9.95	32.81	296.56
OpenCL scan	6.88	10.67	46.73
<b>Operations</b>			
Thread write	11.80	42.64	383.50
Thread single read	10.49	35.37	307.97
OpenCL write	8.84	19.31	122.17
OpenCL single read	7.50	11.72	55.47

Table 5: Amazon EC2 p2.xlarge with Intel Xeon E5-2686v4 processor, 61GB DDR3 RAM, and NVIDIA K80 GPU. Running an SDM with  $n = 256$  bits,  $H = 1,000,000$ , and  $r = 103$ . The SDM settings were: (i)  $n = 256$ ,  $r = 103$ , and  $H = 1,000,000$ ; (ii)  $n = 1,000$ ,  $r = 451$ , and  $H = 1,000,000$ ; and (iii)  $n = 10,000$ ,  $r = 4850$ , and  $H = 1,000,000$ . There is no benchmark for kernel `single_scan5_unroll` because it returns the wrong result in this GPU. The problem is related to the premises of the optimization used by this kernel, which are not true for this GPU. For the histogram of durations, see Figures 17, 14, 15, and 16.

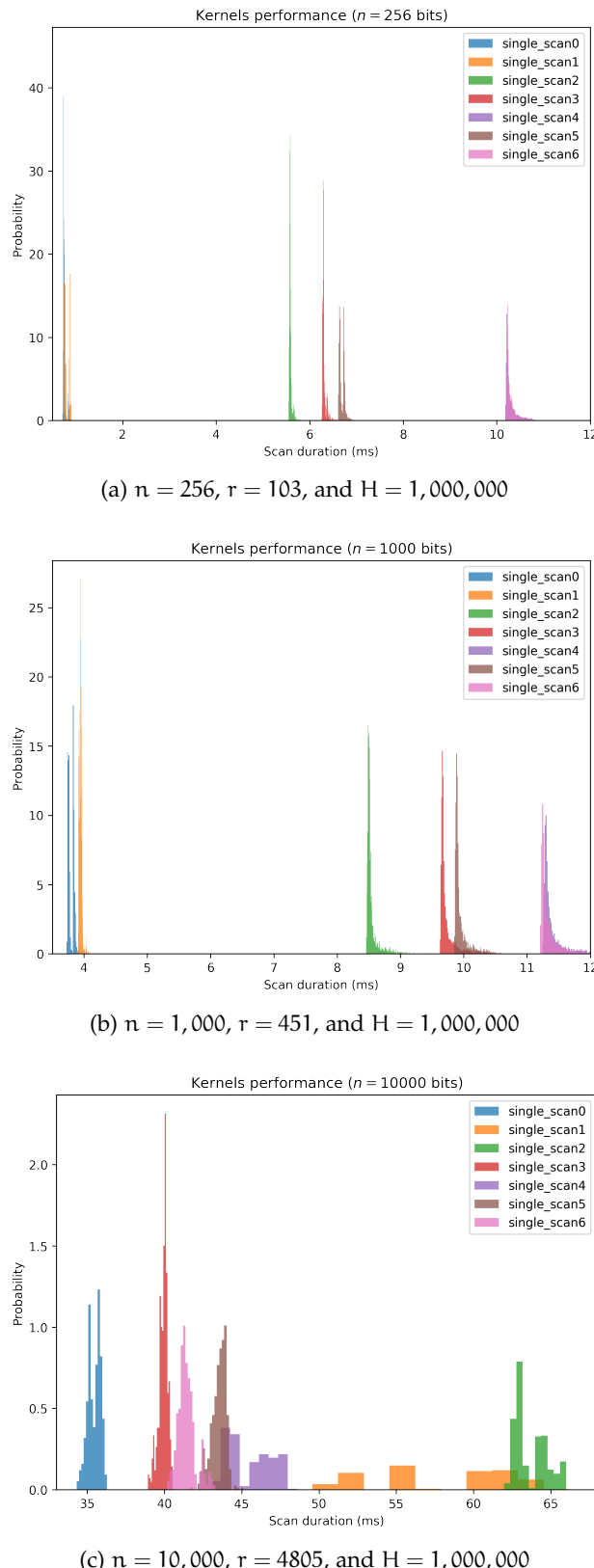


Figure 17: Kernel comparisons for Amazon EC2 p2.xlarge with Intel Xeon E5-2686v4 processor, 61GB DDR3 RAM, and NVIDIA K80 GPU.

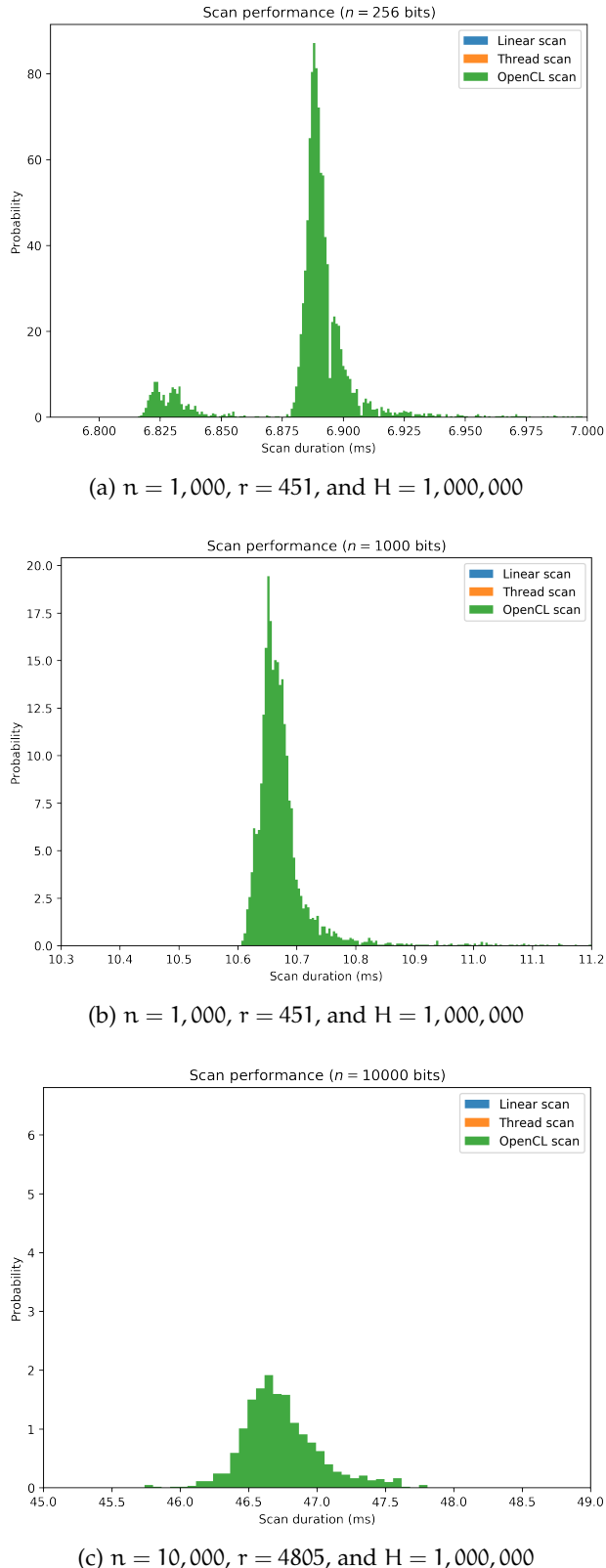


Figure 18: Scanner comparisons for Amazon EC2 p2.xlarge with Intel Xeon E5-2686v4 processor, 61GB DDR3 RAM, and NVIDIA K80 GPU.

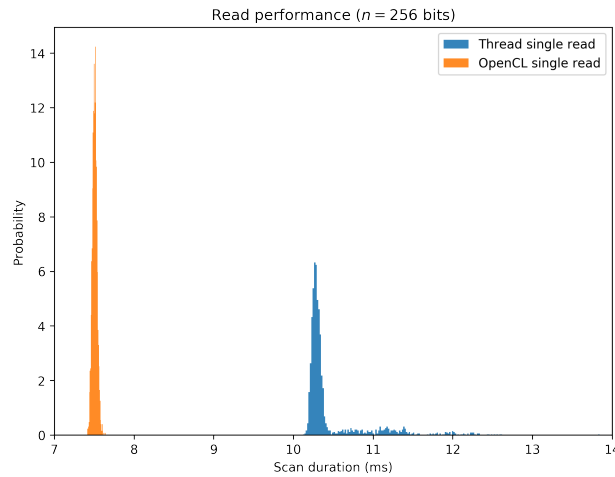
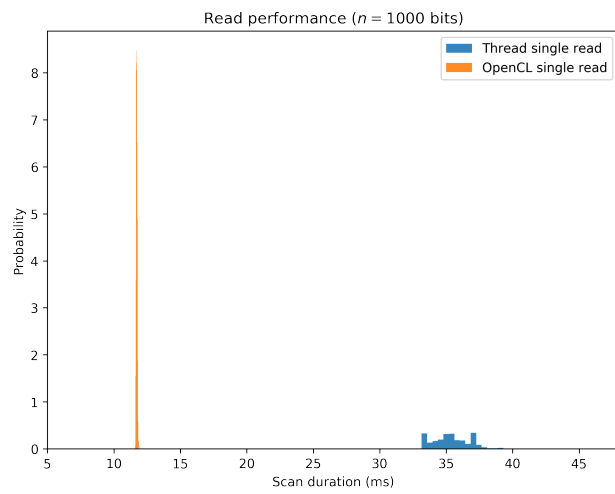
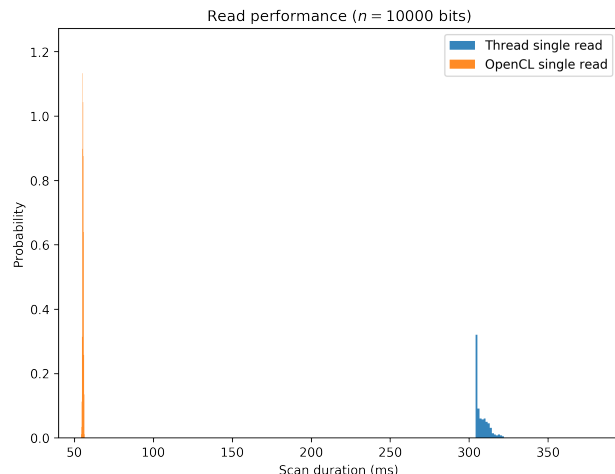
(a)  $n = 1,000$ ,  $r = 451$ , and  $H = 1,000,000$ (b)  $n = 1,000$ ,  $r = 451$ , and  $H = 1,000,000$ (c)  $n = 10,000$ ,  $r = 4805$ , and  $H = 1,000,000$ 

Figure 19: Read operation comparisons for Amazon EC2 p2.xlarge with Intel Xeon E5-2686v4 processor, 61GB DDR3 RAM, and NVIDIA K80 GPU.

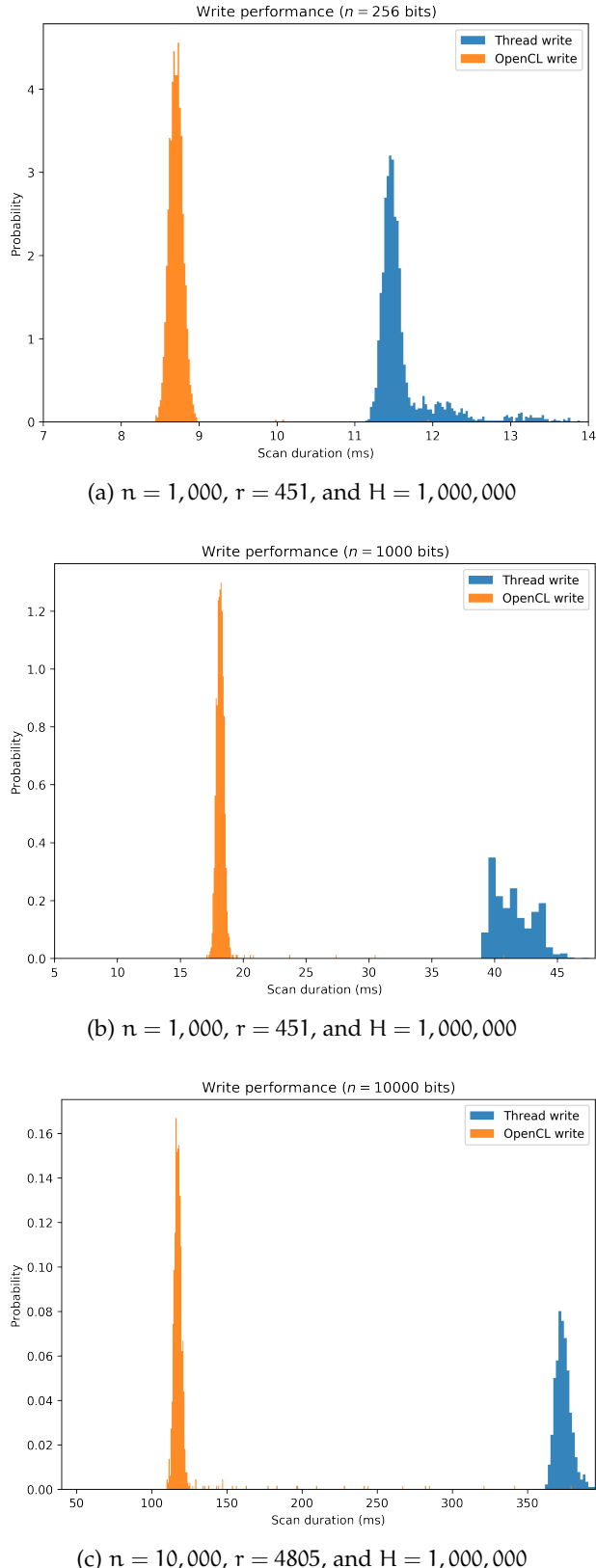


Figure 20: Write operation comparisons for Amazon EC2 p2.xlarge with Intel Xeon E5-2686v4 processor, 61GB DDR3 RAM, and NVIDIA K80 GPU.

	<b>256 bits</b>	<b>1,000 bits</b>	<b>10,000 bits</b>
Kernel	Duration (ms)	Duration (ms)	Duration (ms)
single_scano	0.36	0.69	20.60
single_scan1	0.36	0.54	4.94
single_scan2	0.73	0.85	5.01
single_scan3	0.63	1.02	6.07
single_scan4	1.05	1.10	5.99
single_scan5	0.62	0.95	5.36
single_scan5_unroll			
single_scan6	1.01	1.04	5.96
Scanner	Duration (ms)	Duration (ms)	Duration (ms)
Linear scan	17.60	58.34	540.97
Thread scan	5.19	16.39	198.74
OpenCL scan	0.63	0.85	5.74
Operation	Duration (ms)	Duration (ms)	Duration (ms)
Thread write	7.59	28.47	222.08
Thread single read	6.17	17.44	145.01
OpenCL write	2.33	8.77	80.48
OpenCL single read	1.01	1.82	13.99

Table 6: Amazon EC2 p3.2xlarge with Intel Xeon E5-2686v4 processor, 488GB DDR3 RAM, and NVIDIA Tesla V100 GPU. The SDM settings were: (i)  $n = 256$ ,  $r = 103$ , and  $H = 1,000,000$ ; (ii)  $n = 1,000$ ,  $r = 451$ , and  $H = 1,000,000$ ; and (iii)  $n = 10,000$ ,  $r = 4850$ , and  $H = 1,000,000$ . There is no benchmark for kernel `single_scan5_unroll` because it returns the wrong result in this GPU. The problem is related with the premises of the optimization used by this kernel, which are not true for this GPU. For the histogram of durations, see Figures 21, 22, 23, and 24.

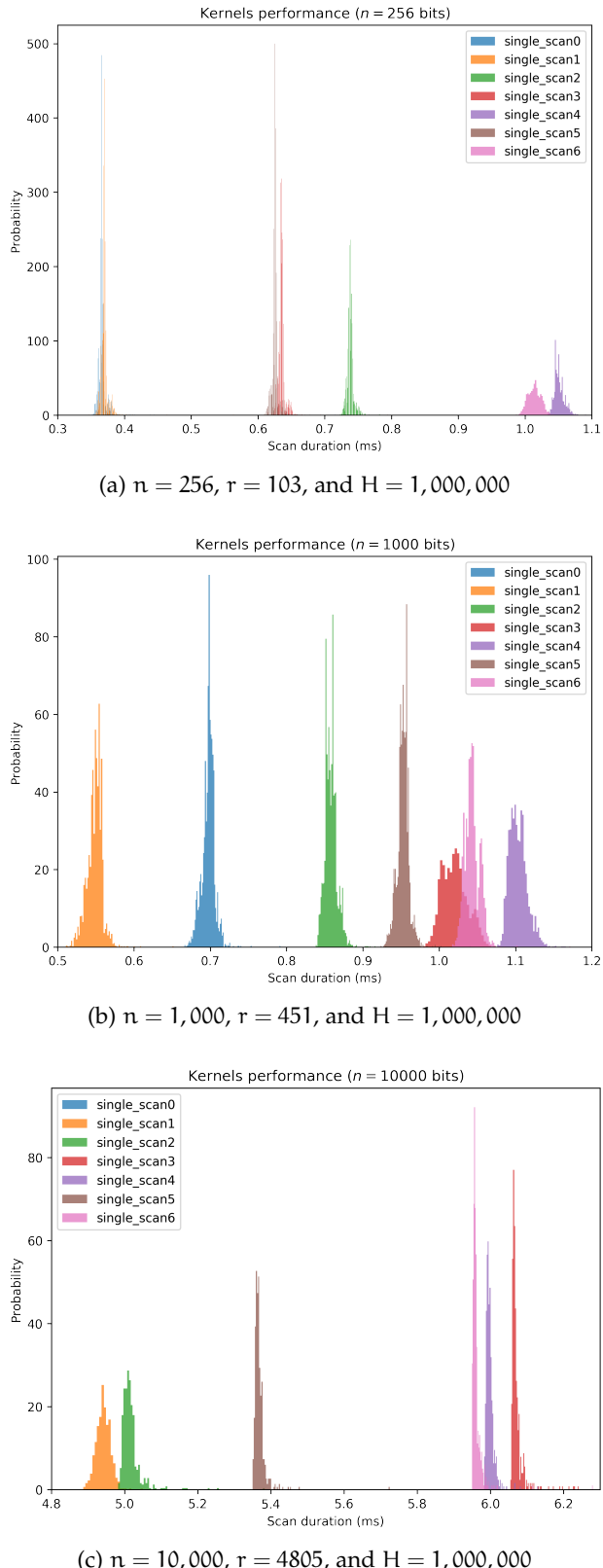


Figure 21: Kernel comparisons for Amazon EC2 p3.2xlarge with Intel Xeon E5-2686v4 processor, 488GB DDR3 RAM, and NVIDIA Tesla V100 GPU.

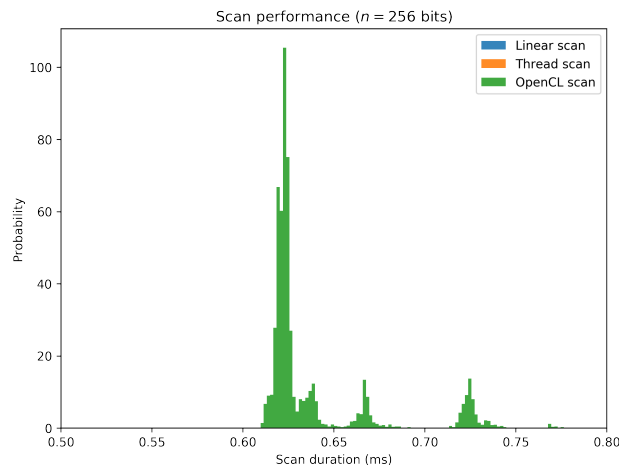
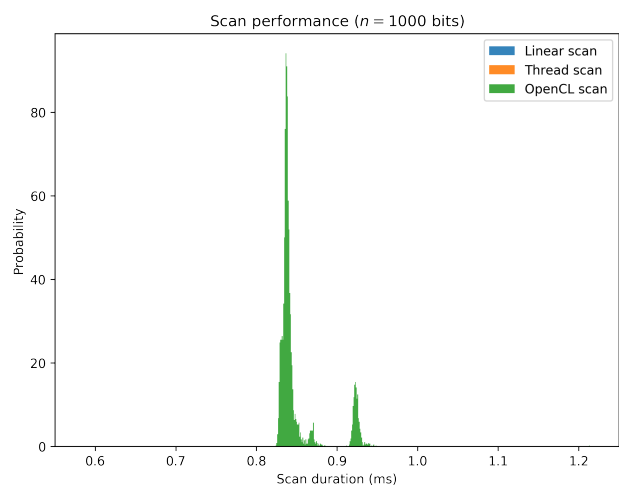
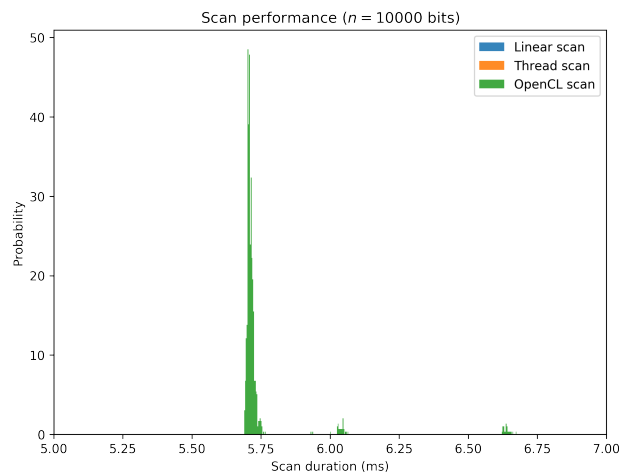
(a)  $n = 1,000$ ,  $r = 451$ , and  $H = 1,000,000$ (b)  $n = 1,000$ ,  $r = 451$ , and  $H = 1,000,000$ (c)  $n = 10,000$ ,  $r = 4805$ , and  $H = 1,000,000$ 

Figure 22: Scanner comparisons for Amazon EC2 p3.2xlarge with Intel Xeon E5-2686v4 processor, 488GB DDR3 RAM, and NVIDIA Tesla V100 GPU.

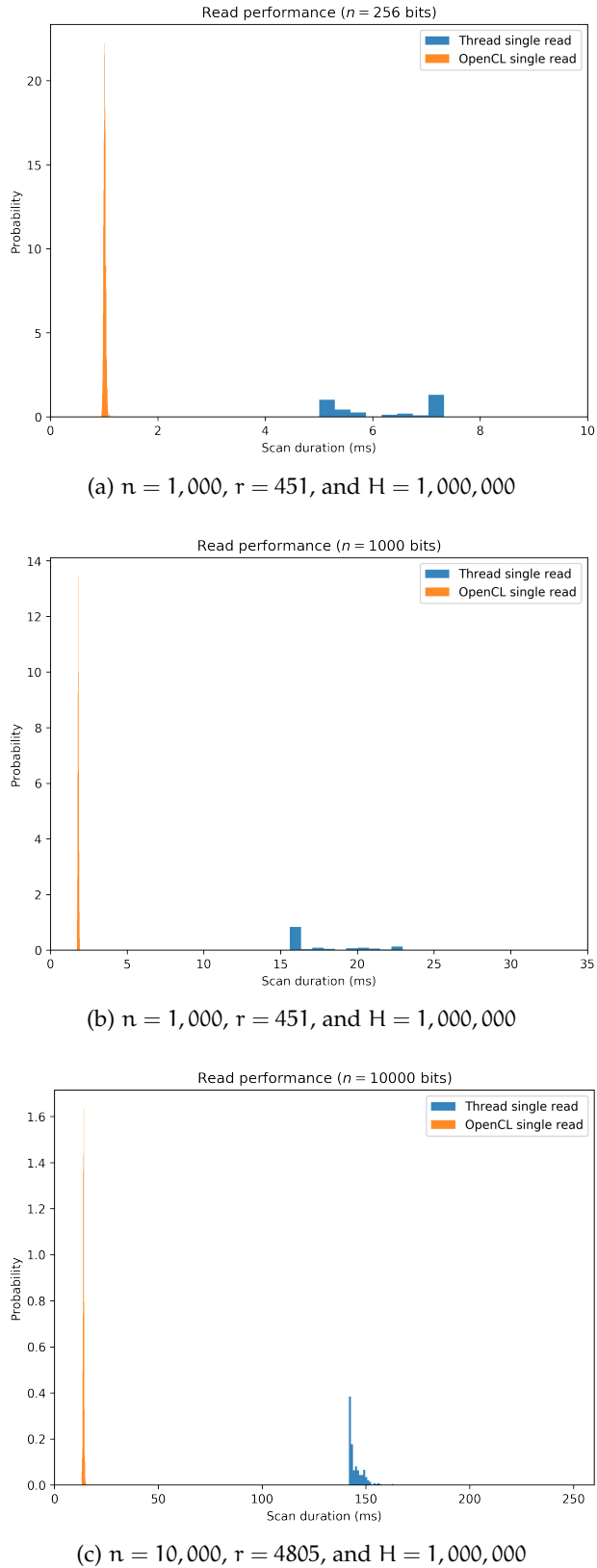


Figure 23: Read operation comparisons for Amazon EC2 p3.2xlarge with Intel Xeon E5-2686v4 processor, 488GB DDR3 RAM, and NVIDIA Tesla V100 GPU.

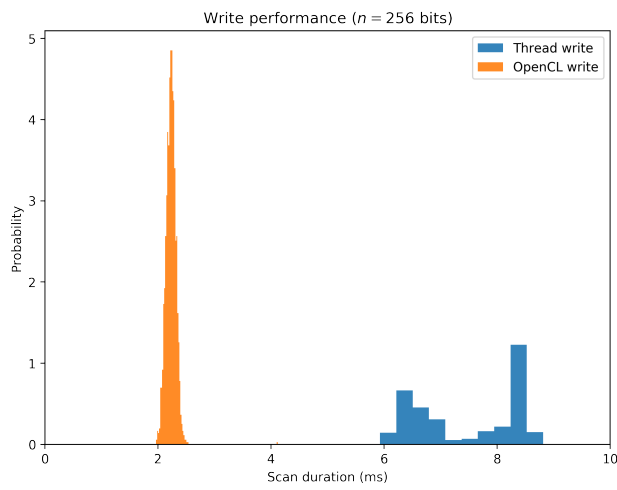
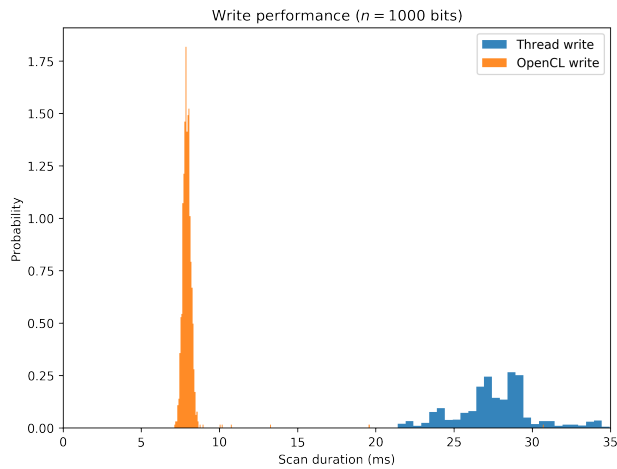
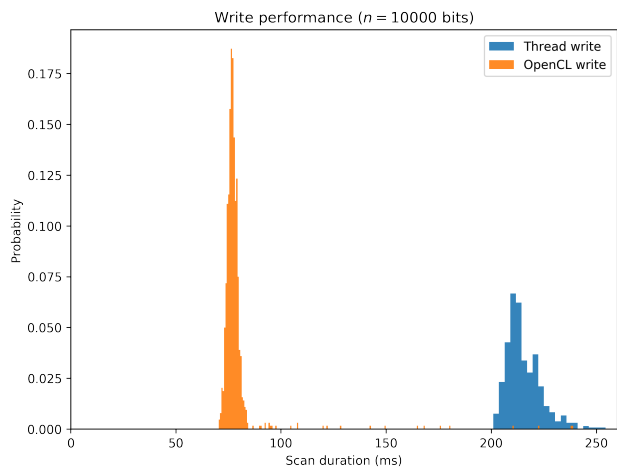
(a)  $n = 1,000$ ,  $r = 451$ , and  $H = 1,000,000$ (b)  $n = 1,000$ ,  $r = 451$ , and  $H = 1,000,000$ (c)  $n = 10,000$ ,  $r = 4805$ , and  $H = 1,000,000$ 

Figure 24: Write operation comparisons for Amazon EC2 p3.2xlarge with Intel Xeon E5-2686v4 processor, 488GB DDR3 RAM, and NVIDIA Tesla V100 GPU.



# 6

## RESULTS (II): FRAMEWORK VALIDATION

The framework has been validated comparing its results with the expected results from Kanerva [41]. Thus, we run simulations which were then compared to the theoretical analysis conducted some decades ago.

### 6.1 DISTANCE BETWEEN RANDOM BITSTRINGS

As shown by Kanerva [41], the distance between two bitstrings follows a binomial distribution with mean  $\mu = n/2$  and standard deviation  $\sigma = \sqrt{n}/2$ . For large values of  $n$ , it may be approximated by a normal distribution with the same mean and standard deviation.

In order to validate our random bitstring generation algorithm, we have calculated 10,000 distances between two random bitstrings with  $n = 1,000$  bits. In total, 20,000 random bitstrings have been generated during the simulation. The code is available in the “Distance between bitstrings” notebook [8].

In figure 25, we can notice that the theoretical model and the simulation results matches. Hence, it seems the random bitstring generation algorithm works appropriately.

This also validates the algorithm used to calculate the distance between two bitstrings. In this simulation, we have used the built-in `_popcnt()` function.

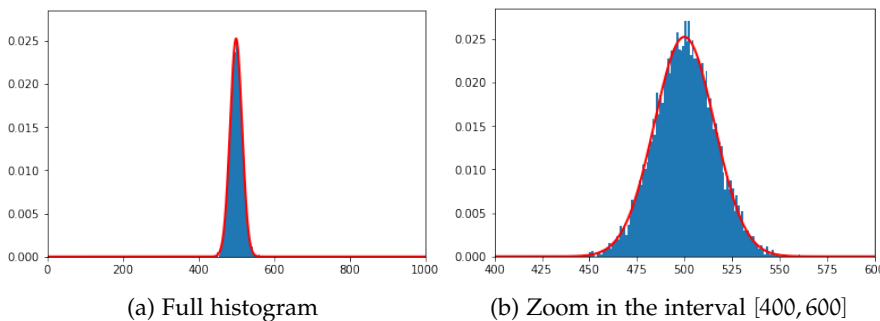


Figure 25: Histogram of 10,000 distances between two random bitstrings with 1,000 bits. The curve in red is the theoretical normal distribution with  $\mu = 500$  and  $\sigma = \sqrt{500}/2$ .

## 6.2 NUMBER OF ACTIVATED HARD LOCATIONS

In his seminal work, Kanerva proposed to use a sample of 1,000,000 hard locations in a 1,000 bits SDM. He also proposed to activate only 1,000 of them, on average. He calculated that an access radius of  $r = 451$  would activate, on average, 0.00107185004892 of the whole space, or, in this case, 1,071.85 hard locations.

We extended his results, calculating the distribution of the number of activated hard locations. As each hard location has probability  $p = 0.00107185004892$  of being activated, the probability of activating exactly  $a$  out of  $H$  hard locations follows a binomial distribution with mean  $\mu = pH$  and standard deviation  $\sigma = \sqrt{Hp(p-1)}$ . In this case,  $\mu = 1071.85$  and  $\sigma = 32.72$ .

In order to validate our scan algorithm, we have run 10,000 scans from a random bitstring and counted the number of activated hard locations. The code is available in the “Number of activated hard locations” notebook [8].

In figure 26, we can notice that the theoretical model and the simulation matches. Hence, it seems that both the address space generation algorithm and the scan algorithm work properly. Notice that the curve is almost the same for  $n = 1,000$  and  $n = 256$ . This difference happens because the access radius is adjusted to get  $p$  as close as possible to 0.001, which mean they are very close, but not the same.

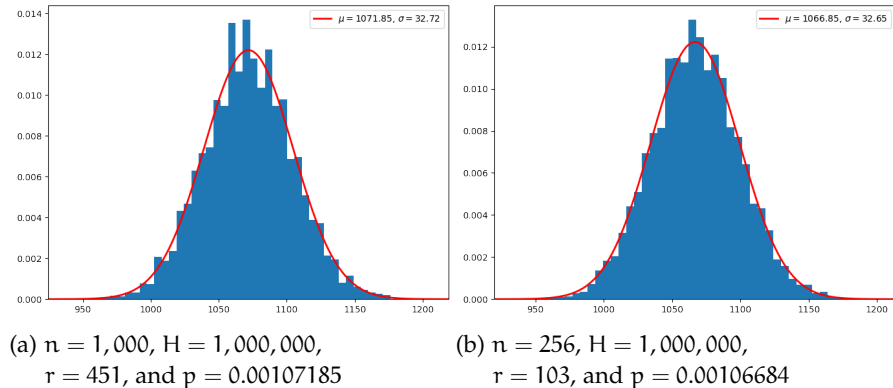


Figure 26: Histogram of the number of activated hard locations in 10,000 scans from a random bitstring. The curve in red is the theoretical normal distribution with  $\mu = Hp$  and  $\sigma = p(p-1)H$ .

Besides the number of activated hard locations, we have also extended Kanerva’s results to calculate the distribution of distances between the center of the circle and the activated hard locations. Let  $A$  be the set of activated hard locations,  $\xi$  be the center of the circle, and  $r$  be the access radius, then:

$$P(d(a, \xi) = x | a \in A) = \frac{P(d(a, \xi) = x)}{P(a \in A)} \quad (1)$$

$$= \frac{\binom{n}{x}}{\sum_{k=0}^r \binom{n}{k}} \quad (2)$$

In order to check Equation 2, we have calculated the distances of the activated hard locations to the center of 1,000 random circles. The code is available in the “Distances of activated hard locations” notebook [8].

In figure 27, we can notice that the theoretical model and the simulation matches.

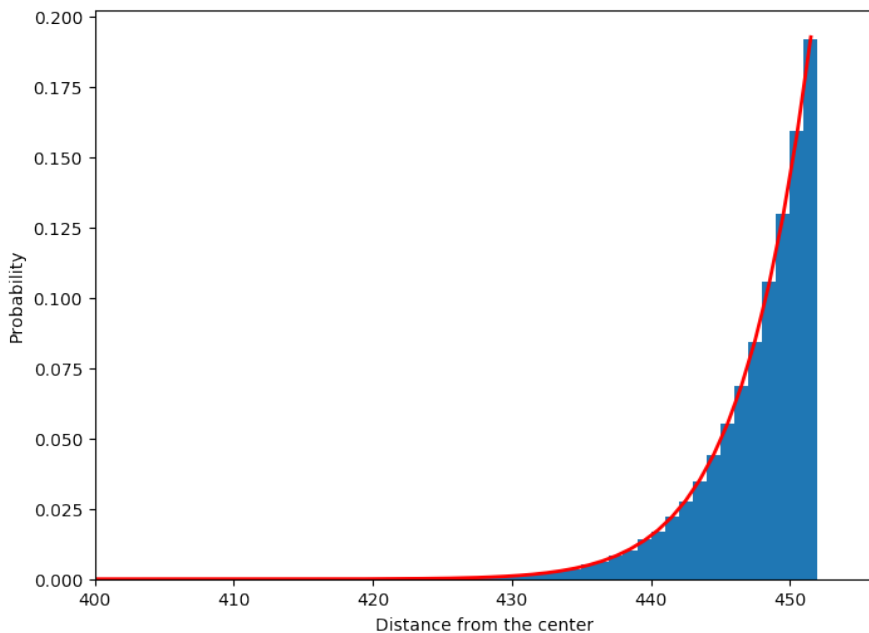


Figure 27: Histogram of the distances of activated hard locations to the center of the circles. The curve in red is the theoretical distribution of Equation 2

### 6.3 INTERSECTION OF TWO CIRCLES

Kanerva has calculated the intersection of two circles according to the distance between their centers. The intersection is important to understand how SDM works because it directly affects the critical distance. When  $\eta_d$  is inside the critical distance, then it will converge to  $\eta$ . In fact, it converges because they share a sufficient amount of hard locations, i.e., the intersection of the circle around  $\eta_d$  and  $\eta$  is enough to converge. For further information about the relation between the critical distance and the intersection, see Brogliato et al. [9].

We have calculated the intersection between a random bitstring ( $bs_1$ ) and another bitstring ( $bs_2$ ) exactly  $d$  bits away. The former ( $bs_1$ ) is just a random bitstring. The latter ( $bs_2$ ) was generated randomly flipping  $d$  bits of  $bs_1$ . The code is available in the “Kanerva’s Figure 1.2” notebook [8].

In Figure 28, we can notice that we have obtained the same results as Kanerva. It seems that the random flipping bits algorithm and the scan algorithm work properly.

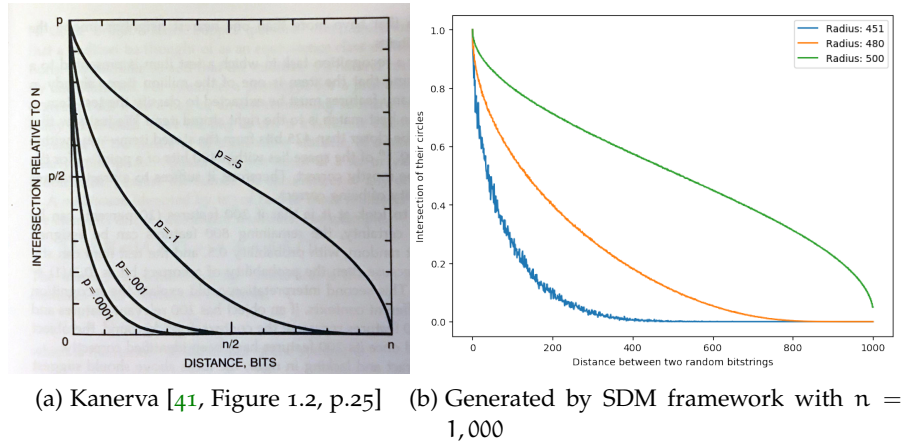


Figure 28: Number of hard locations in the intersection of circles around two bitstrings  $x$  bits away.

#### 6.4 STORAGE AND RETRIEVAL OF SEQUENCES

Kanerva [41, Ch.8] presented an approach to store and retrieve sequences using  $k$  different SDMs, namely  $sdm_1, sdm_2, \dots, sdm_k$ .

Let  $a_0, a_1, a_2, \dots, a_n$  be a sequence to be stored in a  $k$ -fold memory. So, all pointers of the form  $a_i \rightarrow a_{i+k}$  will be written to  $sdm_k$  memory, i.e., in  $sdm_1$ , the following pointers will be written:  $a_0 \rightarrow a_1, a_1 \rightarrow a_2, \dots, a_{n-1} \rightarrow a_n$ ; while in  $sdm_2$ , the following pointers will be written:  $a_0 \rightarrow a_2, a_2 \rightarrow a_3, \dots, a_{n-2} \rightarrow a_n$ ; and so forth.

We have tested the same example presented in Kanerva [41], p.85. We wrote two sequences to a 3-fold memory:  $\langle A, B, C, D \rangle$  and  $\langle E, B, C, F \rangle$ . Then, after reading the sequences  $\langle A, B, C \rangle$  and  $\langle E, B, C \rangle$ , we have obtained  $D$  and  $F$ , respectively.

Each reading operation was performed summing the counters of all activated hard locations from all three memories. For instance, to read the sequence  $\langle A, B, C \rangle$ , we have activated the hard locations around  $C$  in  $sdm_1$ , we have also activated the hard locations around  $D$  in  $sdm_2$ , and, finally, we have also activated the hard locations around  $A$  in  $sdm_3$ . After summing the counters of all those hard locations, we evaluate the resulting bitstring just as in the original read operation.

The code is available in the “Sequences (Kanerva Ch 8)” notebook [8].

The logic behind how it works is that, when reading the sequence  $\langle A, B, C \rangle$ , we have A pointing to D, while both B and C point to D and F. Thus, D appeared more often than F and ended up being the result.

Hence, as we have replicated the theoretical results from Kanerva, we have one more evidence that our framework works appropriately.

#### 6.4.1 *k-fold memory using only one SDM*

We have extended Kanerva’s ideas to be able to store and retrieve sequences in k-fold memories using only one SDM (instead of k SDMs).

Our idea was to create k random bitstrings, one for each fold. We have performed writing and reading exactly as Kanerva’s original idea, but, instead of writing to  $sdm_k$ , we have written  $a_{i+k}$  into the address  $a_i \oplus tag_k$ , and, instead of reading from  $sdm_k$ , we have read from address  $a_i \oplus tag_k$ , where  $\oplus$  is the exclusive or (XOR) operator.

It worked as if we had split SDM into k regions with low intersection between two of them. So, as the interference is minimal, they work like independent SDMs. The major disadvantage of this approach is that memory capacity may be reached faster.

Splitting the memory into regions may be an interesting strategy to other sorts of problems, mostly the ones which would need many SDMs and, consequently, would use a lot of RAM.



# 7

## RESULTS (III): LOSS OF NEURONS

---

In SDM, the data is written distributed among millions of hard locations, which theoretically gives SDM robustness against loss of neurons. In other words, SDM should keep converging correctly even when some neurons are dead. The question is: how robust it really is? How many neurons may die before it starts to forget things? These questions have never been addressed before.

Looking for answers to these questions, we run simulations in which we kept killing some neurons and checking whether SDM remained converging to a given bitstring or not. In these simulations, 10,000 random bitstrings were written to a 1,000-bit SDM with 1,000,000 hard locations, and we choose one of them as our target. As the bitstrings were all written exactly once, we may generalize the results. The code is available in the “Resetting hard locations” notebook [8].

As neurons are hard locations in SDM, when we say that a neuron has been killed, we mean that its counters have been zeroed and a new random bitstring address has been assigned. During our simulations, no other bitstring has been written after the 10,000. Consequently, as their counters will remain zero, it is exactly like ignoring the dead hard locations in the subsequent reading operations.

In Figure 29, we can notice that SDM is robust up to 200,000 neuron deaths which are 20% of all hard locations. Its robustness is astonishing. In fact, SDM begins to be significantly affected by the loss of neurons after 600,000 neuron deaths (Figure 30) and obviously forgets everything when all neurons are dead.

It is interesting that 500,000 neuron deaths have a minor effect on SDM’s recall capability (see Figure 31). It is analogous to do a hemispherectomy in a person and, after the procedure, the person being able to recall and learn almost just like before. In fact, there are clinical reports of children submitted to hemispherectomy who live an almost normal life with minor function problems.

An important observation is that around 800,000 neuron deaths (80% of all neurons) the critical distance becomes small, i.e., SDM recall capacity is hugely diminished. After 900,000 neuron deaths, the critical distance is zero, and everything has been lost.

Although there is some decrease in SDM recall after 600,000 neuron deaths, it is curious that there is a sudden change between 900,000 (90%) and 1,000,000 (100%). In Figure 32 we can see the details of this

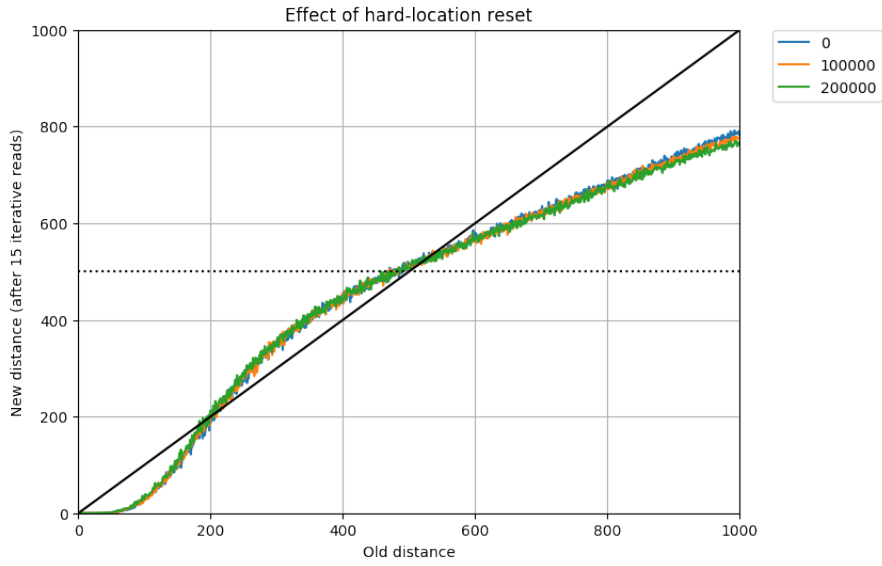


Figure 29: This graph shows the SDM's robustness against loss of neurons in a SDM with  $n = 1,000$  and  $H = 1,000,000$ . It shows that a loss of 200,000 neurons, 20% of the total, does not seem to affect SDM whatsoever.

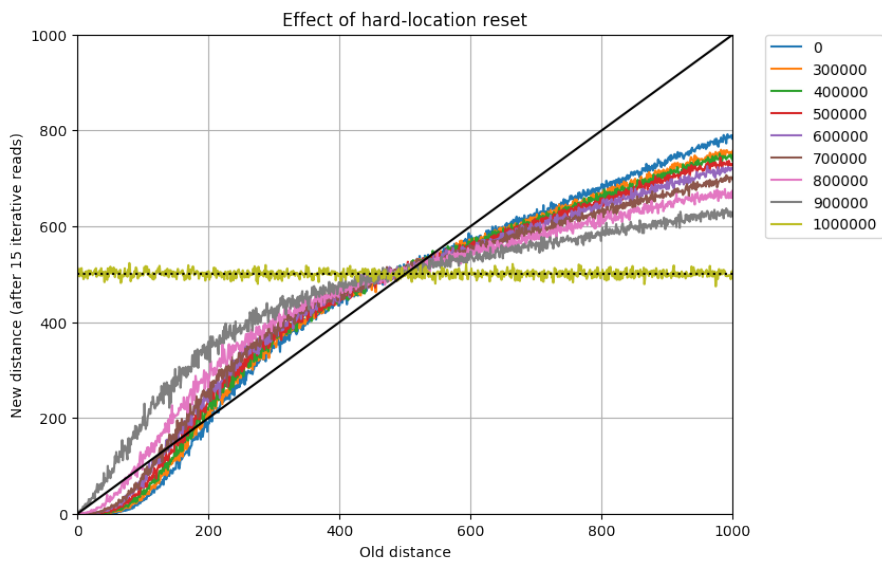


Figure 30: This graph shows the SDM's robustness against loss of neurons in a SDM with  $n = 1,000$  and  $H = 1,000,000$ . The more neurons are lost, the smaller the critical distance, i.e., the worse the SDM recall.

non-linear change. Notice that after 950,000 even the exact clue  $\eta_0$  does not converge to  $\eta$ .

We run the same simulation for a 256-bit SDM with 1,000,000 hard locations. The results were even more surprising, as the 256-bit SDM seems to be more robust to loss of neurons than the 1,000-bit SDM (see Figure 33). Notice that the loss of 50% of neurons barely affected the 256-bit SDM... and it even remained functional when facing an enormous loss of 90% of neurons! What these results seem to imply is not only that the memory is extremely robust, but that a very small expected number of neurons activated in each access radius would preserve the most valueable information. This may have implications as to the number of standard deviations to define the access radius, as we will discuss in Section 14.2. Is there a thing such as excessive robustness, and, if so, when does robustness become waste?<sup>1</sup>

---

<sup>1</sup> Consider, for instance, error-correcting codes in Information Theory or the analogous computer ECC memory in Electrical Engineering: tradeoffs between robustness and waste must be considered at each design decision; Why should it be different in the modeling of human memory?

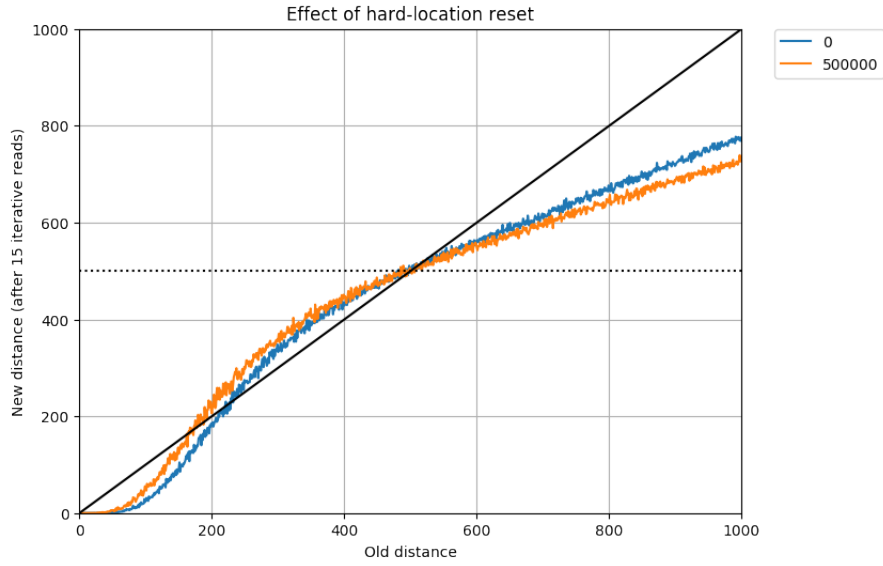


Figure 31: This graph shows the SDM's robustness against loss of neurons in a SDM with  $n = 1,000$  and  $H = 1,000,000$ . Even when 50% of neurons are dead, SDM recall is barely affected, which is an impressive result and matches with some clinical results of children submitted to hemispherectomy.

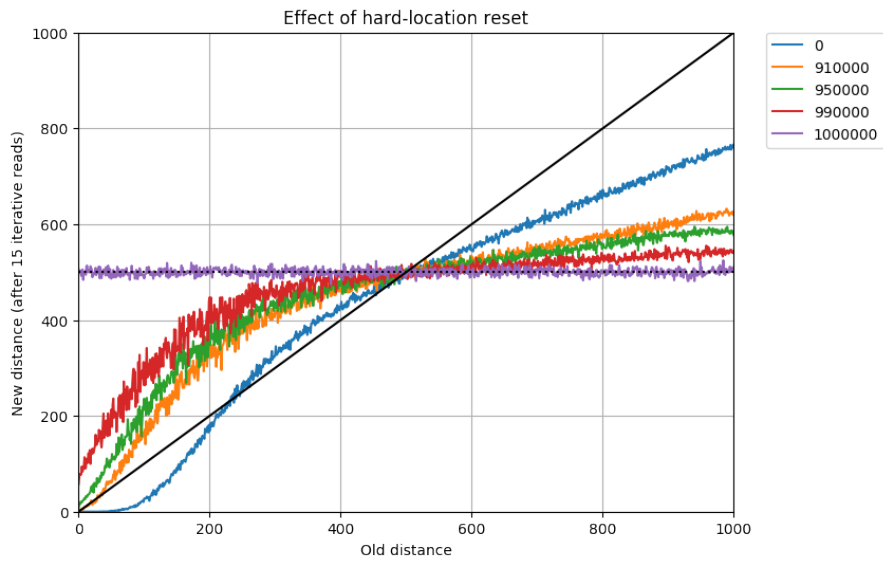


Figure 32: This graph shows the SDM's robustness against loss of neurons in a SDM with  $n = 1,000$  and  $H = 1,000,000$ .

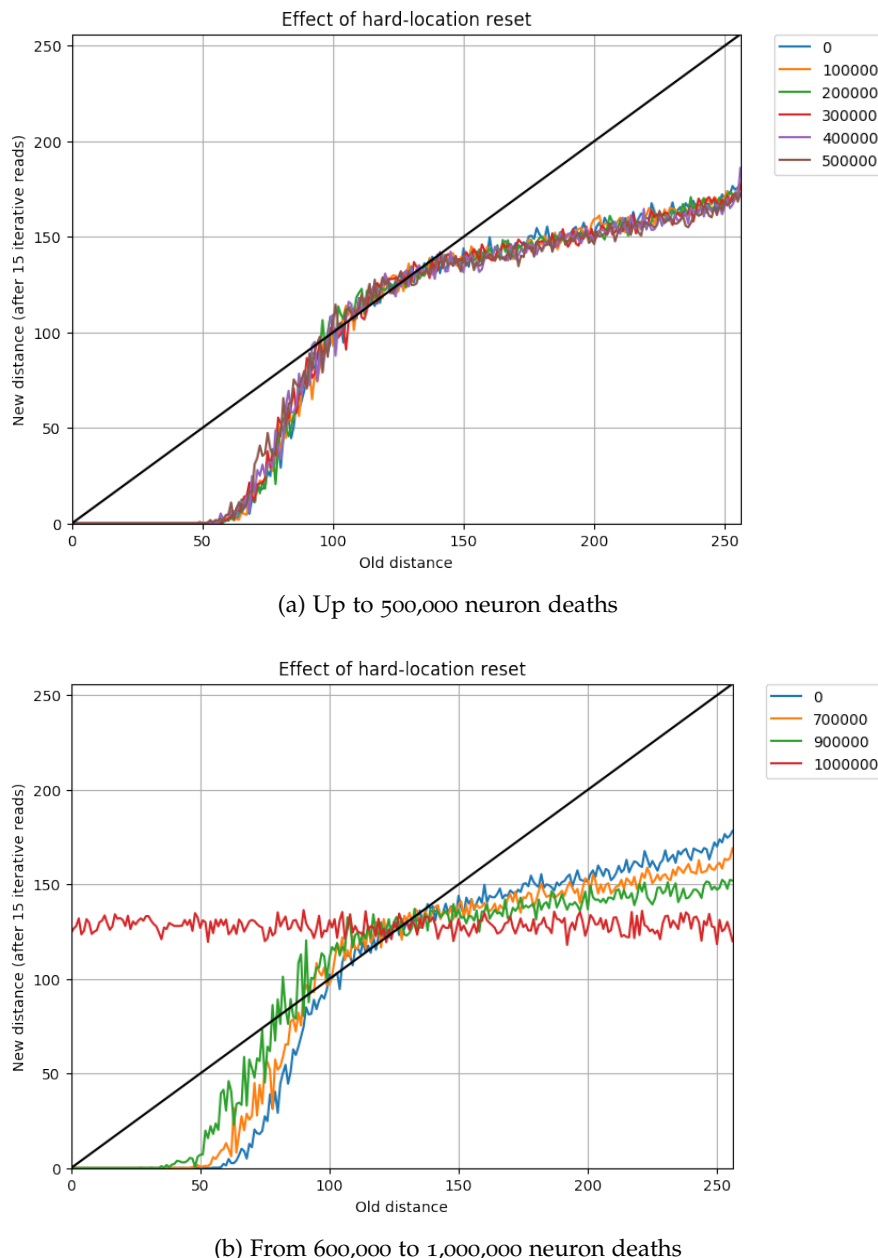


Figure 33: This graph shows the SDM's robustness against loss of neurons in a SDM with  $n = 256$  and  $H = 1,000,000$ .



# 8

## RESULTS (IV): CRITICAL DISTANCE

One particular analysis of Kanerva's interest is given by the limits of recovery. That is, given an item read at a distance  $x$  from a previously stored  $\eta$ , does this reading at a  $\eta_x$  recover the original? Suppose an SDM is trying to read an item written at  $\eta$ , but the cues received so far lead to a point of distance  $x$  from  $\eta$ . As one reads at  $\eta_x$ , a new bitstring  $\beta$  is obtained, leading to Kanerva's question: what is the new distance from  $\eta$  to  $\beta$ ? Is it smaller or larger than  $x$ ? That, of course, depends on the ratio between  $x$  and the number of dimensions of the memory.

Kanerva [41, p.70] originally predicted a ~500-bit distance after a point (Figure 34). The original prediction considered that the read distance would decline when inside the critical distance and increase afterward, converging to a ~500-bit distance. At this point, each read would lead to a different, orthogonal, ~500-bit distance bitstring. He analyzed specifically an SDM with 1,000 bits and 10,000 random bitstrings written into it.

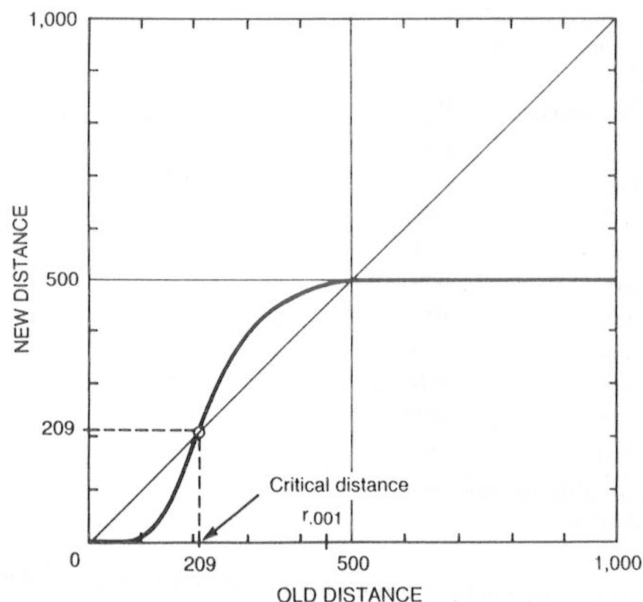


Figure 7.3  
New distance to target as a function of old distance.

Figure 34: Kanerva's original Figure 7.3 (p. 70) predicting a ~500-bit distance after a point.

As we ran the simulations, this one, in particular, struck our attention: The new distances obtained after a read operation were not perfectly predicted by the theoretical model. We have strictly followed Kanerva's configuration and, even so, we have found out some deviations from Kanerva's original theoretical analysis and the results obtained by simulation.

In details, we have created a SDM with  $n = 1,000$ ,  $H = 1,000,000$ , and  $r = 451$ . Then, we have generated 10,000 random bitstrings and written them into the memory. Then, we have generated a reference bitstring (`bs_ref`) and written it into the memory. Then, we have executed the following steps with  $x$  from 0 to 1,000: (i) copy `bs_ref` into a new bitstring; (ii) randomly flipped  $x$  bits of the copy; (iii) read from the memory in the copy address; and (iv) stored the distance between the returned bitstring and `bs_ref`. Finally, we have plotted Figure 35.

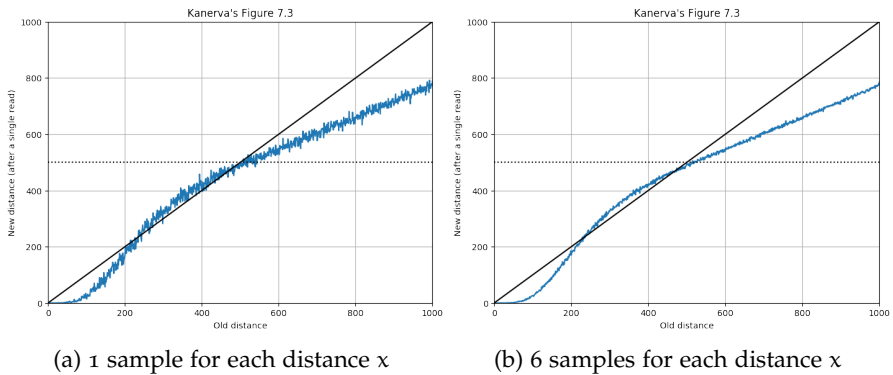


Figure 35: Results generated by the framework diverging from Kanerva's original Figure 7.3. Here we had a 1,000 bit, 1,000,000 hard location SDM with 10,000 random bitstrings written into it, which was also Kanerva's configuration.

Figure 35a has a lot of noise because we have read only once for each distance  $x$  and Kanerva has predicted the average distance. So, we have changed the steps to run  $k$  reads and store the average new distance. We run with  $k = 6$ , and the results can be seen in Figure 35b, which has much lower noise and still holds the divergence.

Our results show that the theoretical prediction is not accurate. There are interaction effects from one or more of the attractors created by the 10,000 writes, and these attractors seem to raise the distance beyond  $\sim 500$  bits (Figure 35).

Obviously, these small deviations from Kanerva's original theoretical predictions deserve a qualification. Kanerva was working in the 1980s and the 1990s, and had no access to the immense computational power that we do today. It is no surprise that some small interaction effects should exist as machines allow us to explore the ideas of his monumental work.

However, when we reduced the number of random bitstrings written in the SDM from 10,000 to only 100, the results reflected very well the Kanerva's theoretical expectation (Figure 36a). This result strengthens our hypothesis that the disparities in the computational outcomes are due to the interaction effect of high numbers of different attractors. In Figure 36b we can notice that the more random bitstrings are written, the stronger the attractors.

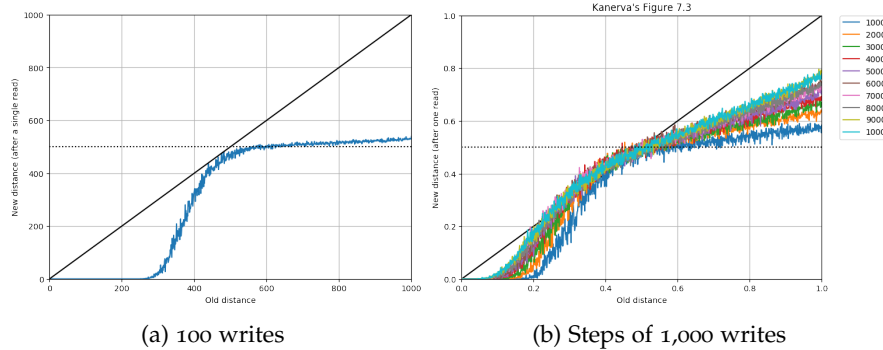


Figure 36: Results generated by the framework similar to Kanerva's original Figure 7.3. Here we have a 1,000 bit, 1,000,000 hard location SDM with (a) just 100 random bitstrings written into it and (b) steps of 1,000 random bitstrings written into it.

To obtain the results from Figures 35 and 36, we had to write 10,000 random bitstrings to an SDM, and then randomly choose one of those bitstrings to be our origin. Finally, we randomly flipped some bits from the origin bitstring and executed a reading operation in the SDM. Thereby, in order to show the interaction effects more clearly, we changed the single read for a 15-iterative read. As we can see in Figure 37, after a distance of 500 bits, all bitstrings converged to 500-bit distance bitstrings, just as described by Kanerva.

Hence, our understanding is that the attractors are just preventing the bitstrings to converge directly to 500-bit distance bitstrings, requiring more reading steps to do so. They are in other orthogonal bitstrings' critical distance, but sufficiently far not to converge in a single read.

Going further in the analysis, we calculated the probability of missing a bit when reading from SDM. After all, that is how Kanerva has originally found the curve. To do this, we used the following equations from our previous work [9]. Let  $d$  be the distance to the target,  $h$  be the number of hard locations activated during reading and write operations,  $s$  be the number of total stored bitstrings,  $H$  be the number of total hard locations,  $w$  be the number of times the target was written into SDM,  $\theta$  be the total random bitstrings in all  $h$  hard locations activated by read operation, and  $\phi(d)$  be the average number of shared hard locations activated two bitstrings  $d$  bits away.

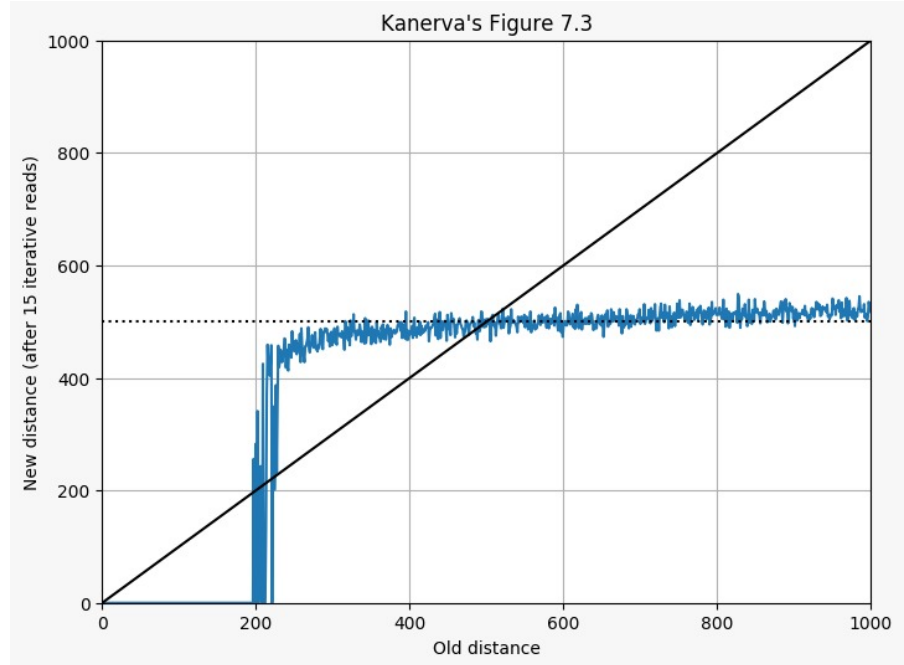


Figure 37: This graph shows the interaction effects more clearly. As we change the single read to a 6-iterative read, the effect has vanished, and all bitstrings above  $x = 500$  have converged to 500-bit distance bitstrings. Here we have precisely the same configuration of Figure 35, except for the iterative read.

$$\theta = \frac{sh^2}{H} - w \cdot \phi(d) \quad (3)$$

$$P(\text{miss}|\text{bit} = 0) = 1 - P\left(\sum_{i=1}^{\theta} X_i < \frac{sh^2}{2H}\right) \quad (4)$$

$$P(\text{miss}|\text{bit} = 1) = P\left(\sum_{i=1}^{\theta} X_i < \frac{sh^2}{2H} - w \cdot \phi(d)\right) \quad (5)$$

$$P(\text{miss}) = \frac{1}{2} \cdot [P(\text{miss}|\text{bit} = 0) + P(\text{miss}|\text{bit} = 1)] \quad (6)$$

For details and the proof of this equation, see Brogliato et al. [9]. Although Kanerva has found a formula for  $\phi(d)$  through an unsolved integral, and de Pádua Braga and Aleksander [22] have proposed another way to calculate  $\phi(d)$ , we have used our framework to estimate the values of  $d$ . In order to do that, we used a Monte Carlo approach, generating many pairs of random bitstrings  $d$  bits away from them and calculating the average number of shared hard locations between them. The code is available in the “Calculate critical distance” notebook [8].

Kanerva’s settings according to the parameters of the equation were:  $s = 10,000$ ,  $H = 1,000,000$ , and  $w = 1$ . We have calculated  $\phi(d)$  as explained, and  $h = H \cdot 2^{-n} \sum_{i=0}^r \binom{n}{i}$ , where  $n = 1,000$  and

$r = 451$ . Finally,  $h = 1,071.85$  and changing  $d$  from 0 to 1000, we got Figure 38.

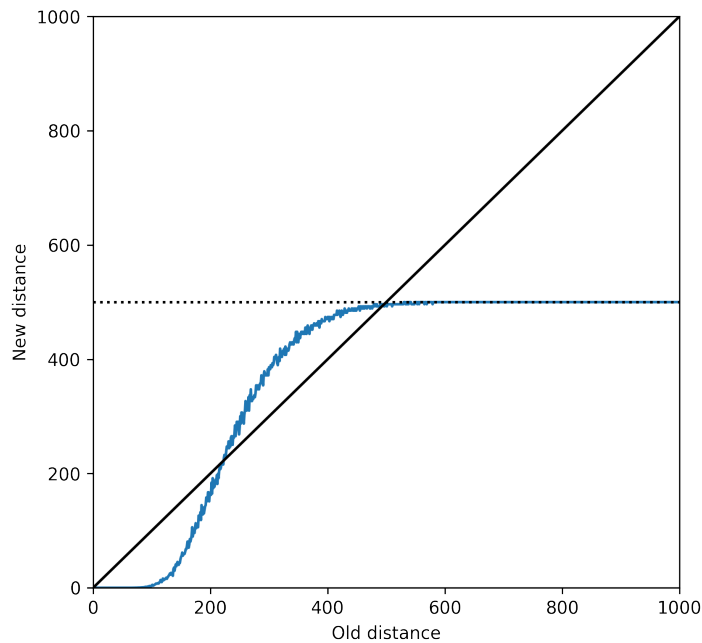


Figure 38: Kanerva's original Figure 7.3 generated using the equations from Brogliato et al. [9].

As one can easily notice, we have got exactly the same curve as Kanerva. Both his and our model expect that, after reading, say, from 550 bits of distance from a written bitstring, we should obtain the expected  $n/2$  equator distance. This question has intrigued us, and here we look for a more analytic explanation than merely interference from the other written attractors. Let us turn back to mathematics to study this anomaly.

### 8.1 A DEVIATION FROM THE EQUATOR DISTANCE?

Explain equator distance<sup>1</sup>.

Kanerva writes<sup>2</sup>:

You have done an incredibly thorough analysis of SDM. I like the puzzle in your message and believe that your simulations are correct and to be learned from. So what to make of the difference compared to my Figure 7.3 (and your Figure 38)? I think the difference comes from my not having accounted fully for the effect of the other

<sup>1</sup> explain equator distance

<sup>2</sup> Email thread 'SDM: A puzzling issue and an invitation', started March 16th 2018, in which we discussed the aforementioned discrepancy. To think that some centuries ago, all scientific publishing was the exchange of such letters.

9,999 vectors that are stored in the memory. You say in it

"Our results show that the theoretical prediction is not accurate. There are interaction effects from one or more of the attractors created by the 10,000 writes, and these attractors seem to raise the distance beyond 500 bits (Figure 35)."

I think that is correct. It also brings to mind a comment Louis Jaeckel made when we worked at NASA Ames. He pointed out that autoassociative storage (each vector is stored with itself as the address) introduces autocorrelation that my formula for Figure 7.2 did not take into account. When we read from memory, each stored vector exerts a pull toward itself, which also means that each bit of a retrieved vector is slightly biased toward the same bit of the read address, regardless of the read address. We never worked out the math.

This is an important observation. A hard location is activated because it shares many dimensions with the items read from or written onto it. Imagine the 'counter's eye view': each individual counter 'likes' to write on its own corresponding bit-address value more than it likes the opposite; as each hard-location has a say in its own area — and nowhere else.

### 8.1.1 Bitmatches at i.

Let  $x$  and  $y$  be random bitstrings and  $n$  be the number of dimensions in the memory; let  $x_i$  and  $y_i$  be the  $i$ -th bit of  $x$  and  $y$ , respectively; and  $d(x, y)$  be the Hamming distance. Whilst the probability of a shared bit-value between same dimension-bits in two random addresses is  $1/2$ , an address only activates hard-locations close to it. Let us call these shared bitvalues a *bitmatch in dimension i*.

So, what is the probability of bitmatches given that we know the access radius  $r$  between the address and a hard-location?

**Theorem 1.** Each dimension  $i$  has a small pull bias, which can be measured by  $P(x_i = y_i | d(x, y) \leq r) = \frac{\sum_{k=0}^r \binom{n-1}{k}}{\sum_{k=0}^r \binom{n}{k}}$ .

*Proof.* The left-hand expression  $P(x_i = y_i | d(x, y) \leq r)$  computes the probability of a bitmatch in  $i$ , given that we know that  $x$  and  $y$  are in the access radius defined by  $r$ , i.e.,  $d(x, y) \leq r$ .

Applying the law of total probability to the left-hand expression we obtain

$$\sum_{k=0}^r P(x_i = y_i | d(x, y) = k \leq r) P(d(x, y) = k | d(x, y) \leq r) \quad (7)$$

We also know that

$$P(x_i = y_i | d(x, y) = k) = \frac{n-k}{n} \quad (8)$$

$$P(d(x, y) = k | d(x, y) \leq r) = \frac{\binom{n}{k}}{\sum_{j=0}^r \binom{n}{j}} \quad (9)$$

Hence,

$$P(x_i = y_i | d(x, y) \leq r) = \frac{\sum_{k=0}^r \frac{n-k}{n} \binom{n}{k}}{\sum_{j=0}^r \binom{n}{j}} \quad (10)$$

Finally, the combinatorial identity

$$\frac{n-k}{n} \binom{n}{k} = \binom{n-1}{k} \quad (11)$$

closes the theorem.  $\square$

Theorem 1 is valid for both “x written at x” (autoassociative memory) and “random written at x” (heteroassociative memory). When  $n = 1,000$  and  $r = 451$ ,  $P(x_i = y_i | d(x, y) \leq r) = p = 0.552905$ . Each bit of a hard location does indeed have a small pull bias. What is meant by this is that each particular dimension has a small preference toward positive values if its address bit is set to 1, and negative values if set to 0 — an intuition developed in Figure 39.

A natural question is what happens to this pull bias as  $n$  grows? Let  $f = P(d(x, y) \leq r) = 2^{-n} \sum_{k=0}^r \binom{n}{k}$ . Then, we have:

**Lemma 2.** *Let  $r$  be the access radius given that  $f$  is the ratio of the hard locations activated. Then,  $\lim_{n \rightarrow \infty} r/n = 1/2$ .*

*Proof.* As the bits of the hard locations’ addresses are randomly chosen, the distance between two hard locations follow a Binomial distribution with  $n$  samples and probability  $1/2$ ,  $B(n, 1/2)$ . For  $n$  sufficiently large, the Binomial distribution can be approximated by a Normal distribution, i.e.,  $B(n, 1/2) \rightarrow N(\mu = n/2, \sigma^2 = n/4)$ .

Let  $\Phi(x)$  be the cdf of the standard normal distribution. If  $z = \frac{r-n/2}{\sqrt{n}/2}$ ,  $z$  is, hence, measuring the number of standard deviations from the average in the Gaussian<sup>3</sup>. Thus,  $P(d(x, y) \leq r) = \Phi(z)$ . As  $f = P(d(x, y) \leq r)$ , then,  $f = \Phi(z)$  for our fixed  $r$ .

---

<sup>3</sup> MARCELO, CHEQUE ESTA ULTIMA FRASE PLEASE?

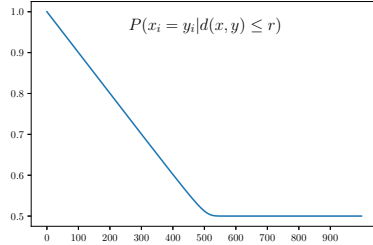


Figure 39: The threshold size  $r$  of hard-locations bring about the autocorrelation of Theorem 1. Consider, for instance, the extremes  $\{0, n\}$ . Let us start with  $n$  (in our case,  $n = 1000$  dimensions): given the information that  $d(x, y) \leq n$ , the probability of a bitmatch in dimension  $i$  is  $p = 1/2$ ; as  $\forall x, y \in \{0, 1\}^N, d(x, y) \leq n$ . At the other extreme, consider that we have the information that  $d(x, y) \leq 0$ : in this case  $x = y$  and the probability of a bitmatch, in any dimension, is  $p = 1$ . The autocorrelation hence drops monotonically until convergence at  $p = 1/2$  as the distance grows.

Calculating the inverse,  $z = \Phi^{-1}(f)$ . Then,

$$z = \Phi^{-1}(f) \quad (12)$$

$$\frac{r - n/2}{\sqrt{n}/2} = \Phi^{-1}(f) \quad (13)$$

$$r = \frac{n}{2} + \Phi^{-1}(f) \frac{\sqrt{n}}{2} \quad (14)$$

$$\frac{r}{n} = \frac{1}{2} + \Phi^{-1}(f) \frac{1}{2\sqrt{n}} \quad (15)$$

Therefore,  $n \rightarrow \infty \Rightarrow r/n \rightarrow 1/2$ .  $\square$

As seen on Fig. 39, the bias disappears as  $r$  grows. Numerically, our results converge to precisely  $p = 1/2$  only after  $d(x, y) \geq 83$  for  $n = 100$ ,  $d(x, y) \geq 607$  for  $n = 1000$ ;  $d(x, y) \geq 5332$  for  $n = 10000$ . This can be seen in Lemma 2.

**Lemma 3.** *Let  $\Phi(x)$  be the cdf of the standard normal distribution. Then,  $n \rightarrow \infty \Rightarrow P(x_i = y_i | d(x, y) \leq r) = \frac{1}{2} \frac{\Phi(z_1)}{\Phi(z_2)}$ , where  $z_1 = \frac{2r-n+1}{\sqrt{n-1}}$  and  $z_2 = \frac{2r-n}{\sqrt{n}}$ .*

*Proof.* From the approximation of the Binomial distribution  $B(a, 0.5)$  by the Normal distribution  $N(\mu = a/2, \sigma^2 = a/4)$ , we conclude that, for  $a$  sufficiently large, the cdf of the Binomial is approximately equal to the cdf of the Normal distribution. Thus,

$$\frac{1}{2^a} \sum_{k=0}^b \binom{a}{k} = \Phi\left(\frac{b-a/2}{\sqrt{a}/2}\right) = \Phi\left(\frac{2b-a}{\sqrt{a}}\right)$$

Thus,

$$\sum_{k=0}^b \binom{a}{k} = 2^a \Phi\left(\frac{2b-a}{\sqrt{a}}\right)$$

The result comes directly from applying the equation above in  $P(x_i = y_i | d(x, y) \leq r)$ .  $\square$

**Theorem 4.** *The autocorrelation vanishes when  $n \rightarrow \infty$ , i.e.,  $\lim_{n \rightarrow \infty} P(x_i = y_i | d(x, y) \leq r) = 1/2$ .*

*Proof.* From Lemma 2, we know that  $r = n/2$  for  $n$  sufficiently large. Thus, replacing  $r = n/2$  in Lemma 3,  $P(x_i = y_i | d(x, y) \leq r) = \frac{\Phi(z_1)}{2\Phi(z_2)}$ , where  $z_1 = \frac{1}{\sqrt{n-1}}$  and  $z_2 = 0$ .

As  $n \rightarrow \infty$ ,  $z_1 \rightarrow 0$ , and  $P(x_i = y_i | d(x, y) \leq r) = \frac{\Phi(0)}{2\Phi(0)} = 1/2$ .  $\square$

Another way to prove is to divide into two cases: Suppose that  $n$  is an even integer, then,

$$\sum_{k=0}^r \binom{n}{k} = \sum_{k=0}^{n/2} \binom{n}{k} = \frac{1}{2} \sum_{k=0}^n \binom{n}{k} = \frac{2^n}{2} = 2^{n-1}$$

And, also,

$$\begin{aligned} \sum_{k=0}^r \binom{n-1}{k} &= \sum_{k=0}^{n/2} \binom{n-1}{k} \\ &= \frac{1}{2} \left[ \sum_{k=0}^{n-1} \binom{n-1}{k} - \binom{n-1}{n/2} \right] \\ &= \frac{1}{2} \left[ 2^{n-1} - \binom{n-1}{n/2} \right] \\ &= 2^{n-2} - \frac{1}{2} \binom{n-1}{n/2} \end{aligned}$$

Finally,

$$P(x_i = y_i | d(x, y) \leq r) = \frac{\sum_{k=0}^r \binom{n-1}{k}}{\sum_{k=0}^r \binom{n}{k}} \quad (16)$$

$$= \frac{2^{n-2} - \frac{1}{2} \binom{n-1}{n/2}}{2^{n-1}} \quad (17)$$

$$= \frac{2^{n-2}}{2^{n-1}} - \frac{1}{2^n} \binom{n-1}{n/2} \quad (18)$$

$$= \frac{1}{2} - \frac{1}{2^n} \binom{n-1}{n/2} \quad (19)$$

Stirling's approximation yields that, for  $n$  sufficiently large,  $\binom{n}{n/2} \sim \frac{2^n}{\sqrt{\pi n/2}}$ . Thus,  $\frac{1}{2^n} \binom{n}{n/2} \sim \frac{\sqrt{2}}{\sqrt{\pi n}}$ , which yields

$\lim_{n \rightarrow \infty} \frac{1}{2^n} \binom{n}{n/2} = 0$ . Finally, as  $\binom{n-1}{n/2} \leq \binom{n}{n/2}$ , by the squeeze theorem,  $\lim_{n \rightarrow \infty} \frac{1}{2^n} \binom{n-1}{n/2} = 0$ , which closes the proof for  $n$  even.

When  $n$  is an odd integer, the steps of the proof are similar. Therefore, the proof is complete.  $\square$

In Figure 40, with  $n = 10,000$  and  $r = 4,845$ , we can notice that the autocorrelation has reduced significantly—as predicted by Theorem 4. In fact, in this case, using Lemma 3,  $P(x_i = y_i | d(x, y) \leq r) = 0.516876$ .

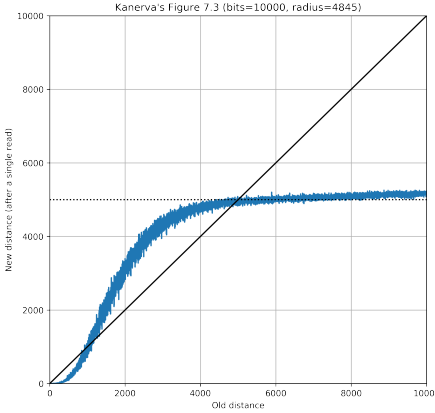


Figure 40: The same setup as in Figure 35, but for  $n = 10,000$ . It shows that the interference has almost gone away when  $n$  is sufficiently large.

So far we have looked only at a single pair of bitstrings: the probability of a single bitmatch between bitstrings within the access radius distance. Now let us consider the number of activated hard locations exhibiting this bitmatch.

Let  $h$  be the number of activated hard locations. As the probability of activating a specific hard location is a constant  $h \sim \text{Binomial}(H, p_1)$ . Thus,  $E[h] = \mu_h = Hp_1$  and  $V[h] = \sigma_h^2 = Hp_1(1 - p_1)$ , where  $p_1 = 2^{-n} \sum_{k=0}^r \binom{n}{k}$ .

Let  $Z$  be the number of activated hard locations with the same bit as the reading address. Then,  $Z = \sum_{i=1}^h X_i$ , where  $X_i \sim \text{Bernoulli}(p)$ , where  $p = P(x_i = y_i | d(x, y) \leq r)$ .<sup>4</sup>

**Theorem 5.** *Given a reading address  $x$  and a dimension  $i$ , the number of activated hard-locations with bitmatches at  $i$  follows a normal distribution with  $E[Z] = \mu_Z = p\mu_h$  and  $V[Z] = \sigma_Z^2 = p(1 - p)\mu_h + p^2\sigma_h^2$ .*

*Proof.* By the central limit theorem,  $Z$  is normally distributed.

Applying the law of total averages and the law of total variance,  $E[Z] = E[E[Z|h]] = E[ph] = pE[h] = ph$ , and  $V[Z] = E[V[Z|h]] + V[E[Z|h]] = E[hp(1 - p)] + V[ph] = p(1 - p)E[h] + p^2V[h] = hp(1 - p) + p^2Hp_1(1 - p_1)$ .

---

<sup>4</sup> TRANSITION!!!

Applying the law of total variance,  $\mathbf{V}[Z] = \mathbf{E}[\mathbf{V}[Z|h]] + \mathbf{V}[\mathbf{E}[Z|h]] = \mathbf{E}[hp(1-p)] + \mathbf{V}[ph] = p(1-p)\mathbf{E}[h] + p^2\mathbf{V}[h] = p(1-p)\mu_h + p^2\sigma_h^2$ .  $\square$

As, in our case,  $P(973 < h < 1170) = 0.997$ , by the central limit theorem,  $Z$  may be approximated by a normal distribution. Figure 41 provides a comparison between the theoretical model and a simulation.

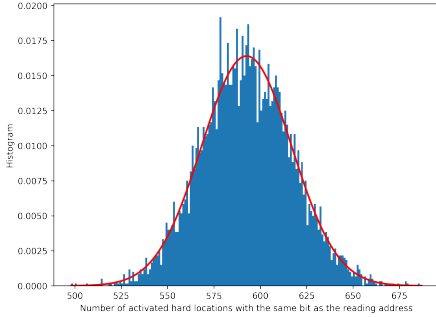


Figure 41: Given an address  $x$  and a dimension  $i$ , how many hard locations with bitmatches in  $i$  are activated by reading at  $x$ ? The histogram was obtained through numerical simulation. The red curve is the theoretical normal distribution found in Theorem 5.

## 8.2 COUNTER BIAS

The previous theorems show that there is bias in the counters. In this section we show that there is a small counter bias, as a function of the bitmatch in dimension  $i$ . If the Hard location's address bit is set to 1, the mean will be above zero. And the mean will be below zero if the address bit is set to 0.

Let us analyze the  $i$ th counter of a hard location. Let  $s$  be the number of bitstrings written into memory (in our case,  $s = 10,000$ ) and  $addr_i$  be the  $i$ th bit of the hard location's address.

Let  $\theta$  be the average number of bitstrings written in each hard location. As there are  $s$  bitstrings written into the memory, and the probability of activating a specific hard location is constant,  $\theta \sim \text{Binomial}(s, p_1)$ . Thus,  $E[\theta] = \mu_\theta = sp_1$  and  $\mathbf{V}[\theta] = \sigma_\theta^2 = sp_1(1-p_1)$ .

Let us introduce another random variable. Let  $Y_i$  be the number of bitmatches in the  $i$ th dimension of a hard location's address after  $s$  written bitstrings. Then,  $Y_i = \sum_{k=1}^{\theta} X_k$ .

**Theorem 6.** *Given the number of written bitstrings  $s$ ,  $E[Y_i] = \mu_Y = p\mu_\theta$  and  $\mathbf{V}[Y_i] = \sigma_Y^2 = p(1-p)\mu_\theta + p^2\sigma_\theta^2$ .*

*Proof.* Applying the law of total expectation,  $E[Y] = \mathbf{E}[\mathbf{E}[Y|\theta]] = \mathbf{E}[p\theta] = pE[\theta] = p\mu_\theta$ .

Applying the law of total variance,  
 $\mathbf{V}[Y] = \mathbf{E}[\mathbf{V}[Y|\theta]] + \mathbf{V}[\mathbf{E}[Y|\theta]] = \mathbf{E}[\theta p(1-p)] + \mathbf{V}[p\theta] = p(1-p)\mathbf{E}[\theta] + p^2\mathbf{V}[\theta] = p(1-p)\mu_\theta + p^2\sigma_\theta^2.$   $\square$

During a write operation, the counters are incremented for every bit 1 and decremented for every bit 0. So, after  $s$  writes, there will be  $\theta$  bitstrings written in each hard location with  $Y_i$  bitmatches and  $\theta - Y_i$  non-bitmatches. Thus,  $[cnt_i|addr_i = 1] = (Y_i) - (\theta - Y_i) = 2Y_i - \theta$  and  $[cnt_i|addr_i = 0] = \theta - 2Y_i.$

**Theorem 7.**  $\mathbf{E}[cnt_i|addr_i = 1] = \mu_{cnt} = (2p - 1)\mu_\theta$  and  $\mathbf{V}[cnt_i|addr_i = 1] = \sigma_{cnt}^2 = 4p(1-p)\mu_\theta + (2p - 1)^2\sigma_\theta^2.$

*Proof.*  $\mathbf{E}[cnt_i|addr_i = 1] = \mathbf{E}[2Y_i - \theta] = \mathbf{E}[2Y_i] - \mathbf{E}[\theta] = 2\mathbf{E}[Y_i] - \mu_\theta = 2p\mu_\theta - \mu_\theta = (2p - 1)\mu_\theta.$

Applying the law of total variance,  $\mathbf{V}[cnt_i|addr_i = 1] = \mathbf{V}[2Y_i - \theta] = \mathbf{E}[\mathbf{V}[2Y_i - \theta|\theta]] + \mathbf{V}[\mathbf{E}[2Y_i - \theta|\theta]].$

Let us solve each part independently. Thus,

$$\mathbf{V}[2Y_i - \theta|\theta] = \mathbf{V}[2Y_i|\theta] = 4\mathbf{V}[Y_i|\theta] = 4\mathbf{V}[\sum_{k=1}^{\theta} X_k] = 4\theta p(1-p).$$

$$\mathbf{E}[\mathbf{V}[2Y_i - \theta|\theta]] = \mathbf{E}[4\theta p(1-p)] = 4p(1-p)\mathbf{E}[\theta] = 4p(1-p)\mu_\theta.$$

Finally,

$$\mathbf{E}[2Y_i - \theta|\theta] = 2\mathbf{E}[Y_i|\theta] - \mathbf{E}[\theta|\theta] = 2p\theta - \theta = (2p - 1)\theta.$$

$$\mathbf{V}[\mathbf{E}[2Y_i - \theta|\theta]] = \mathbf{V}[(2p - 1)\theta] = (2p - 1)^2\mathbf{V}[\theta] = (2p - 1)^2\sigma_\theta^2. \quad \square$$

**Theorem 8.**  $\mathbf{E}[cnt_i|addr_i = 0] = -\mu_{cnt}$  and  $\mathbf{V}[cnt_i|addr_i = 1] = \sigma_{cnt}^2.$

*Proof.* Notice that  $[cnt_i|addr_i = 0] = -[cnt_i|addr_i = 1].$  Thus,  $\mathbf{E}[cnt_i|addr_i = 0] = -\mathbf{E}[cnt_i|addr_i = 1]$  and  $\mathbf{V}[cnt_i|addr_i = 0] = \mathbf{V}[cnt_i|addr_i = 1].$   $\square$

In summary, what we learn is that

$$[cnt_i|addr_i = 1] \sim \mathcal{N}(\mu_{cnt}, \sigma_{cnt}^2) \tag{20}$$

$$[cnt_i|addr_i = 0] \sim \mathcal{N}(-\mu_{cnt}, \sigma_{cnt}^2) \tag{21}$$

In our case,  $p = 0.5529$ ,  $s = 10,000$ , and  $H = 1,000,000$ , so  $[cnt_i|addr_i = 1] \sim \mathcal{N}(\mu = 1.1341, \sigma^2 = 10.7184)$ . For “random at x”,  $p = 0.5$ , so  $\mu = 0$  and  $\sigma^2 = 10.7185$ . The slight bias above or below 0 can be seen in Figure 42.

Finally,

$$\mathbf{P}(cnt_i \geq 0|addr_i = 1) = \mathbf{P}(cnt_i \leq 0|addr_i = 0) \tag{22}$$

$$= 1 - \mathcal{N}.cdf(0) \tag{23}$$

For “random written at x”,  $p = 0.5$  implies  $\mu_{cnt} = 0$ , which implies  $\mathbf{P}(cnt_i \geq 0|addr_i = 1) = \mathbf{P}(cnt_i \leq 0|addr_i = 0) = 0.5$ , independently of the parameters because they will only affect the variance and the normal distribution is symmetrical around the average.

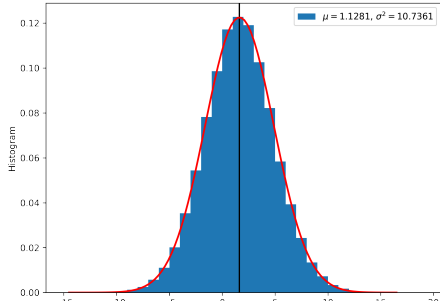
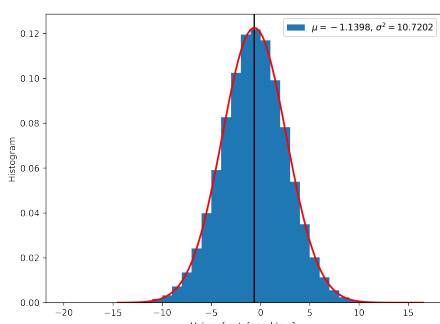
(a)  $\text{addr}_i = 1$ (b)  $\text{addr}_i = 0$ 

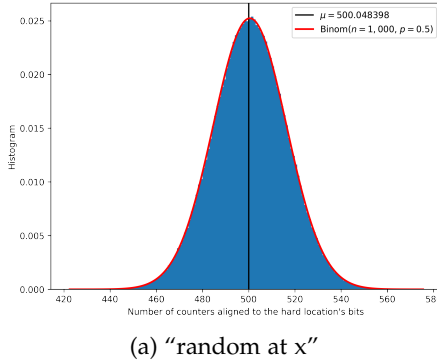
Figure 42: The value of the counters after  $s = 10,000$  writes shows the auto-correlation in the counters in autoassociative memories (“x at x”). The histogram was obtained through simulation. The red curve is the theoretical normal distribution found in equations (20) and (21).

However, for “x written at x”,  $p = 0.5529$  and the probabilities depend on  $s$ . For  $s = 10,000$ , they are equal to 0.6354. For  $s = 20,000$ , they are equal to 0.6867. For  $s = 30,000$ , they are equal to 0.7232. The more random bitstrings are written into the memory, the more the hard locations point to themselves.

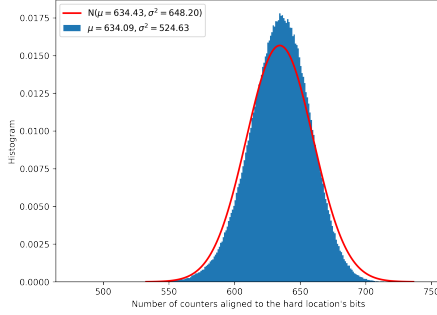
Let  $D$  be the number of counters aligned with  $\text{addr}_i$ . The standard deviation was calculated using the fact that  $[D|\theta] \sim \text{Binomial}(1000, q = P(\text{cnt}_i > 0 | \text{addr}_i = 1, \theta))$ .

Applying the law of total variance,  $V[D] = E[V[D|\theta]] + V[E[D|\theta]] = E[1000q(1-q)] + V[1000q] = 1000E[q - q^2] + 1000^2V[q] = 1000E[q](1 - E[q]) + 1000(1000 - 1)V[q]$ , where  $E[q] = \sum_{\theta} P(\text{cnt}_i > 0 | \text{addr}_i = 1, \theta)P(\theta)$  and  $E[q^2] = \sum_{\theta} [P(\text{cnt}_i > 0 | \text{addr}_i = 1, \theta)]^2P(\theta)$ .

Doing the math,  $E[q] = 0.402922$  and  $E[q^2] = 0.634433$ . Thus,  $V[q] = E[q^2] - (E[q])^2 = 0.0004166$ . Hence,  $V[D] = 648.2041$ . See Figure 43 and notice that I still have to figure out why the mean is correct, but the standard deviation is not.



(a) "random at x"



(b) "x at x"

Figure 43: Autocorrelation in the counters in autoassociative memories ("x written at x"). The histogram was obtained through simulation. The red curve is the theoretical distribution.

### 8.3 READ BIAS

Now that we know the distribution of  $\text{cnt}_i | \text{addr}_i$ , we may go to the read operation. During the read operation, on average,  $h$  hard locations are activated and their counters are summed up. So, for the  $i$ th bit,

$$\text{acc}_i = \sum_{k=1}^h \text{cnt}_k \quad (24)$$

Let  $\eta$  be the reading address and  $\eta_i$  the  $i$ th bit of it. Then, let's split the  $h$  activated hard locations into two groups: (i) the ones with the same bit as  $\eta_i$  with  $Z$  hard locations, and (ii) the ones with the opposite bit as  $\eta_i$  with  $h - Z$  hard locations.

$$[\text{acc}_i | \eta_i] = \sum_{k=1}^Z [\text{cnt}_k | \text{addr}_k = \eta_i] + \sum_{k=1}^{h-Z} [\text{cnt}_k | \text{addr}_k \neq \eta_i] \quad (25)$$

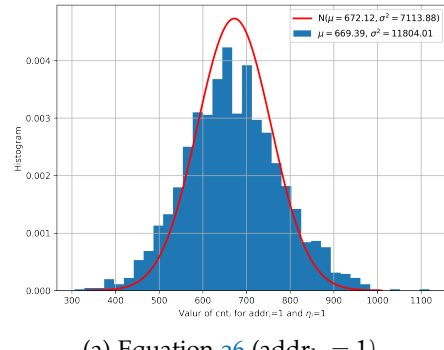
Each sum is a sum of normally distributed random variables, so

$$\sum_{k=1}^Z [cnt_k | addr_k = \eta_1] \sim \mathcal{N}(\mu = \mu_{cnt}\mu_Z, \sigma^2 = \sigma_{cnt}^2\mu_Z + \mu_{cnt}^2\sigma_Z^2) \quad (26)$$

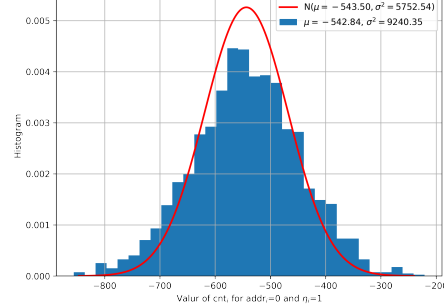
, and, respectively:

$$\sum_{k=1}^{h-Z} [cnt_k | addr_k \neq \eta_1] \sim \mathcal{N}(\mu = -\mu_{cnt}(1-p)\mu_h, \sigma^2 = \sigma_{cnt}^2(1-p)\mu_h + \mu_{cnt}^2\sigma_{h-Z}^2) \quad (27)$$

In our case,  $\sum_{k=1}^Z [cnt_k | addr_k = 1] \sim \mathcal{N}(\mu = 672.12, \sigma^2 = 7113.87)$ , and  $\sum_{k=1}^Z [cnt_k | addr_k = 0] \sim \mathcal{N}(\mu = -543.49, \sigma^2 = 5752.54)$ . See Figure 44 — we can notice that the average is correct but the variance is too small.



(a) Equation 26 ( $addr_k = 1$ )



(b) Equation 27 ( $addr_k = 0$ )

Figure 44: The histogram was obtained through simulation. The red curve is the theoretical normal distribution.

Hence,

$$[acc_i | \eta_i = 1] \sim \mathcal{N}(\mu = (2p - 1)^2 \mu_\theta \mu_h, \sigma^2 = \sigma_{cnt}^2 \mu_h + 2\mu_{cnt}^2 \sigma_h^2) \quad (28)$$

$$[acc_i | \eta_i = 0] \sim \mathcal{N}(\mu = -(2p - 1)^2 \mu_\theta \mu_h, \sigma^2 = \sigma_{cnt}^2 \mu_h + 2\mu_{cnt}^2 \sigma_h^2) \quad (29)$$

In our case,  $[acc_i | \eta_i = 1] \sim \mathcal{N}(\mu = 128.62, \sigma^2 = 12865.69)$ , and  $[acc_i | \eta_i = 0] \sim \mathcal{N}(\mu = -128.62, \sigma^2 = 12865.69)$ . See Figure 45 — we can notice that the variance issue from Figure 44 propagates directly here.

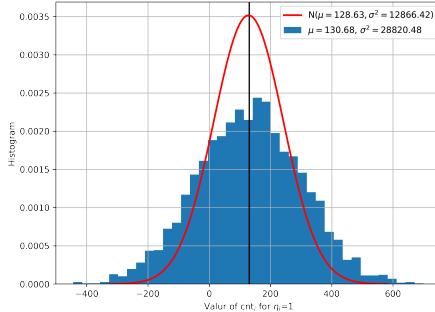
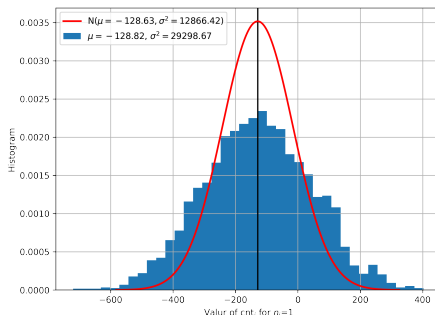
(a) Equation 28 ( $\eta_k = 1$ )(b) Equation 29 ( $\eta_k = 0$ )

Figure 45: The histogram was obtained through simulation. The red curve is the theoretical normal distribution.

Finally,

$$\begin{aligned}
 P(\text{wrong}) &= P(acc_i < 0 | \eta_i = 1) \cdot P(\eta_i = 1) \\
 &\quad + P(acc_i > 0 | \eta_i = 0) \cdot P(\eta_i = 0) \\
 &= \frac{\mathcal{N}_{\eta_i=1}.cdf(0)}{2} + \frac{1 - \mathcal{N}_{\eta_i=0}.cdf(0)}{2} \\
 &= \frac{\mathcal{N}_{\eta_i=1}.cdf(0)}{2} + \frac{\mathcal{N}_{\eta_i=1}.cdf(0)}{2} \\
 &= \mathcal{N}_{\eta_i=1}.cdf(0)
 \end{aligned}$$

Using the empirical variance of  $\sigma^2 = 27838.3029$ , we calculate  $P(\text{wrong}) = 0.220377$ .

In order to check this probability, we have run a simulation reading from 1,000 random bitstrings (which have never been written into memory) and calculated the distance from the result of a single read. As the  $P(\text{wrong}) = 0.22037$ , we expected to get an average distance of 220.37 with a standard deviation of 13.10. See Figure 46 for the comparison between the simulated and the theoretical outcomes.

Figure 47 shows the new distance between  $\eta_d$  and  $\text{read}(\eta_d)$ , where  $\eta_d$  is  $d$  bits away from  $\eta$ . As for  $d \geq 520$  there is no intersection between  $\eta$  and  $\eta_d$ , our model applies and explains the horizontal line around distance 220.

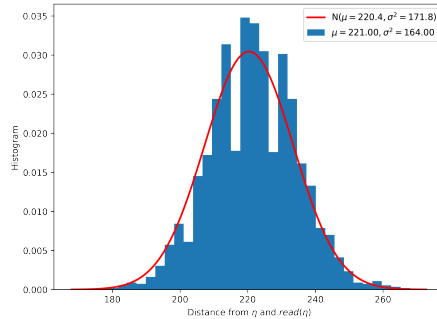


Figure 46: The histogram was obtained through simulation. The red curve is the theoretical normal distribution.

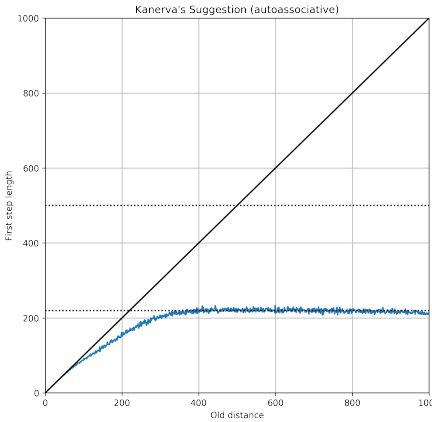
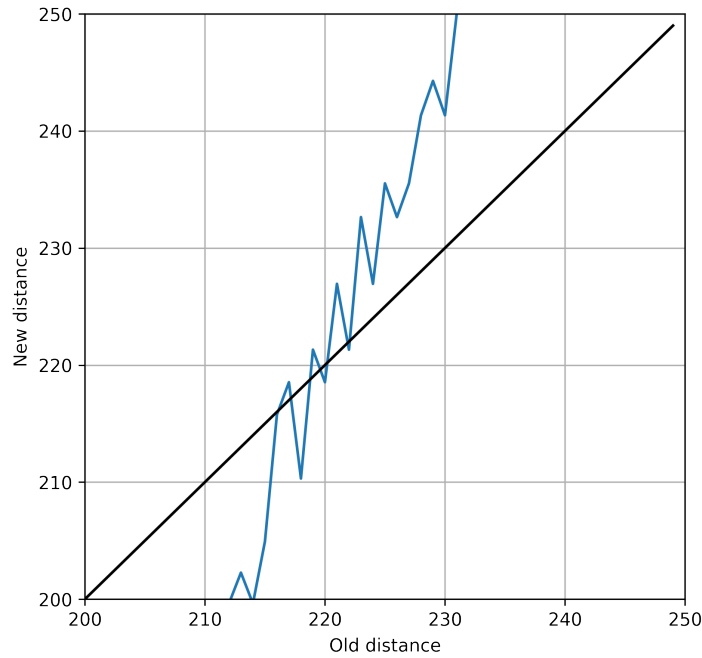


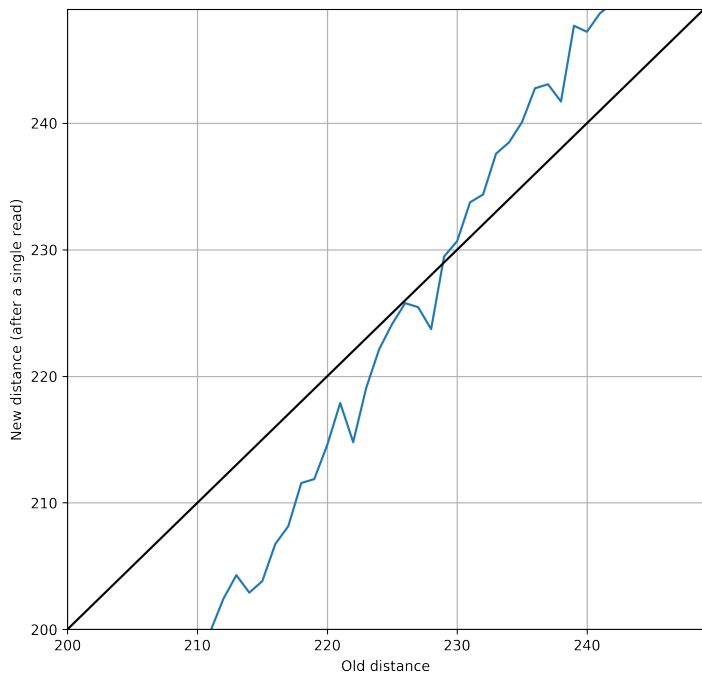
Figure 47: New distance after a single read operation in a bitstring  $\eta_d$ , which is  $d$  bits away from  $\eta$ . The new distance was calculated between  $\eta_d$  and  $\text{read}(\eta_d)$ . Notice that when  $d \geq 520$ , the intersection between  $\eta$  and  $\eta_d$  is zero, which means there is only random bitstrings written into the activated hard locations. The distance 220 equals  $1000 \cdot 0.220$  which is the probability found in Figure 46.

#### 8.4 CRITICAL DISTANCE OF 209

The critical distance is defined as  $d$  where  $P(\text{miss}) = d/n$ , or, in Figure 38, the point where the curve meets with the identity function (the black diagonal line). Thus, we plot a zoom-in of Figure 38 around  $d = 209$  in Figure 48 using the same equations [9]. It was surprising that the meeting does not happen at  $d = 209$ , but around  $d = 221$ .

Figure 48: Zoom-in around  $d = 209$  of Figure 38.

To confirm that the critical distance is not around 209, but around 221, we also plot a zoom-in of Figure 35 around  $d = 209$  in Figure 49. In order to reduce the noise, we increased the samples to  $k = 180$ .

Figure 49: Zoom-in around  $d = 209$  of Figure 35.

# 9

## RESULTS (V): GENERALIZED READ OPERATION

---

Dr. Murilo observed that the models of Kanerva's read ( $z = 1$ ) and Chada's read ( $z = 0$ ) were simple variations of a generalized read with an exponent  $z$ , which suggests experimenting with different values. Mathematically, let  $A$  be the set of the counters of the activated hard location, and  $c_i$  be the counter of the  $i$ th bit. Then,

$$s_i = \sum_{c \in A} \frac{c_i}{|c_i|} |c_i|^z$$

The sum of  $|c_i|^z$  turns the intermediate values from integers to floating point numbers. Thus, we have developed a specific read operation which stored the intermediate values in double variables.

The results, however, have not yielded performance improvements. Though for  $z \leq 1$  results are comparable to  $z = 1$ , for  $z > 1$ , the system shows an evident deterioration, with a smaller critical distance and faster divergence at large-distance reads. This is shown in Figures 50 and 51.

We understand that the critical distance is an important parameter of SDM. The bigger the critical distance, the better, because SDM is able to converge even with farther clues. For  $z > 1$ , the bigger the  $z$ , the smaller the critical distance. For  $z = 6$ , the critical distance almost reaches zero.

It is interesting that Kanerva has proposed  $z = 1$  without realizing the generalized reading. Even so, he proposed the  $z$  with the highest critical distance.

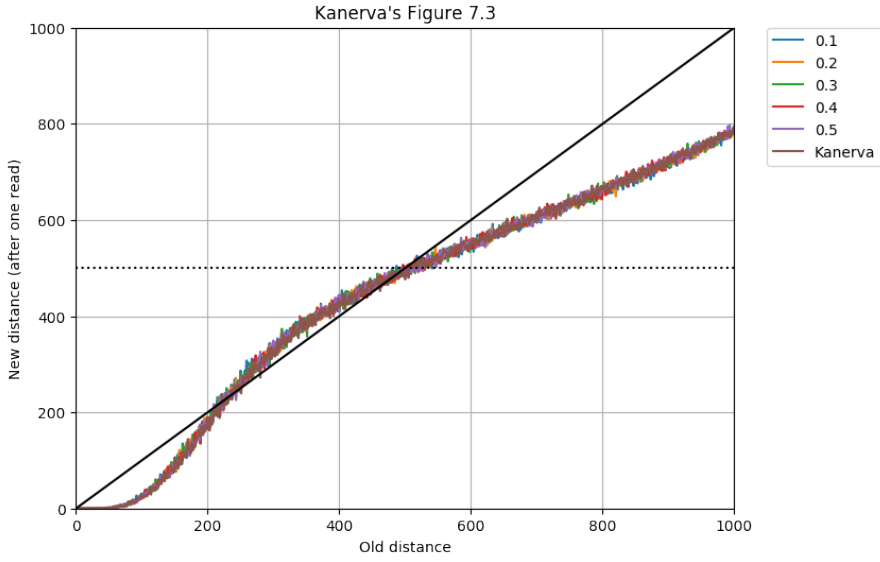
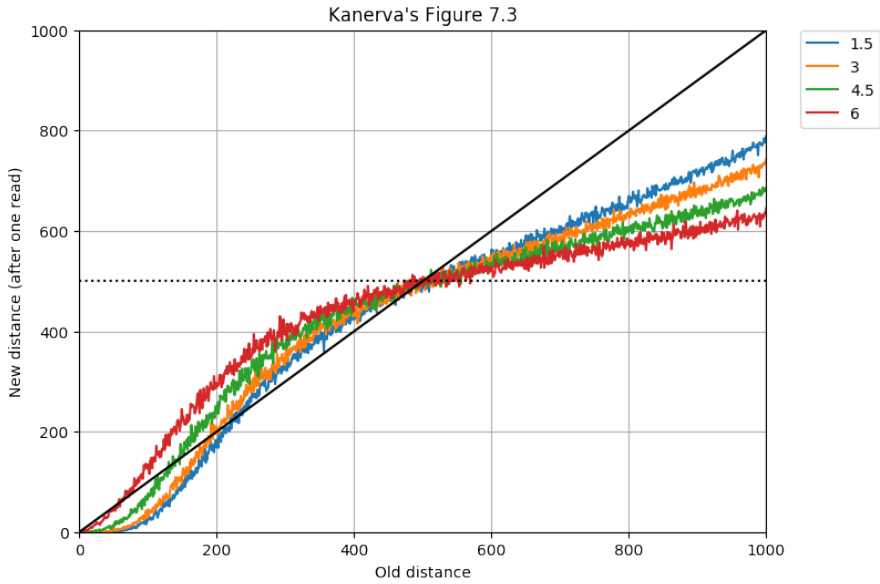
(a) SDM behavior when  $z \in \{0.1, 0.2, 0.3, 0.4, 0.5, 1\}$ (b) SDM behavior when  $z \in \{1.5, 3, 4.5, 6\}$ 

Figure 50: (a) and (b) show the behavior of a single read. As stated previously, we can see a deterioration of convergence, with lower critical distance as  $z > 1$ . Another observation can be made here, concerning the discrepancy of Kanerva's Fig 7.3 and our data. It seems that Kanerva may not have considered that a single read would only 'clean' a small number of dimensions *after the critical distance*. What we observe clearly is that with a single read, as the distance grows, the system only 'cleans' towards the orthogonal distance 500 after a number of iterative readings.

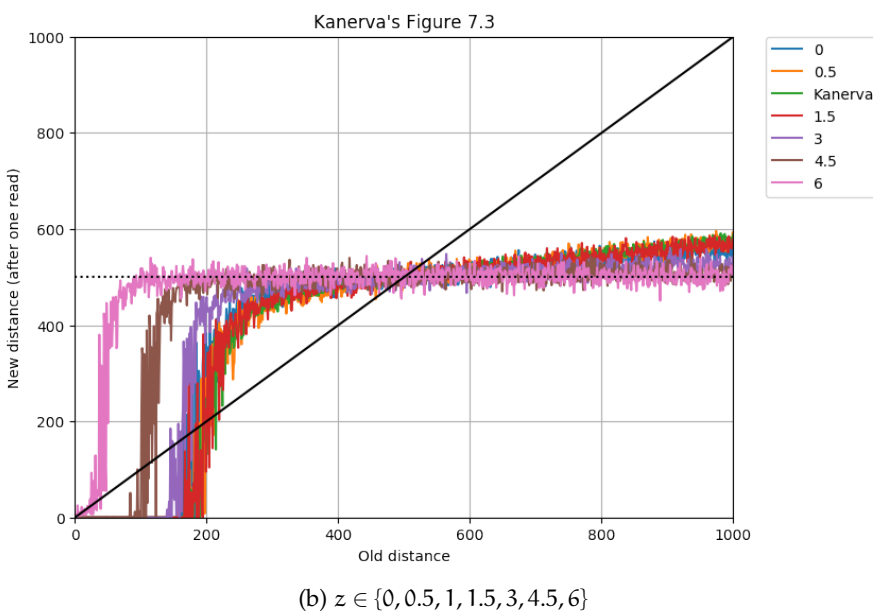
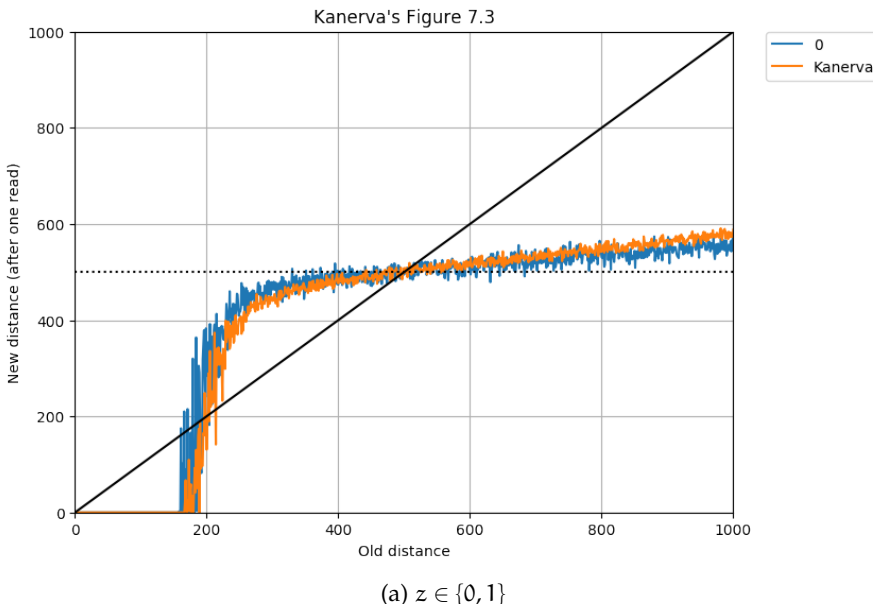


Figure 51: (a) and (b) show the behavior of Figure 50, now executed with 6-iterative reads. What we observe clearly is that with a single read, as the distance grows, the system only ‘cleans’ towards the orthogonal distance 500 after a number of iterative readings.



## RESULTS (VI): SUPERVISED CLASSIFICATION APPLICATION

---

Supervised classification problem consists of categorizing data into groups after seeing some samples from each group. First, it is presented pieces of data with their categories. The algorithm learns from these data, which is known as the learning phase. Then, new pieces of data are presented and the algorithm must classify them into the already known groups. It is named “supervised” because the algorithm will not create the groups itself. It will learn the groups during the learning phase, in which the groups have already been defined and the pieces of data have already been classified into them.

Although this problem has already been studied (REF), our intention here is to show that a pure SDM may also be used to classify data. Fan and Wang [26] has used SDM to solve a classification problem, recognizing handwriting letters from images, but he used a mix of genetic algorithm with SDM, which is very different from the original SDM described by [41]. Even though his algorithm has classified properly, we were intrigued whether a pure SDM would also classify successfully.

Hence, we have developed a supervised classification algorithm based on a pure SDM as our main memory. Our goal was to classify noisy images into their respective letters (case sensitive) and numbers. For some examples, see Figure 52.

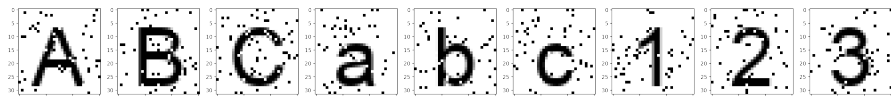


Figure 52: Examples of noisy images with uppercase letters, lowercase letters, and numbers.

The images had 31 pixels of width and 32 pixels of height, totaling 992 pixels per image<sup>1</sup>. Each image was mapped into a 1,000-bit bitstring in which the bits were set according to the color of each pixel of the image. So, white pixels were equal to bit 0, and black

<sup>1</sup> A crucial note is in order. While others have proposed similar models [37], in no way is it claimed here that these bitstrings should form a plausible representation of letters in the human mind (See, for instance, Hofstadter [36] for a marvelous discussion of the subtleties and fluidity involved in that process). These letters should merely be seen as *invariant patterns* that are processed by the memory, which is able to capture their underlying invariant structure even when presented only under heavy noise. Recall that any resizing, any rotation, or any mere shifting of these letters will take them out of the critical distance for SDM reading.

pixels to bit 1. The eight remaining bits were all set to zero. This was a bijective mapping (or one-to-one mapping), i.e., there was only one bitstring for each image, and there was only one image for each bitstring.

A total of 62 classification groups have been trained in the SDM. For each of them, it was generated a random bitstring. Thus, the groups' bitstrings were orthogonal between any two of them. There is one image for each of the 62 groups in Figure 53. Notice that the memory has never seen a single image without noise.

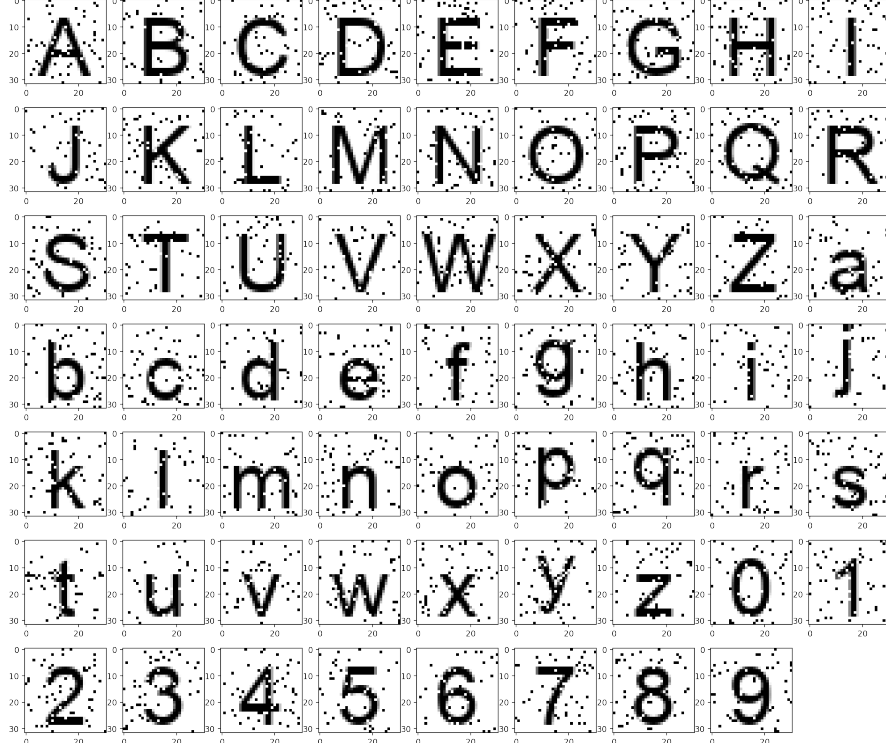


Figure 53: One noisy image for each of the 62 classification groups.

The association of images to groups was stored as sequences in SDM, as detailed by Kanerva [41] in Chapter 8. During the learning phase, the image bitstrings were stored pointing to their group's bitstrings, i.e., `write(addr=bs_image, datum=bs_label)`. Thus, in order to classify an unknown image, we only had to read from its address and check which group has been found.

During the learning phase, we have generated 100 noisy images for each character. The images had 5% of noise, i.e., 5% of their pixels have been randomly flipped. For example, see the generated images for letter A in Figure 54. Then, we have written the classification group bitstring into the bitstring associated to each noisy image, i.e., `write(bs_image, bs_label)`.

Finally, we have assessed the performance of our classifier. We had done it in three different scenarios: high noise (20%), low noise (5%)

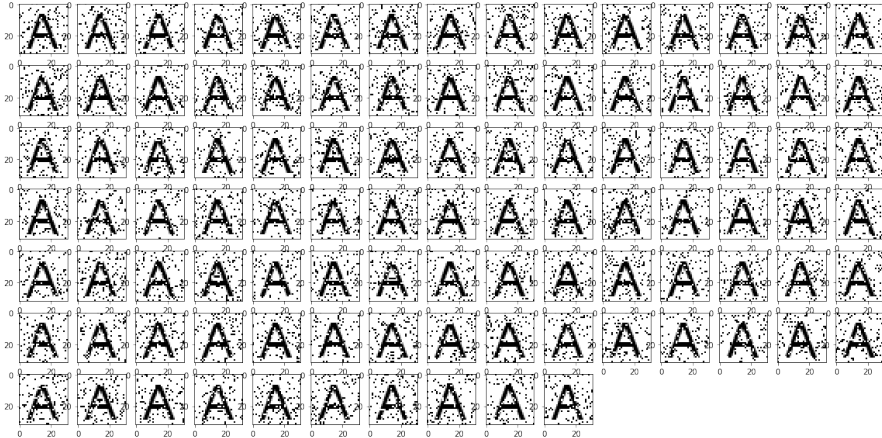


Figure 54: 100 noisy images generated to train label A.

and no noise. See Figures 55 and 56 for images with 20% noise and no noise. The low noise scenario had the same noise as the training set. For each scenario, we had classified 620 unknown images with ten images per group.

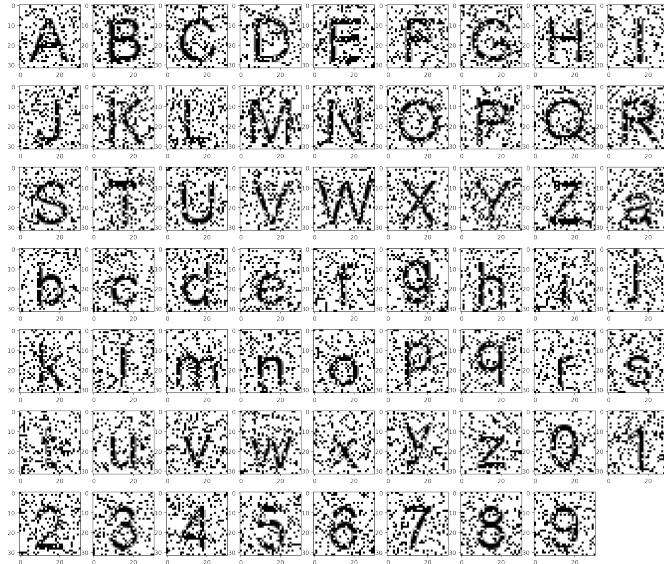


Figure 55: Images generated using a 20% noise for the high noise scenario.

The performance was calculated as the percentage of hits for each group. We did not expect the same performance for all groups because some groups become very similar to other depending on the noise level, and this similarity may even confuse a person (see Figure 57).

In the no noise scenario, the classifier has hit all characters, except letter "l" which was wrongly associated with the group of "i". We believe that it happened because the classifier had never seen an image with no noise and the difference between the images of "l" and "i" is smaller than the critical distance. So, both groups have been merged

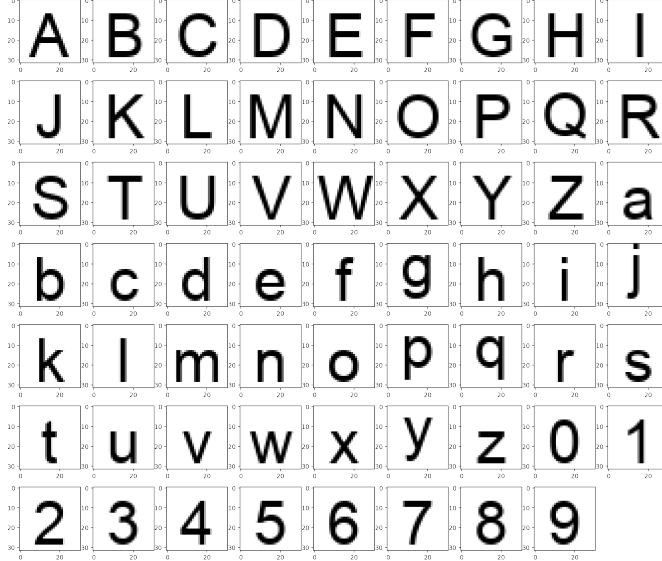


Figure 56: Images generated for the no noise scenario.

and it converged to only one of them. In our simulation, it happened to be the group of “i”.

In the low noise scenario, it has made few mistakes. It correctly classified all images but some from characters “b”, “e”, “f”, “l”, “t”, and “9”. It completely classified “l” images to the “i” group. In the other cases, it made just a few mistakes. See Figure 58 to check the images and their classification.

The high noise scenario is the most interesting, because, even in a high noise level, the classifier has hit most of the characters. It has hit all images for 44 out of 62 groups and made at least one miss for the other 18 groups. The misses may be seen in details in Figure 57.

The critical distance plays an important role in the classification error. As we have 62 groups and each has been trained with 100 images, there were 6,200 writes to the memory. When an image is being classified, it will have to converge to a group, and the convergence depends on the distance between this image and the images from the training set, i.e., in the noise level.

In our simplified scenario, there is neither translation nor rotation. Future work may explore how sensible this classification algorithm is to these operations. We expect that, with proper training, the algorithm will remain classifying the images with a good hit rate.

These results show that the SDM may be used as a supervised classification algorithm. Although we do not believe that the mapping between images and bitstrings are even close to the way human cognition deals with images, we believe the results are exciting and useful to many possible real-world problems.

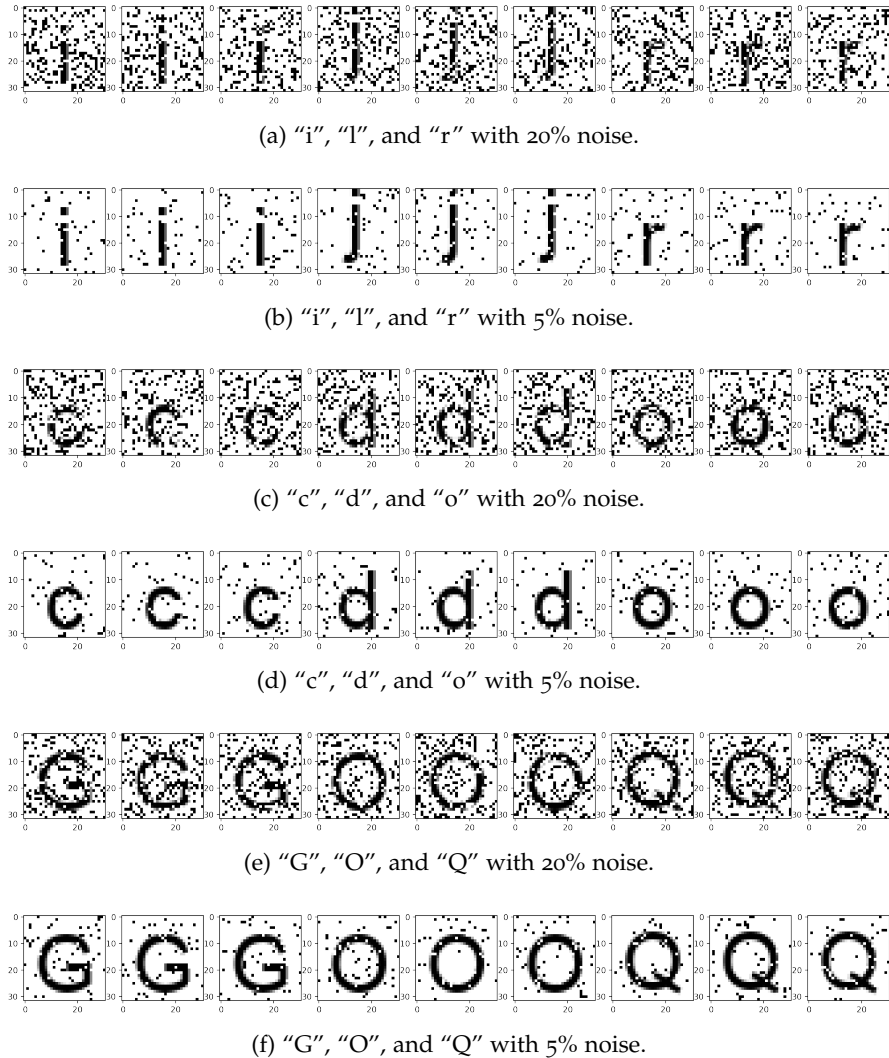


Figure 57: Images of different characters which may be confusing depending on the noise level.

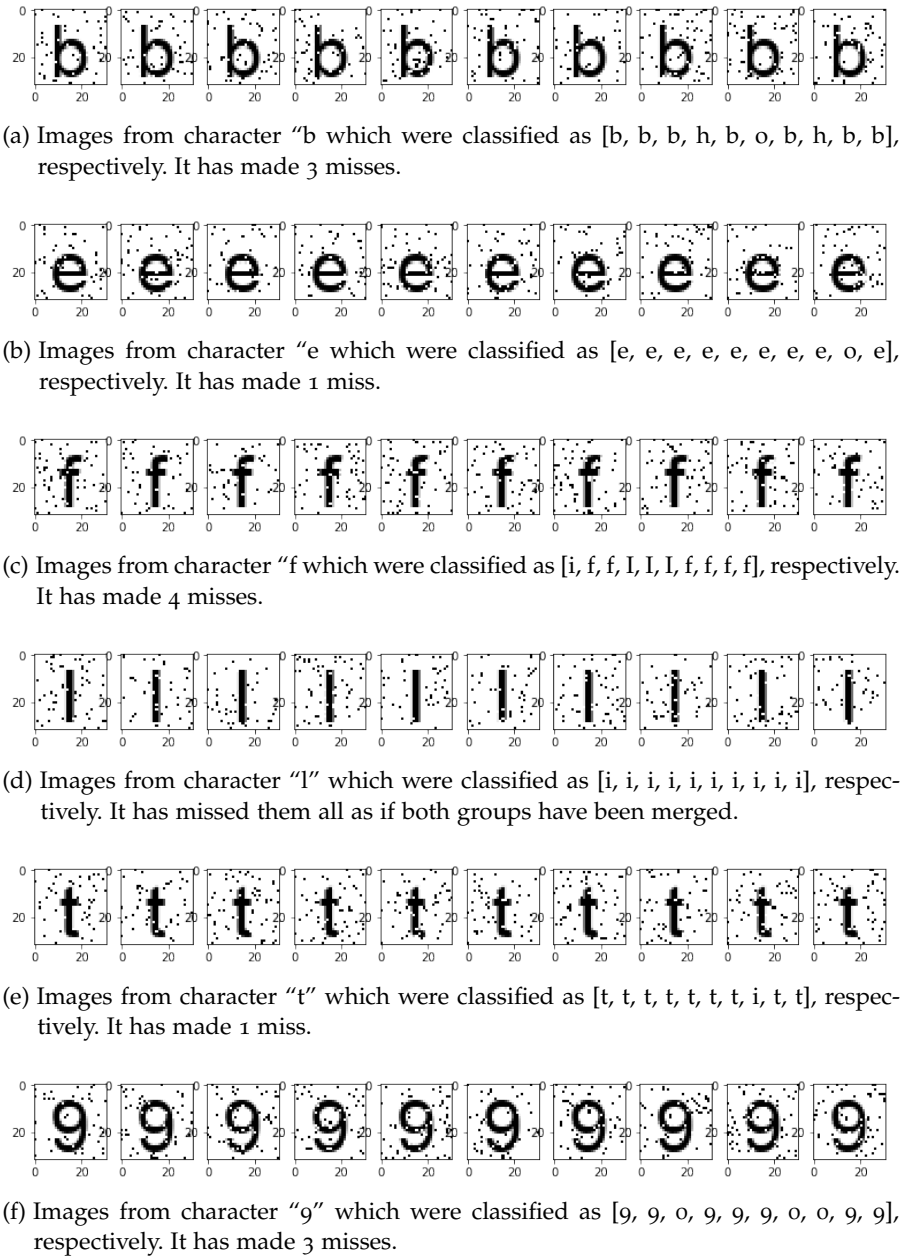
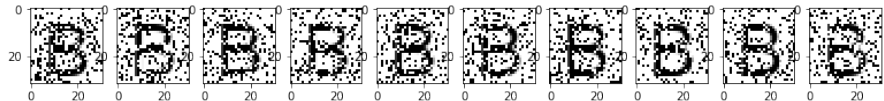
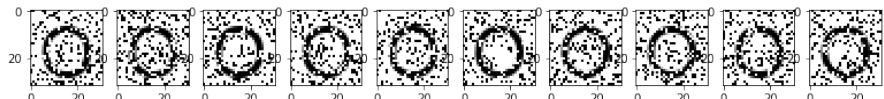


Figure 58: Characters in the low noise scenario in which the classifier has made at least one mistake. In all the other cases, it correctly classified the images. We may notice that the groups of "i" and "l" have been completely merged by the classifier, because it cannot distinguish them, not even with no noise.



(a) Images from character "B" which were classified as [S, B, B, B, B, B, B, B, B, B]. It has made 1 mistake.



(b) Images from character "O" which were classified as [G, G, O, O, O, O, O, O, O, O]. It has made 2 mistakes.



(c) Images from character "T" which were classified as [T, T, T, T, T, I, T, T, T, T]. It has made 1 mistake.



(d) Images from character "Y" which were classified as [Y, I, Y, Y, Y, Y, Y, Y, Y, Y]. It has made 1 mistake.



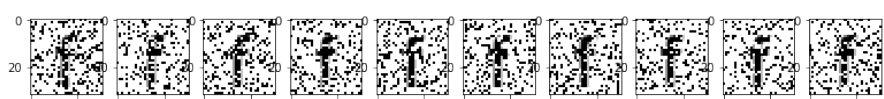
(e) Images from character "b" which were classified as [o, o, o, b, o, h, h, b, b, o]. It has made 7 mistakes.



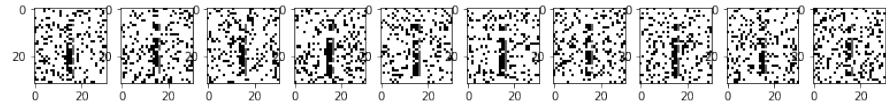
(f) Images from character "c" which were classified as [c, c, c, c, c, o, c, c, c, o]. It has made 2 mistakes.



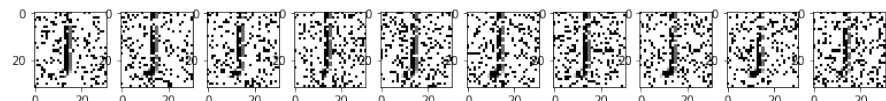
(g) Images from character "e" which were classified as [e, o, e, o, o, o, e, o, o, e]. It has made 6 mistakes.



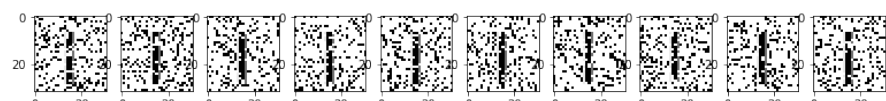
(h) Images from character "f" which were classified as [I, I, I, I, i, I, I, I, I, I]. It has missed them all.



(i) Images from character "i" which were classified as [i, i, i, I, i, i, i, i, I, i]. It has made 2 mistakes.



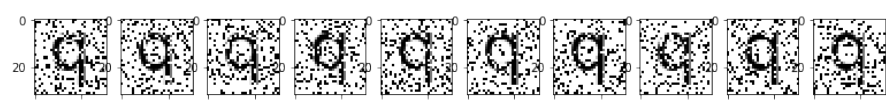
(j) Images from character "j" which were classified as [j, j, j, I, I, j, j, j, I]. It has made 3 mistakes.



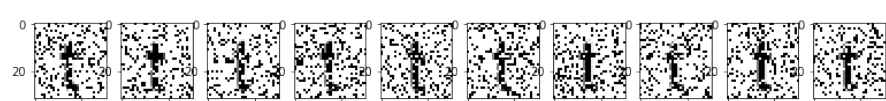
(k) Images from character "l" which were classified as [l, i, l, l, l, l, i, l, l, i]. It has missed them all.



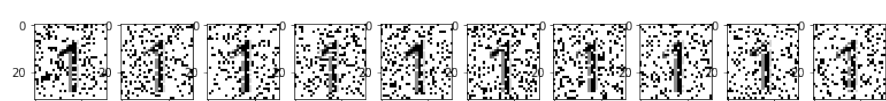
(l) Images from character "n" which were classified as [u, n, n, n, n, n, u, u, u, h]. It has made 5 mistakes.



(m) Images from character "q" which were classified as [q, q, q, q, q, q, q, q, q, g]. It has made 1 mistake.



(n) Images from character "t" which were classified as [l, r, l, i, l, i, i, i, l, i]. It has missed them all.



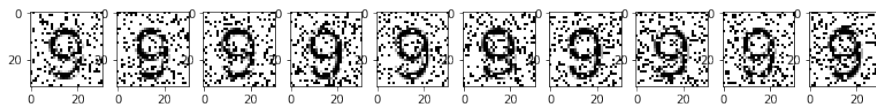
(o) Images from character "1" which were classified as [1, l, 1, l, 1, 1, l, l, 1, l]. It has made 5 mistakes.



(p) Images from character "7" which were classified as [7, 7, 7, l, 7, l, l, 7, 7, 7]. It has made 3 mistakes.



(q) Images from character “8” which were classified as [8, 6, 6, 6, 8, d, 8, 8, d, 6]. It has made 6 mistakes.



(r) Images from character “9” which were classified as [9, o, 6, o, 9, o, o, 9, o, o]. It has made 7 mistakes.

Figure 57: Characters in the high noise scenario in which the classifier has made at least one mistake. In all the other cases, it correctly classified the images.



## RESULTS (VII): IMAGE NOISE FILTERING APPLICATION

---

Image noise filtering consists in removing the noise from an input, in our case an image. Our images are black & white images, and the noise is generated randomly flipping some of their pixels from black to white and vice versa. In Figure 58, we may see an image with different levels of noise, from 0% to 45% in steps of 5%. It makes no sense to apply 50% of noise as it would absolutely randomize the image.

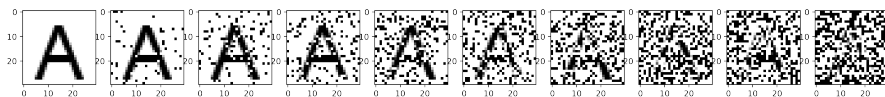


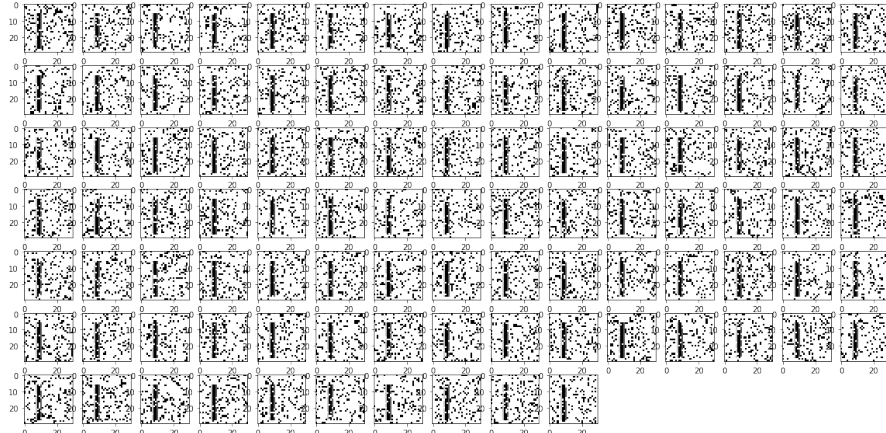
Figure 58: Progressive noise into letter “A”, from 0% to 45% in steps of 5%.

The images have  $30 \times 30$  pixels, totaling 900 pixels per image. Each image is mapped into a bitstring of 1,000 bit in which the bits are set according to the color of each pixel of the image. White pixels are assigned to bit 0, and black pixels to bit 1. The 100 remaining bits are all set to zero. This is a bijective mapping (or one-to-one) from images and bitstrings, i.e., there is one, and only one, bitstring for each image, and vice versa.

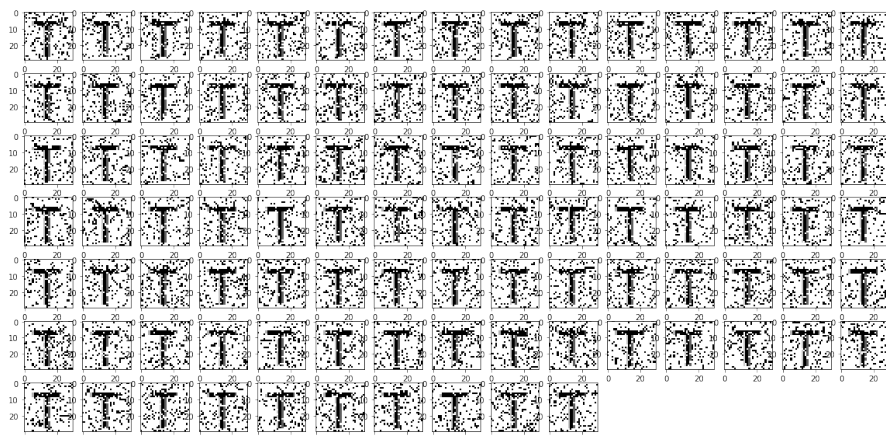
In the learning phase, 200 noisy images were generated and written into SDM. Half of the letter “I” and half of the letter “T” (see Figure 59). They were written into their own addresses, i.e., `write(address=bs_image, datum=bs_image)`, following, for instance, Hong and Chen [37], Marshall and Meeden [63].

Then, in order to test the filtering, we just have read from noisy images, and the results were remarkable. We were able to clean images up to 42% of noise (see Figure 60). While SDM has never seen a clean version of the letters, it just learned from the learning phase which pixels have appeared more frequently and choose them.

A simplified mathematical analysis would be: During the learning phase, 200 images with 15% of noise were written to SDM, so, the average distance between them and the clean image was 150 bits. Thus they shared, on average, 175 hard locations with the clean image. In these 175 hard locations, the counter’s value for a black pixel mapped to bit 1 was  $(1 - 0.15) \cdot 200 - 0.15 \cdot 200 = 140$ . Finally, let’s analyze the reading. When reading from a noisy image with 42% of noise, the average distance between the noisy image and its clean image is 420, which means they share, on average, 6 hard locations. As the average number of activated hard locations is 1,072,

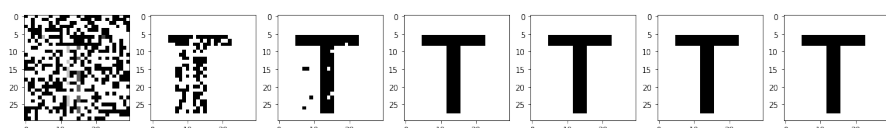


(a) Letter "I" with 15% of noise.

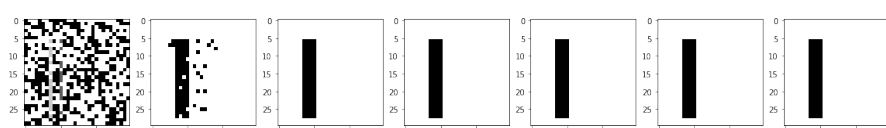


(b) Letter "T" with 15% of noise.

Figure 59: Training images written into the SDM. They were written in their own addresses — `write(address=bs_image, datum=bs_image)`.



(a) Steps of reading from letter "T" with 42% of noise



(b) Steps of reading from letter "I" with 42% of noise

Figure 60: In order to test the SDM as a noise filter, we read from noisy images expecting to get a clean image. It is interesting to highlight that SDM has never seen a clean version letters "T" and "I".

the sum of their counters will be, on average,  $Y = 6 \cdot 140 - \sum_{i=1}^{1072-6} X_i$ , where  $X_i$  is a Bernoulli trial with

probability 0.5. Hence,  $P(\text{black pixel}) = P(Y > 0) = P(6 \cdot 140 - \sum_{i=1}^{1072-6} X_i > 0) = P(\sum_{i=1}^{1066} X_i < 840) = 99.99\%$ . But, when reading from a noisy image with 45% of noise, the average number of hard locations shared with the clean image is only 3. Thus the sum of the activated hard locations' counters will be, on average,  $3 \cdot 140 - \sum_{i=1}^{1072-3} X_i$ , and  $P(\text{black pixel}) = P(\sum_{i=1}^{1069} X_i < 420) = 1.28 \cdot 10^{-12}$ . The probability abruptly drops from 100% to 0% when the noise goes from 42% to 45% (see Figure 61). The analysis for white pixels is exactly the same, but with opposite signs. The code to calculate this probability is available in "Noise filter - Math analysis" notebook [8].

This is a simplified analysis because it does not take into consideration the hard locations shared by the different letters. It works fine for our example because letters "I" and "T" are almost orthogonal and share, on average, only one hard location.

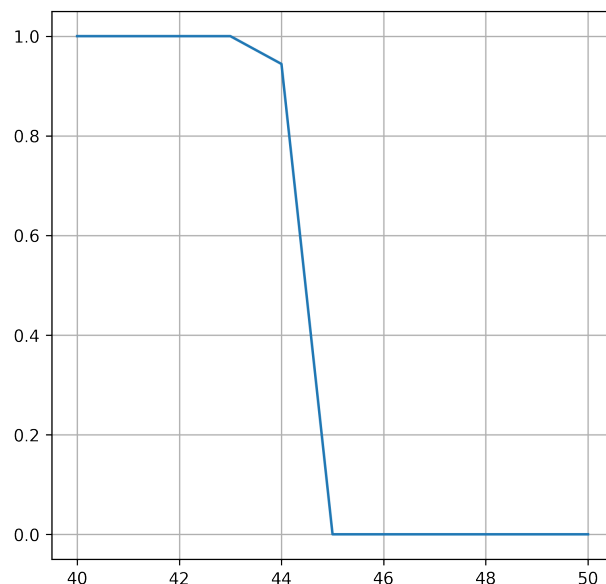
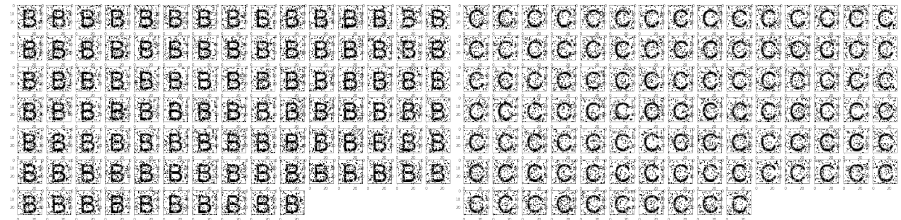


Figure 61: Probability of getting the right pixel when reading from an image with noise  $p$ . It assumes that SDM was trained with 200 images with 15% noise.

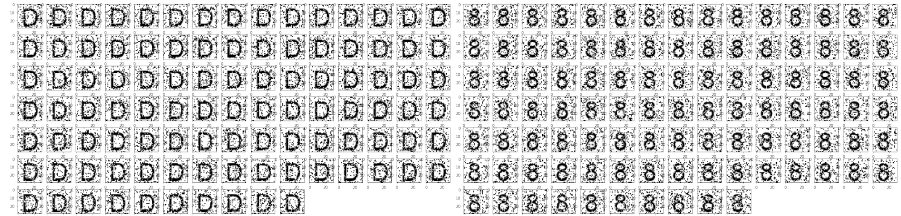
If the intersection between images becomes too high, the noise filter stops working properly. We have confirmed it writing the letters "B", "C", "D" and the numeral "8". They share a high number of hard locations, and our noise filter could not filter their noise correctly. The training sets can be seen in Figure 62 and the results in Figure 63.

A possible solution to this interference problem is to use labels. Each label has a random bitstring, which will be chunked with the images before writing into SDM. Hence, before reading, we also have to chunk the image with the label — which means we need to know the label of each image. The chunk was done using the exclusive



(a) Letter "B" with 15% of noise.

(b) Letter "C" with 15% of noise.



(c) Letter "D" with 15% of noise.

(d) Letter "8" with 15% of noise.

Figure 62: Training images in which the intersection between images is too high. They were written in their own addresses — write(address=bs\_image, datum=bs\_image).

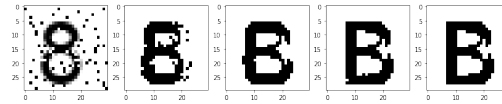
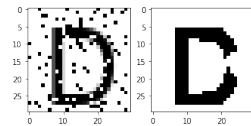
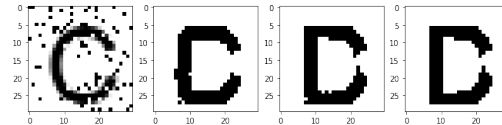
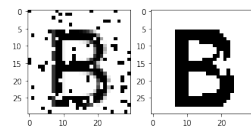


Figure 63: When the intersection between images becomes too high, there appears some interference in the resulting image. All cases have 10% noise. We can notice that the empty space on the right side of the "C" letter generates some white pixels on the right side of both "B" and "D" letters.

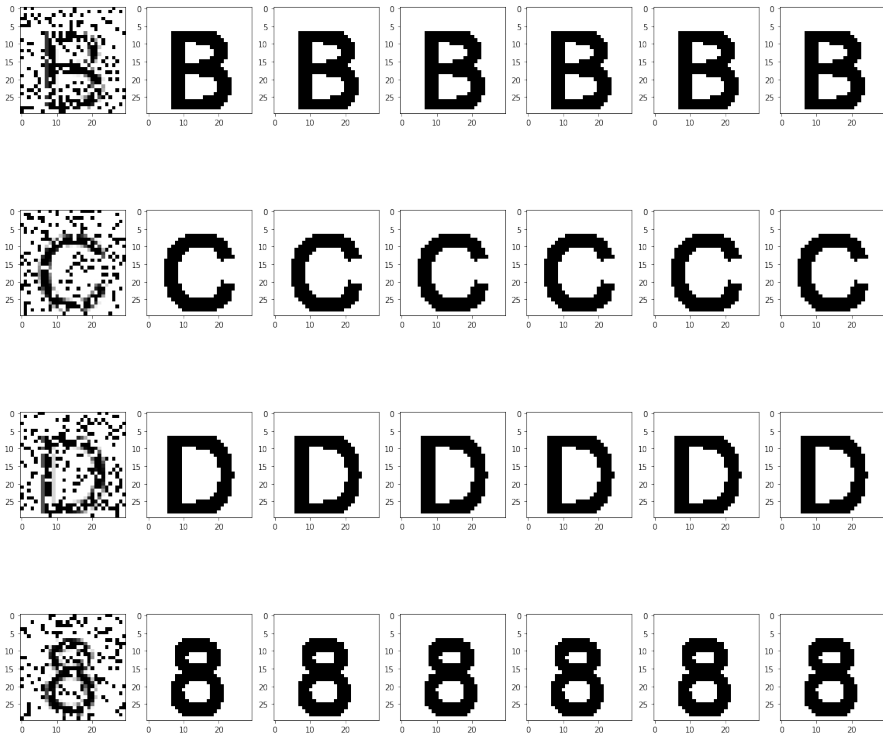


Figure 64: Using labels solves the interference problem when the intersection between images becomes too high. All cases have 20% noise.

OR (XOR) operator, i.e.,  $bs\_chunk = bs\_image \oplus bs\_label$ . In other words, we run `write(address=bs_chunk, datum=bs_label)` during the training, and `read(address=bs_chunk)` during the testing. We used the same training set as before, and the results can be seen in Figure 64.

The chunk through exclusive OR (XOR) works because of Theorem 9, which says that chunking the images with labels will generate, on average, orthogonal bitstrings. Thus, these orthogonal bitstrings will not interfere with each other because they share, on average, only one hard location.

The disadvantage of using labels is that it requires classification of the images. In our example, we just used the correct label with each image, but we could have used our classification algorithm as a pre-processing step, and only then run the noise filter.

**Theorem 9.** If  $v_1$  and  $v_2$  are random bitstrings, then  $\forall a, b, E[d(a \oplus v_1, b \oplus v_2)] = n/2$ .

*Proof.* Let  $A = \{i | a^i = b^i\}$  be the indexes in which the bits of  $a$  are equal to the bits of  $b$ , and  $B = \{i | a^i \neq b^i\}$  be indexes in which the bits of  $a$  are different from the bits of  $b$ . Thus,

$$\begin{aligned}
d(a \oplus v_1, b \oplus v_2) &= \sum_{i=1}^n d(a^i \oplus v_1^i, b^i \oplus v_2^i) \\
&= \sum_{i=1}^n (a^i \oplus v_1^i) \oplus (b^i \oplus v_2^i) \\
&= \sum_{i=1}^n (a^i \oplus b^i) \oplus (v_1^i \oplus v_2^i) \\
&= \sum_{i \in A} (a^i \oplus b^i) \oplus (v_1^i \oplus v_2^i) + \sum_{i \in B} (a^i \oplus b^i) \oplus (v_1^i \oplus v_2^i)
\end{aligned}$$

For  $i \in A$ ,  $a^i \oplus b^i = 0$ , and follows:

$$\begin{aligned}
(a^i \oplus b^i) \oplus (v_1^i \oplus v_2^i) &= 0 \oplus (v_1^i \oplus v_2^i) \\
&= v_1^i \oplus v_2^i \\
&= d(v_1^i, v_2^i)
\end{aligned}$$

Hence,  $E[\sum_{i \in A} d(a^i \oplus v_1^i, b^i \oplus v_2^i)] = E[\sum_{i \in A} d(v_1^i, v_2^i)] = |A|/2$ , because  $v_1$  and  $v_2$  are random bitstrings and their average distance is half the number of bits.

For  $i \in B$ ,  $a^i \oplus b^i = 1$ , and follows:

$$\begin{aligned}
(a^i \oplus b^i) \oplus (v_1^i \oplus v_2^i) &= 1 \oplus (v_1^i \oplus v_2^i) \\
&= d(1, v_1^i \oplus v_2^i)
\end{aligned}$$

Hence,

$$E[\sum_{i \in B} d(a^i \oplus v_1^i, b^i \oplus v_2^i)] = E[\sum_{i \in B} d(1, v_1^i \oplus v_2^i)] = |B|/2.$$

Finally,  $E[d(a \oplus v_1, b \oplus v_2)] = |A|/2 + |B|/2 = n/2$ , since  $|A| + |B| = n$   $\square$

# 12

## RESULTS (VIII): THE POSSIBILITY OF UNSUPERVISED REINFORCEMENT LEARNING

---

Reinforcement learning has increasing prominence in the media after AlphaZero has won all games from both the best chess grandmasters in the world and the best chess engines. What is incredible about these victories is that AlphaZero has almost no knowledge about chess game and has learned all its movement playing against itself for 4 hours. Basically, it knows only the valid movements and had to learn everything from scratch, which it did using a reinforcement learning algorithm<sup>1</sup> [82, 83].

Reinforcement learning is a machine learning algorithm which learns from the rewards of its actions. So, it receives the game state as input, it decides which action will be taken, and then it learns from the rewards of all the actions it has chosen. In theory, it learns after each reward feedback it receives, improving its decision over time and presenting intelligent behavior. A positive reward would indicate that the chosen action should be encouraged, while a negative reward would indicate the opposite. In some algorithms, there may be a neutral reward which would indicate that the chosen action was neither positive nor negative. How each type of reward should be handled depends on each algorithm. For further information, see Sutton and Barto [89].

We have done some experiments with an SDM as a memory for a TicTacToe player. Basically, it receives the current board state and returns which action should be played. At the end of the game, it receives both the sequences of boards and the winner and is supposed to learn from them.

In our approach, there were 9 possible actions: one for each cell of the TicTacToe game. Action 1 means playing in the first cell of the first row; action 2 means playing in the second cell of the first row; and so one. Figure 65 shows the TicTacToe board numbering and the link between each cell and its respective action.

Our algorithm to decide what should be played is simple: it reads the current board from SDM and then it chooses the valid action with the highest score. To calculate the scores, the bitstring is split into 9 parts, one per action (Figure 65). The number of bits 1 in each part indicates the score of its respective action.

After a game has finished, it is time to learn from its decisions. Our algorithm has three rewards: positive, negative, and neutral. It always

---

<sup>1</sup> See also the recent work on modern machine learning and reinforcement learning [2, 96]

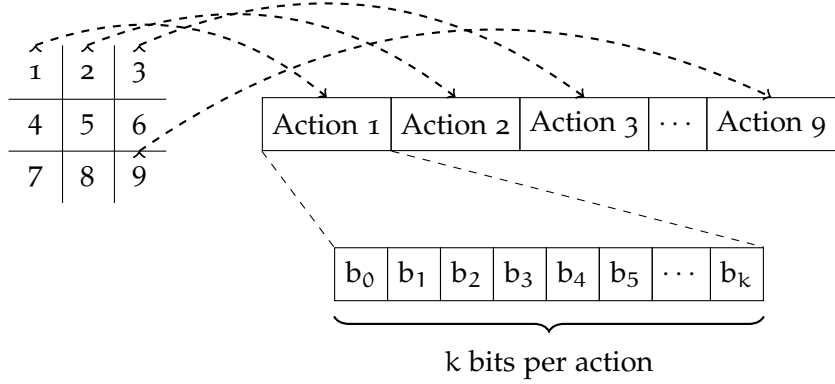


Figure 65: Each action is a cell in the TicTacToe board and is mapped to slice of the bitstring.

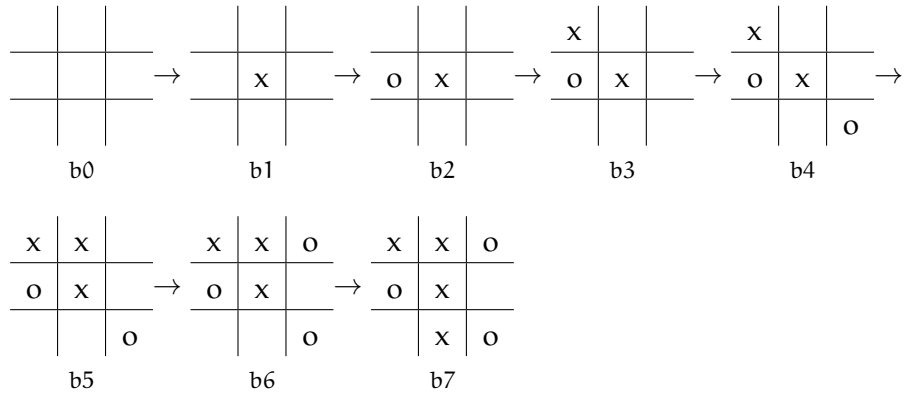


Figure 66: Example of a game with 7 movements in which X wins.

learns from both players, no matter who wins or if it was a draw. The winner's sequence of actions feeds our positive reward learning. The loser's sequence of actions feeds our negative reward learning. If it is a draw, both sequences feed our neutral reward learning.

Each board state has a unique random bitstring. For instance, each board in Figure 66 has its own unique random bitstring. Thus, if a specific board state is reached again, SDM will return the scores for each action.

Let  $b_0, b_1, b_2, \dots, b_n$  be the board sequence of the game (see Figure 66). In order to learn, our algorithm will map each action which goes from  $b_k$  to  $b_{k+1}$  to a reward bitstring and then will write a pointer from  $b_k$  to this reward bitstring, i.e., `write(bs_board, bs_reward)`.

The reward bitstring may be a positive, negative, or neutral bitstring. The positive reward bitstring is randomly generated and then only the bits related to the action will be set to 1 (see Figure 67). The negative reward bitstring is also randomly generated and then only the bits related to the action will be set to 0. Finally, the neutral reward bitstring is only a random bitstring.

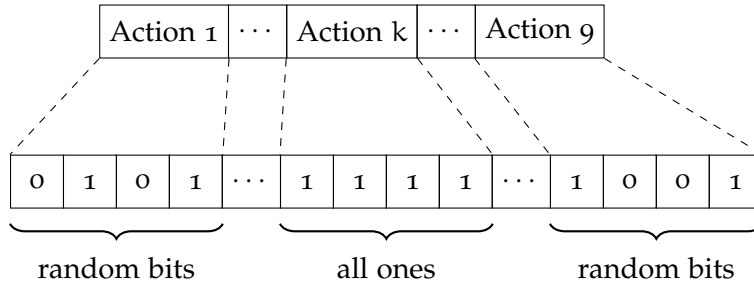


Figure 67: Positive reward bitstrings used in our reinforcement learning algorithm.

The idea behind these reward bitstrings is to increase the score of positive rewards (all bits set to 1), and to decrease the score of negative rewards (all bits set to 0). The neutral reward will have, on average, half of its bits 1 and the other half 0. Thus, it is in the middle of a positive reward and a negative reward.

Let the  $b$  be the sequence of boards and  $a$  be the sequence of actions, then  $b_0 \xrightarrow{a_0} b_1 \xrightarrow{a_1} b_2 \xrightarrow{a_2} \dots \xrightarrow{a_{n-1}} b_n$ . Suppose there is a winner, thus the winner's actions will be the sequence  $a_{n-1}, a_{n-3}, a_{n-5}, \dots$ , while the loser's actions will be the sequence  $a_{n-2}, a_{n-4}, a_{n-6}, \dots$

The positive reward learning will be writing the following pointers in SDM:  $b_{n-1} \rightarrow a_{n-1}$ ,  $b_{n-3} \rightarrow a_{n-3}$ , and so on. The reward bitstring of  $a_{n-1}$  will have all bits set to one in  $a_{n-1}$ 's slice. All other bits will be random.

The negative reward learning will be writing the following pointers in SDM:  $b_{n-2} \rightarrow a_{n-2}$ ,  $b_{n-3} \rightarrow a_{n-3}$ , and so on. The reward bitstring of  $a_{n-2}$  will have all bits set to zero in  $a_{n-2}$ 's slice. All other bits will be random.

If it is a draw, all actions will be mapped to the neutral reward bitstring, which is simply a random bitstring.

There are also weights associated with positive, negative, and neutral rewards. They are used to indicate what goal is more important. For instance, if SDM should try to win in the first place, no matter if it may lead to losing, the weight of the positive reward should be higher than the others. But, if it is more important not to lose, then the weight of the negative reward should be higher.

In the very beginning, SDM is empty, and its counters are zeroed. So, any reading will result in a random bitstring, because it will flip a coin for all counters. Thus, the chosen action will be random, as their scores will follow a binomial distribution. It is precisely the desired behavior — we play randomly until we learn. In fact, it will happen every time an unknown board is seen.

Internally, every board is mapped into a random bitstring and passed to SDM. As every two boards are, on average, orthogonal, SDM knows nothing about the boards themselves, neither whether

they are consecutive or not. It knows only the score of the actions according to the games it has seen and learned from. Hopefully, the actions will lead to a victory or a draw.

In more details, the next movement decision consists in one read from SDM, resulting in a bitstring. Then the scores of the actions are calculated counting the number of 1 in each part of the bitstring. The chosen action is the one which is valid and has the highest score.

### 12.1 TRAINING

Our algorithm learned playing games against opponents. We had four types of opponents: (i) another SDM player, (ii) a random player whose actions are always random; (iii) a smart player whose actions wins when it can, block the opponent when it can, or are random; and (iv) a human player.

The weights of the rewards were chosen to prevent losing. Thus the weight of the negative reward was 5, while the weight of the positive reward was 2 and the neutral was 1. This choice are in accordance to Prospect Theory, which is a behavioral economic theory and states that losses hurt more than gains feel good [40].

Every learn cycle had two parts: (i) 100 games learning and (ii) 100 games testing. So, it has never learned during the testing phase and has not affected the measure of the statistics.

### 12.2 RESULTS

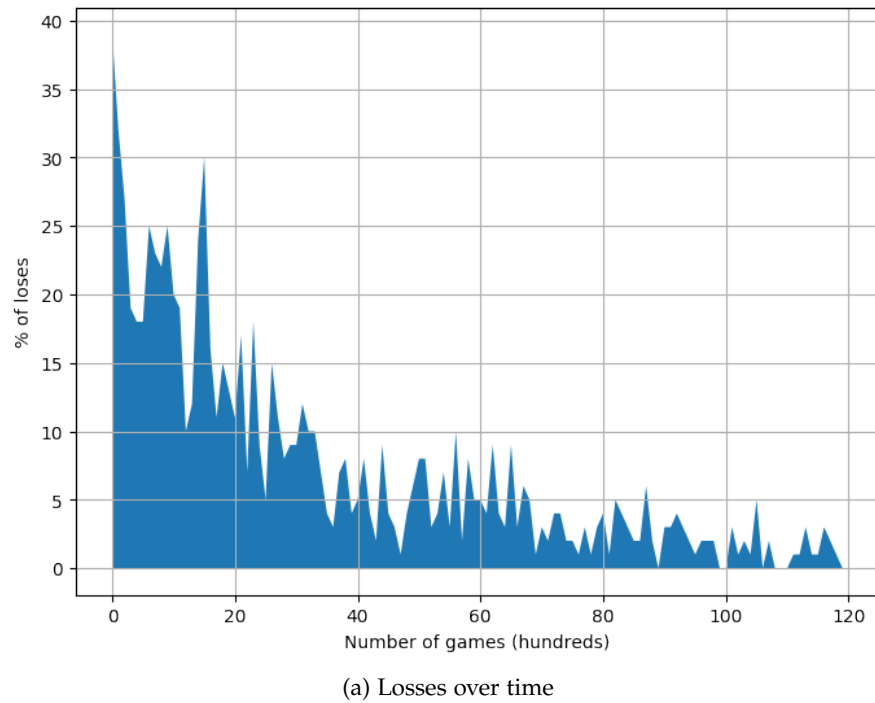
When playing against the random player, SDM has already started improving after the first 100 training games. Its winning rate converges quickly to around 80%, while the drawing rate starts to grow after 2,000 games and keeps rising until the end. The losing rate keeps decreasing until it reaches cycles of 100 games without any loss. See Figure 68.

When playing against the smart player, SDM has started learning how not to lose during the first training cycles. The drawing rate grows quickly in the first 500 games and slowly since then. The winning rate grew to around 20% and remained there until 6,000 games, while the drawing rate kept increasing. Then, after learning how not to lose, SDM started learning how to win, since, after 7,000 games, the winning rate started to increase. See Figure 69.

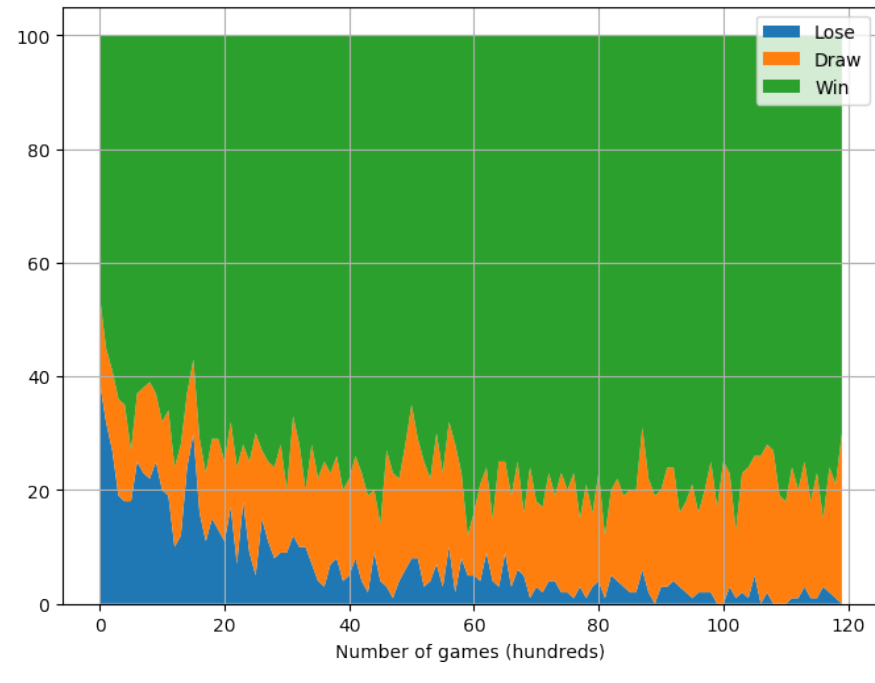
When playing against another SDM player, both player quickly learns how not to lose. During the first 100 testing games, without any learning game, they have behaved like two random players. After the 100 training games, they have learned how not to lose, and the drawing rate grows quickly, reaching 100%. See Figure 70.

When playing against mixed players, SDM has also adapted. In Figure 71, it has played 6,000 games against the random player, the

smart player, and another SDM player. In each cycle, one of them was randomly chosen. The number of losses over time is decreasing, whereas the number of wins and draws change a lot. It is easy to notice when the other SDM player was chosen since all games in that cycle have drawn.

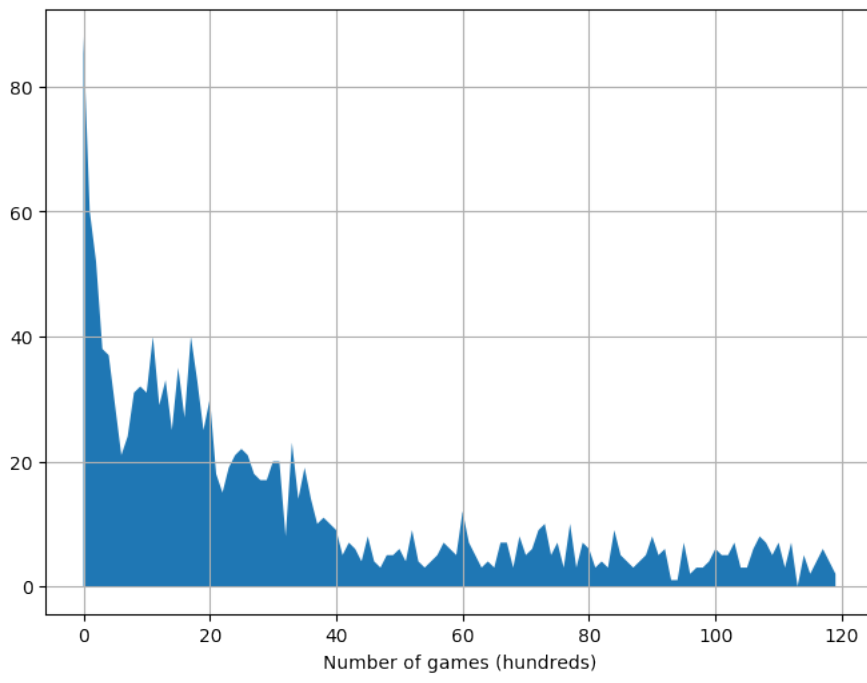


(a) Losses over time

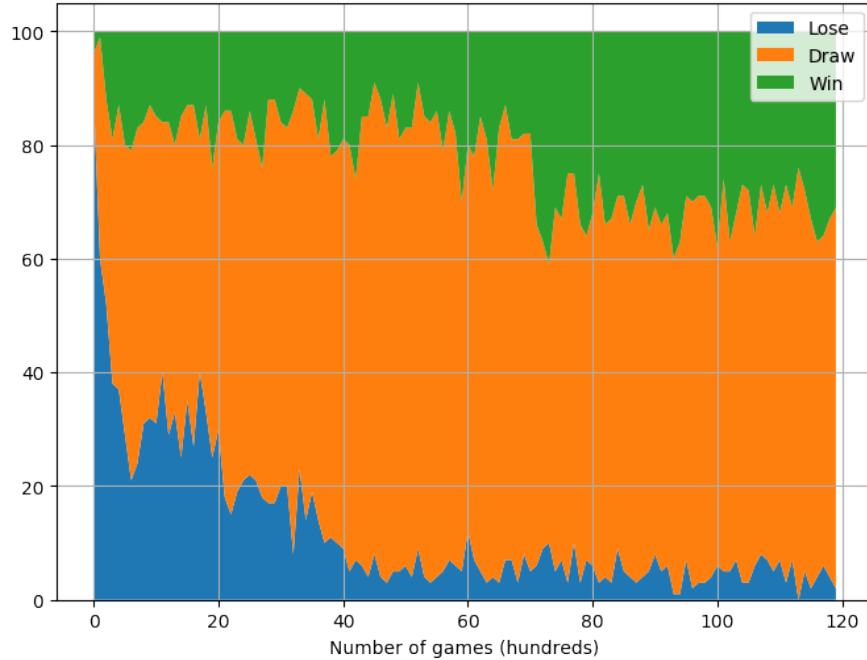


(b) Results over time

Figure 68: Results playing against the random player. Each cycle was made of 100 games for training, and then 100 games for measuring statistics.



(a) Losses over time



(b) Results over time

Figure 69: Results playing against the smart player. Each cycle was made of 100 games for training, and then 100 games for measuring statistics.

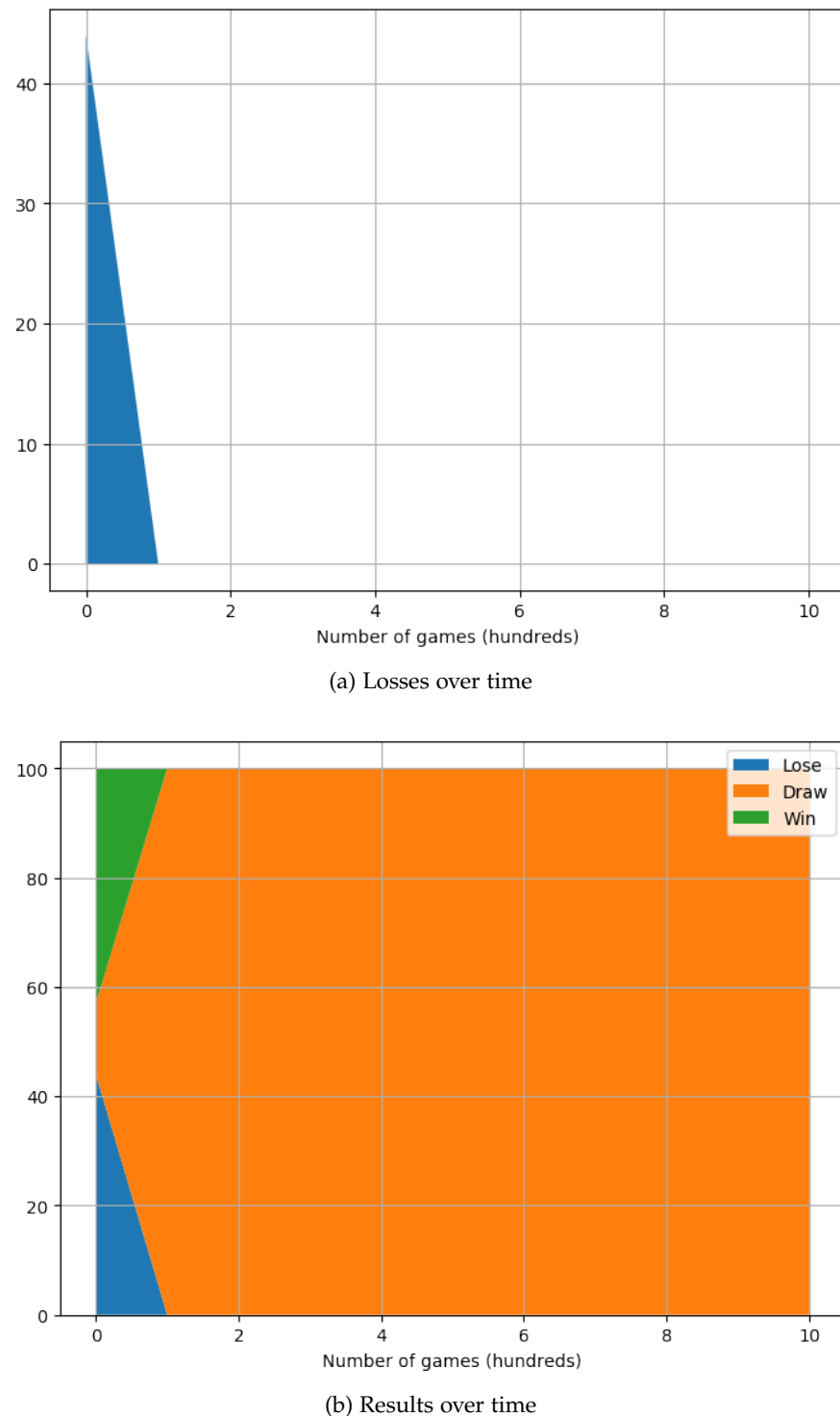


Figure 70: Results playing against another SDM player. Each cycle was made of 100 games for training, and then 100 games for measuring statistics.

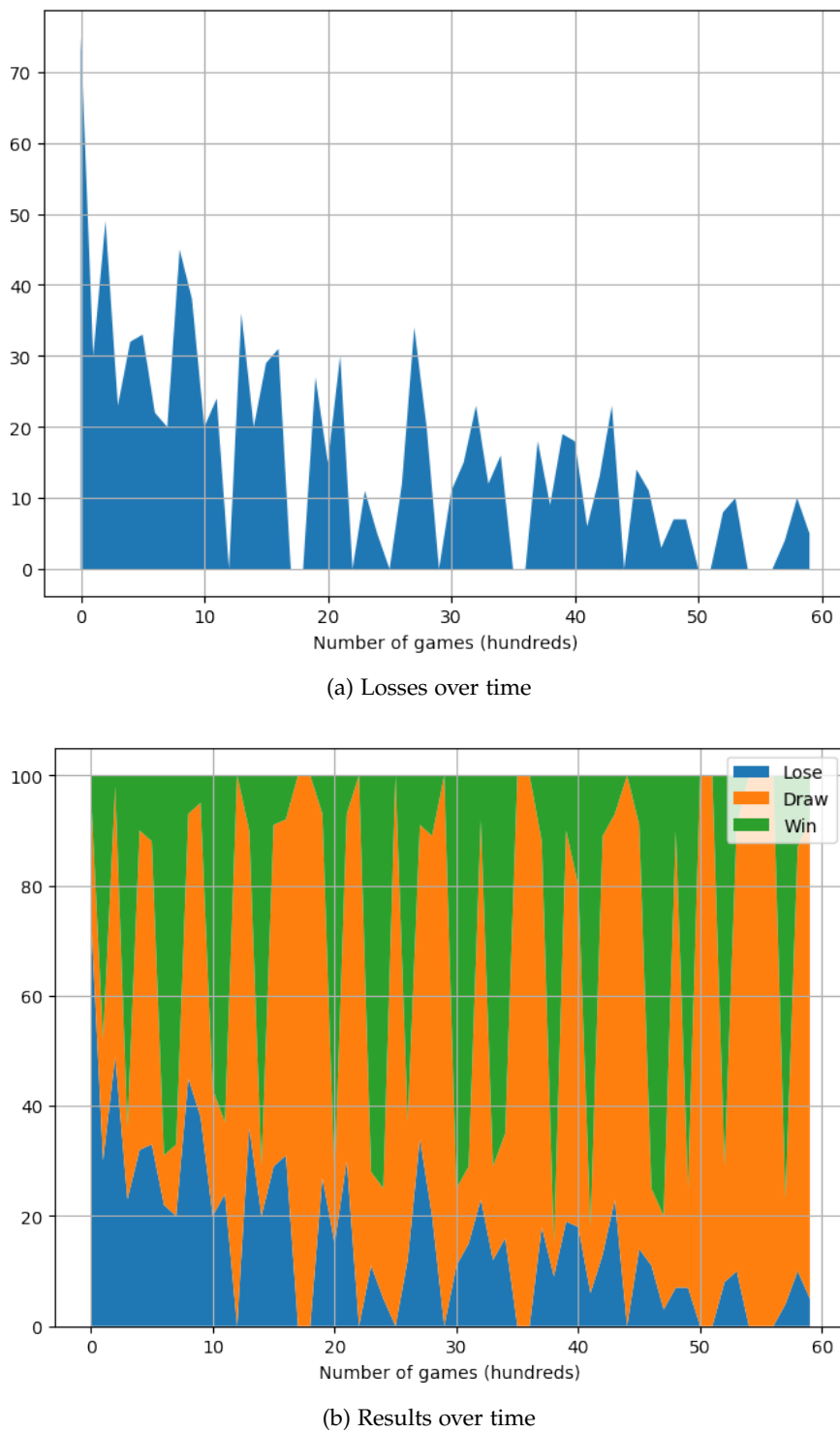


Figure 71: Results playing against a randomly chosen player between random player, smart player, and another SDM player. Each cycle was made of 100 games for training, and then 100 games for measuring statistics.



## RESULTS (IX): INFORMATION-THEORETICAL WRITE OPERATION

---

My advisor, Alexandre Linhares, has proposed another write operation: an information-theoretical weighted write. In it, the sum of the counter's value is weighted based on the distance between each hard location's address and the reading address. The logic behind it is to vary the importance of each hard location inside the circle. It is only natural that one encodes an item in closer hard locations with a stronger signal, and a natural candidate for this signal function is the amount of information contained in the distance between the item and each hard location. Closer hard locations have lower probabilities and therefore should encode more information.

Note that this is not the first time in which a weighted function has been applied to writing in SDM — Hely et al. [34] suggest a rather complex spreading model based on floating point signals in the interval [0.05, 1.0] — they were, however, only able to test their model with 1,000 hard locations.

Consider the following. Information Theory [18] let us compute the precise amount of information in an event when given its probability  $p$ , through the measure of *self-information*:

$$I(p) = -\log_2(p)$$

Now, given any two  $n$ -sized bitstrings, the probability of their Hamming distance being exactly  $d$  is given by  $P(X = d) = 2^{-n} \binom{n}{d}$ , and the probability of it being at most  $d$  is:

$$P(X \leq d) = 2^{-n} \sum_{i=0}^d \binom{n}{i}$$

But we must consider that not all hard locations are activated in each write operation, which changes our probability function. Thus, let  $r$  be the access radius then:

$$\begin{aligned}
P(X = d | X \leq r) &= \frac{P((X = d) \cap (X \leq r))}{P(X \leq r)} \\
&= \frac{P(X = d)}{P(X \leq r)}, \quad \text{as } d \leq r \\
&= \frac{2^{-n} \binom{n}{d}}{2^{-n} \sum_{i=0}^r \binom{n}{i}} \\
&= \frac{\binom{n}{d}}{\sum_{i=0}^r \binom{n}{i}}, \quad d \leq r
\end{aligned}$$

And the probability of it being at most  $d$  is:

$$P(X \leq d | X \leq r) = \frac{\sum_{i=0}^d \binom{n}{i}}{\sum_{i=0}^r \binom{n}{i}}, \quad d \leq r$$

As expected,  $P(X \leq d | X \leq r) = 1$  when  $d = r$ .

Hence the weighted write would, on each hard location, sum (or subtract) using the following weights, as seen in Figure 72:

$$w(d) = -\log_2 (P(X = d | X \leq r)) = -\log_2 \binom{n}{d} + \log_2 \sum_{i=0}^r \binom{n}{i}, \quad d \leq r$$

The initial results of this *Shannon write* operation can be seen in Figure 73 and seem promising. It seems that, when  $n = 1,000$ ,  $H = 1,000,000$ ,  $r = 451$ , and 10,000 written random bitstrings, the critical distance increased from around 221 to around 250. This increase may be interpreted as an improvement in SDM, because it would converge to the correct bitstring even for farther bitstrings. Note that 29 additional bits imply an attractor area  $2^{29}$  times larger than the original. This Shannon write may affect memory capacity [16, 17, 84] — possibly increasing it. Another point to keep in mind is that, since the modulus of the vectors are not uniform in this approach, the shape of the attractor may have asymmetries. Whereas these are just some initial tests, the idea seems meritorious so far. As for future research, we will execute all tests in the thesis and compare this Shannon write with the original Kanerva model.

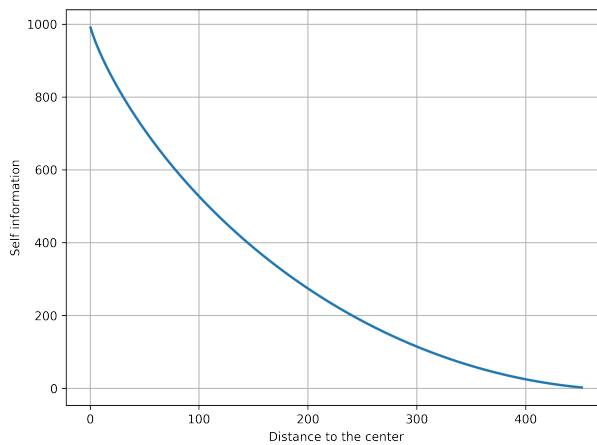
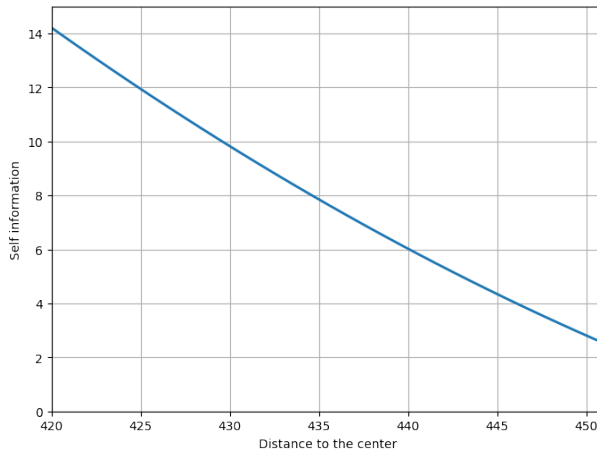
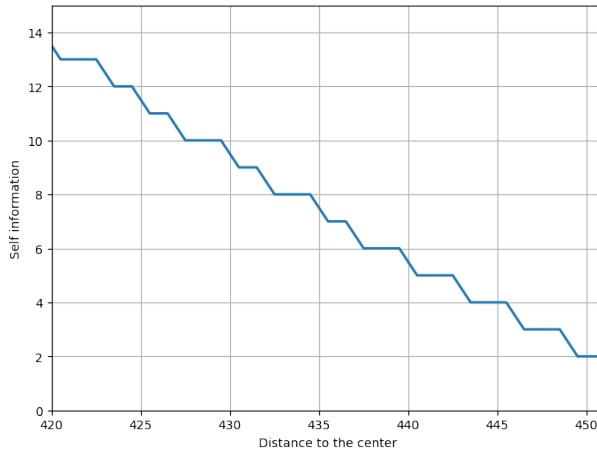
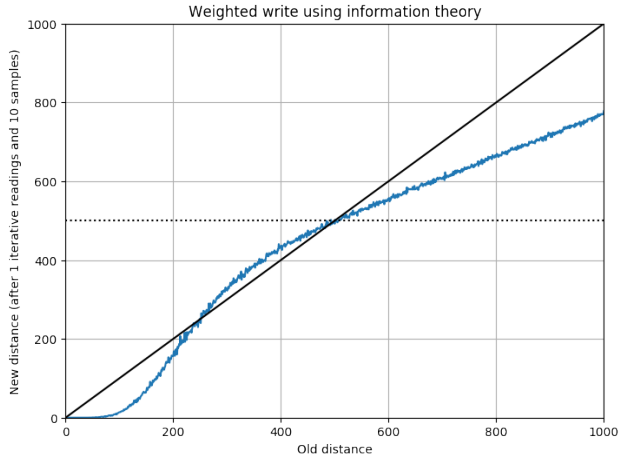
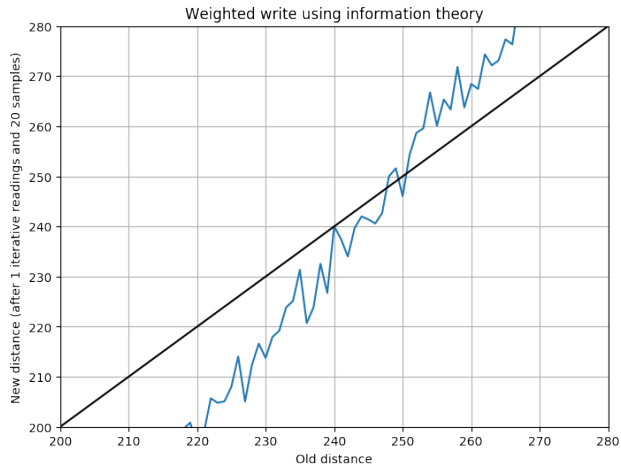
(a)  $w(d)$ ,  $d \in \{1, 2, \dots, n\}$ .(b)  $w(d)$  for the desired range.(c) Stepwise  $[w(d)]$  for fast integer computation.

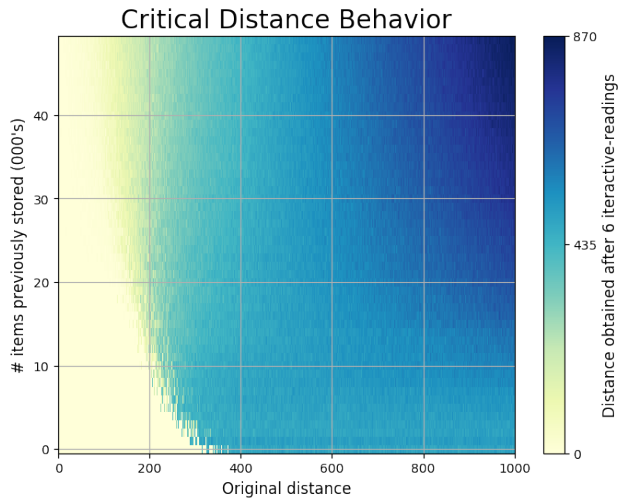
Figure 72: Shannon write operation: Computing the amount of information of a signal to each hard location in its access radius. (a) entirety of the space; (b) region of interest; (c) Fast integer computation is possible through a stepwise function.



(a) Write process weighted by the amount of information contained in the distance between the written bitstring and each hard location



(b) Zoom in Figure 73a



(c) Behavior of weighted write operation according to the distance from the center and the number of items previously stored in the memory

Figure 73: Behavior of the critical distance under the information-theoretic weighted write operation when  $n = 1,000$ ,  $H = 1,000,000$  and  $r = 451$ .

## CONCLUSION

---

*The most exciting phrase to hear in science, the one that heralds new discoveries, is not ‘Eureka!’ (I found it!) but “That’s funny...”*

— Isaac Asimov

Sparse Distributed Memory is a viable model of human memory, yet it does require researchers to (re-)implement a number of parallel algorithms in different architectures.

We provide a new, open-source, cross-platform, highly parallel framework in which researchers may be able to create hypotheses and test them computationally with minimal effort. The framework is well-documented for public release at this time (<http://sdm-framework.readthedocs.io>), it has already served as the backbone of Chada’s Ph.D. thesis [13]. The single-line command “`pip install sdm`” will install the framework on posix-like systems, and single-line commands will let users test the framework, generate some of the figures from Kanerva’s theoretical predictions in their own machines, and — if interested enough —, test their own theories and improve the framework, and the benchmarks used to evaluate the framework, in open-source fashion. It is our belief that such work is a necessary component towards accelerating research in this promising field.

Here are interesting questions that have been considered during this work, but have had to be left for future research.

### 14.1 ANOTHER ‘FUNNY THING’...

Over the course of this work we looked into a ‘funny thing’ that had appeared in my master’s thesis: the graphs of convergence did not reflect the original expectations put forth by Kanerva, and neither my own previous calculations. These numerical results pointed us back to the math and to some interesting random variables not studied before.

Another funny thing that has appeared in my master’s thesis was that the critical distance collapsed when the network was exclusively writing ‘random-at-x’. This is something I would like to look into but have not had the time to conduct a proper study yet.

## 14.2 MAGIC NUMBERS

Kanerva suggests, in his book, the use of 1,000 dimensions and 1,000,000 hard locations. More recently, he suggested the use of 10,000 dimensions, and on personal discussions suggested that this should be a minimum; as he has been concerned in latent semantic analysis and seems to be the proper scale in that application.

Each parameter set choice like this will lead to particular numbers — many of them emergent —, such as the access radius size, critical distance, memory capacity, and so forth. For example, the number of dimensions  $n$  leads to the number of standard deviations available on the space:  $2\sqrt{n}$ . One then must choose a proper multiple  $m \times \sigma$ : Kanerva (and most in the literature) have been using  $m = 3$ , as  $\mu - 3\sigma$  selects approximately 1/1000 of the space. These constants will determine the size of the access radius. Then one must choose the number of hard locations, which will determine how many hard-locations are activated on average; and so on and so forth...

One intriguing question here is: is there a ‘better’ number of dimensions and hard locations? If so, can such numbers be better studied algebraically or numerically? How should these parameters be compared? What are the tradeoffs that should be considered? What are the ‘best’ benchmarks possible?

## 14.3 SYMMETRICAL, RAPIDLY ACCESSIBLE, HARD LOCATIONS

A hypercube with  $n$  dimensions can be divided by two hypercubes with  $n - 1$  dimensions. Is there an algorithm that separates the area of each hard location in such a form that there exists a function mapping each bitstring in  $\{0,1\}^n$  to the set of hard locations it ‘belongs to’? Though this would break Kanerva’s assumption of a randomly yet uniformly distributed set of hard locations — for a perfectly symmetrical set of hard locations —, there could be large performance gains if such a mapping function from a bitstring to its corresponding set of nearest hard locations exists. Note that others have attempted heuristic approaches to this<sup>1</sup>.

Consider the hypercube with  $n$  dimensions. We want to select a subset of its vertices with cardinality  $2^{20}$  that is symmetrically distributed over the space. Afterward,  $\forall b \in \{0,1\}^n$ , we want an algorithm  $A$  that yields the particular list of hard locations for  $b$  and all hard locations respect the desired properties of the memory.

A reduction from measuring the distance to  $2^{20}$  hard locations to a computation of  $2^{10}$  hard locations might yield astonishing

---

<sup>1</sup> Kanerva [42] has recently mentioned that ‘The computationally most efficient implementation of it, by Karlsson [51], is equivalent to the RAM-based WISARD of Alek-sander et al. [3].’ Note, however, that Karlsson’s model may introduce non-uniform asymmetries in the space, and seems to require a staggering  $O(2^n)$  hard-locations.

performance gains, depending, of course, on our optimistic assumptions concerning existence and complexity of such algorithm. At large scales of computing, the very ability to perform some experiments is a function of sheer performance. The horizon of experiments — and possibly of knowledge — expands *as a function of computational demands*. A little more on this will follow below.

#### 14.4 "I" VERSUS "L"

The classification algorithm had some problems classifying the patterns "i" and "l", due to the low distance between them. In this case, SDM could not discriminate the differences — it has only considered the big picture. Although this behavior is close to how humans see things, we also have the ability to zoom and focus on the details, clearly discerning letter "i" from letter "l".

I have run the classification algorithm under the MNIST database of handwritten digits [23]. First, SDM has been trained with the 60,000 training images, and then it classified the 10,000 testing images. In these initial tests, the memory has given the correct classification for 79.22% of the images, which is inferior to the specialized algorithms. For instance, in 1998, LeCun et al. [57] have developed algorithms which achieve from 88% through a linear classifier, to 99.7% through a convolutional net. For a review of algorithms' performance in the MNIST database, see [23].

Looking into the reason behind images incorrectly classified, I have found that the issue is very related to the "i" versus "l" issue. Some handwritten digits are very close to others, and a "2" or a "7" may look like a "1", for instance. So, how can we solve this issue without using anything specific to images? Machine learning algorithms use specific techniques to improve performance. I would like to unveil a solution psychologically closer to how we behave — even if that eventually leads to lower performance.

An unexplored idea is to use multiple SDMs which communicate. A first SDM would write the whole picture, just like we have done. Another SDM would write specific regions of the image, just like our eye focusing on specific regions. When reading, they may compose the counters and give a more precise classification.

#### 14.5 DEEP LEARNING, MULTIPLE SDMS — AND THE INCREDIBLE ANIMAL BEHAVIOR OF DR. LINHARES

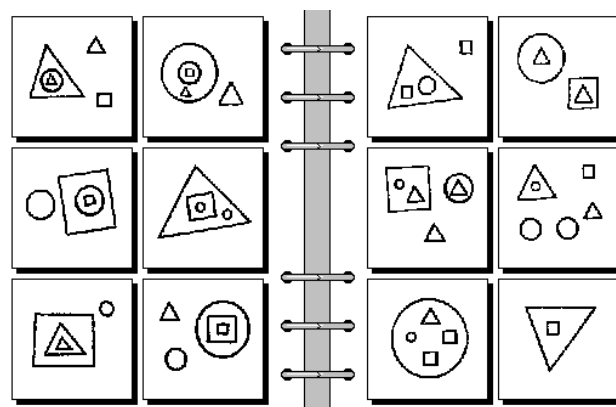
There is the intention of studying what, if any, capabilities do multiple SDMs have... yet it is probably advisable to leave the following comments as originally made by my advisor, Dr. Linhares. To quote:

System 1	System 2
Unconscious Reasoning	Conscious Reasoning
Implicit	Explicit
Automatic	Controlled
Low Effort	High Effort
Large Capacity	Small Capacity
Rapid	Slow
Default Process	Inhibitory
Associative	Rule-Based
Contextualized	Abstract
Domain Specific	Domain General
Evolutionarily Old	Evolutionarily Recent
Nonverbal	Linked to language
Includes recognition, perception, orientation	Includes rule following, comparisons, weighing of options
Modular Cognition	Fluid Intelligence
Independent of working memory	Limited by working memory capacity
Non-Logical	Logical
Parallel	Serial

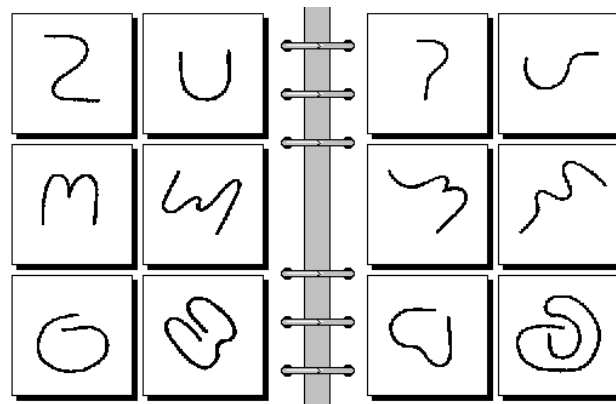
Table 7: Dual process theories.

Those deep neural networks... alphaGo... alphazero... very impressive, and to me very right and proper in a sense and also very wrong and misguided in another. I have not seriously studied the topic. Eric Nichols explained it to me in a napkin, and I watched some youtube videos and browsed the books. So what follows, like all great science, is completely based on gossip and hearsay, prejudice and anecdote. Or at least that's how I believe all great *hunches* over what is promising and what is a dead-end come from; that aesthetic sense that forms over time and seems to guide us towards what feels beautiful and correct and away from what seems foolish and wasteful...

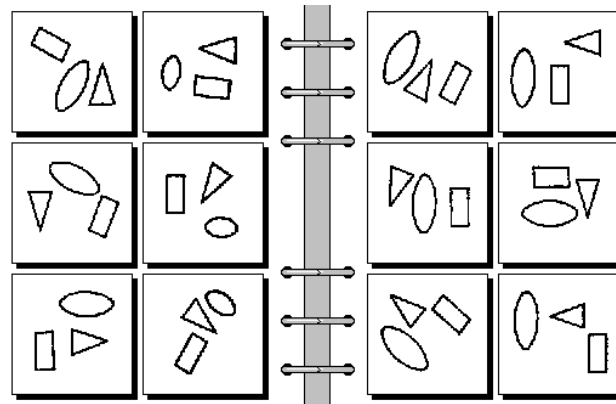
So here is my hunch: *SDM is System 1 and System 1 is SDM* (e.g., as in Table 7). I haven't seen anyone say this out loud, but Kanerva has pretty much nailed system 1 — I feel he is at least 90% right.



(a) Bongard problem 71



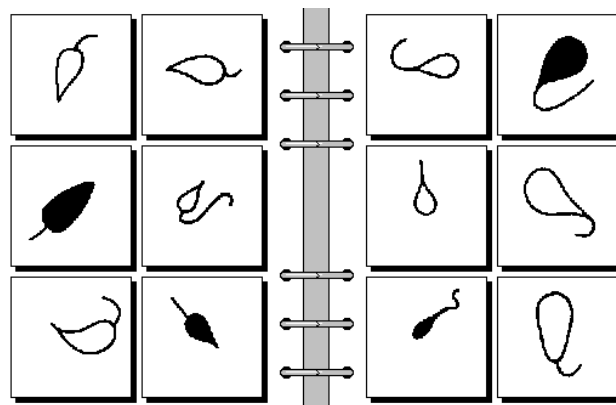
(b) Bongard problem 72



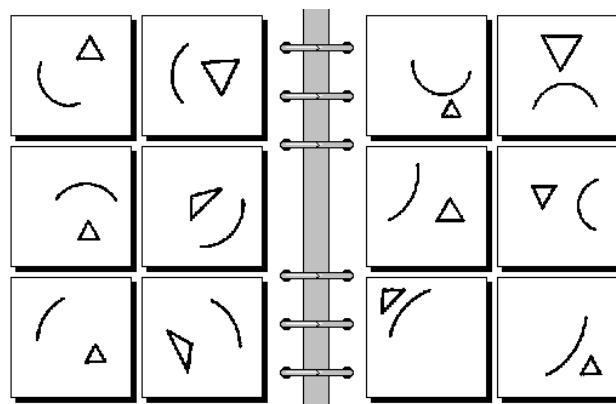
(c) Bongard problem 73

Figure 74: Bongard problems 71 - 73, courtesy of noted Bongardologist, Dr. Harry Foundalis. What distinguishes the boxes on the left hand side to those on the right hand side?

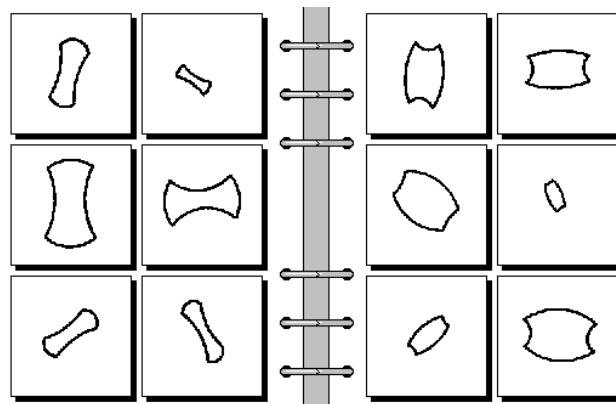
You know those animals that create those burrows underground, creatures like the prairie dogs? There, underground, they build all sorts of passageways from here to where they want to go; and in the process they discover all that *can't be passageway*. What can't be



(a) Bongard problem 74

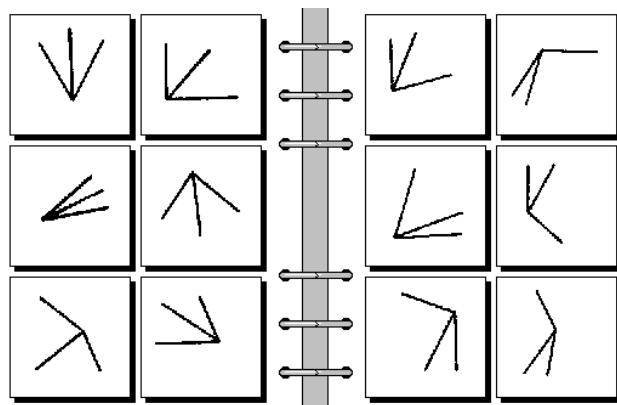


(b) Bongard problem 75

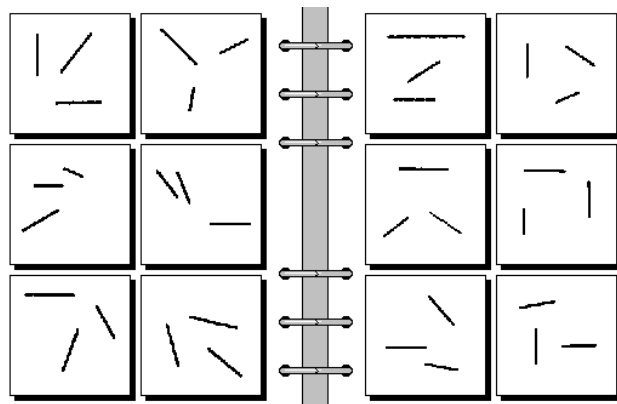


(c) Bongard problem 76

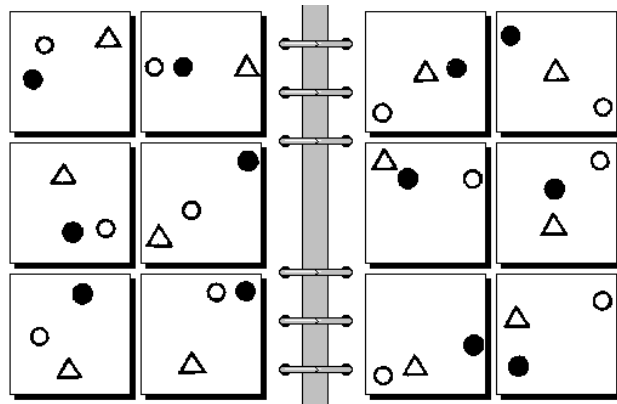
passageway — what can't be corridor — will never be used as passageway, by definition. And most of the world can't be passageway. Think about the animal behavior: endless dead-end nooks and crannies yet the beast won't give up! To me it's all very similar to what these systems seem to be doing... it seems they are crafting and molding a model of their problem; discovering what can't be passageway and finding some other route, very tortuous if need be... You have these monstrous networks



(a) Bongard problem 77



(b) Bongard problem 78



(c) Bongard problem 79

creating layers upon layers in which they differentiate and distribute the errors throughout all the nooks and crannies of, say, a domain like the game of Go. Then, after some biblical number-crunching, it seems that there may be a very subtle way... however tortuous, however tight, however improbable, however uncomfortable.

And these machines are exhibiting intelligence. The victories in the game of Go seem to have shown that

alphaGo did have vague, non-explicit, non-formal, but very strong intuitions about what the nooks and crannies of the Go universe looks like. So here is what I like and I find beautiful: These gigantic clusters of inter-related micro impressions that the system has acquired and can relate to. I imagine multiple SDMs exchanging information; gossiping to each other about all the dead-ends out there and trying to find some tiny tortuous pathway, and it feels to me that that's a good and proper way to move forward in research.

But it feels like a mistake to say that that is thinking. It's not. It is to me a great model of someone getting so attuned into an area that they are able to simply flow through tasks; in the positive psychology sense of the word flow. It's very powerful and very intelligent: but it is a form of intelligence without thinking. Intelligence that can't make leaps from one arena to another; Intelligence that can't work on Bongard problems. So what I would fear as a dead-end in research would be to have another AI winter... decades of massive, massive number-crunching and machine learning of this type... in disregard to big questions such as the interaction of short-term memory with SDM and, again, tasks like Bongard problems (Figure 74). Bongard problems demand high-gossip between system 1 and system 2; they demand a high dose of imagination and mental imagery manipulation; they demand discrimination and demand clusterization, among many other things that have been spelled out before by Bongard [6], Hofstadter [35], Linhares [60] and the landmark, deep, study being Foundalis [30].

Cognitive Science has to study the *plausible* interaction between system 1 and system 2. We can't continue to study, say, a silly, implausible, model of system 1 and a great model of system 2 (or vice-versa). We need both system 1 and system 2 to be plausible, in the psychological sense and in the neuroscientific sense. AlphaGo, for instance, has this wonderful model of the game, reflecting many of the properties of system 1... but then falls back into silliness as soon as it turns to the other side of the problem: it uses montecarlo methods in very efficient fashion to probe some 70,000 thousands of positions per second and go on to the next probing of this wonderful system 1...

It works; it is impressive; it is intelligent; but it is not thinking; and it hasn't thought us much about our cognition.

Hofstadter has nailed the interactions and the content... analogies, fluid concepts, things seen through a different perspective, abstract roles, variations on a theme, etc. Kanerva has nailed system 1, long-term-memory, and its theoretical neuroscience; micro neuro-firings bringing a memory back to life. Isn't it time to work on System 2 models that are counterparts to SDM — in fact, isn't it obvious that that's our glaring omission? Attaching something as beautiful as SDM to, say, some centralized hyper-efficient montecarlo algorithm is nothing short of heresy against all the gods of science for which the villain shall be put to death without clemency or mercy. Seems like the only reasonable path going forward...

#### 14.6 NOT A REAL CONCLUSION

Project	Observation
Source-code	C, OpenCL, Python (NVIDIA CUDA, FP-GAs desirable in the future)
Step-by-step notebook studies	replication and dissemination of studies
Documentation of framework	100+ pages currently
Open-Source Creative Commons Book	Under consideration (to be created from this thesis)
Collection of SDM links, results, resources	modeled after 'Awesome Machine Learning' <a href="#">[69]</a> and 'Awesome Artificial Intelligence' <a href="#">[58]</a> lists, community managed
Slides from the Jupyter Notebooks	online course, currently in planning phase
Videos following the Course Slides	online course, currently in planning phase

Table 8: Desiderata of open-source, creative-common deliverables, longer-term. Some of these items are mature for wide dissemination, whereas others are in planning phase. For an online SDM course, for instance, we might partner with a Ph.D. program in the Teaching of Mathematics and Physics, such as IM/UFRJ [\[38\]](#), who are intent on developing and measuring the effects of new educational tools.

Let us revisit, in these concluding thoughts, the emphasis employed over speed of computation. At first sight, that might seem like a typical objective of efficiency in computer science. But we are not only interested in the computer science effects here — the ambition is different. More important than this ‘computer-scency’ goal, i.e., a beautiful, clean, efficient algorithm with the primary effect of enhanced speed, however, is the secondary effect on the sociology of science: communities form around open-source code, specialists in a particular arena magnify the capabilities of the code, debates and meetings are regularly held, and deep divisive disagreements lead to community splits in multiple potential directions of exploration. In a very real sense, given a shared code to work and experiment on, we can see farther.

Beyond speed, I have also strived for *ease of use* and *replicable studies*. All the simulations and graphics generated in this thesis are promptly available to be re-executed and explored by those interested. Most importantly, they also serve as a tutorial for learning about the framework’s design, and perhaps as a teaching tool for SDM itself. I have generated a Docker image, which makes it even easier to explore the framework by delegating heavy computational work to cloud services. After running the container, a Jupyter Notebook is available with sdm-framework and other tools already installed. We invite the reader to take a look and explore a little bit.

The overarching intention here is to not only provide a starting point, but to provide a documented Framework in which SDM research can be conducted. Consider having the ability to compare the results of a new (‘forked’) model to the previous ‘best’ (under a particular benchmark set). For example, some of the benchmarks that we plan to develop in future research are: how fast is convergence through iterative reading? How large is the attractor of the critical distance? How well does the system filter noise? How well does the system work under the supervised learning task? And other authors may be able to improve this benchmark set themselves, as is usual in open source development. It is perhaps this facility of ease to build on top of previous work that seems most exciting at this stage.

Consider the misunderstanding concerning the SDM read operation: Dr. Stan Franklin describes Kanerva’s read operation in a way that each hard location, at each dimension, provides only a single bit of information to the read operation (instead of Kanerva’s full counter). We have referred to this modified read operation as Chada read<sup>2</sup>. Having an open, testable, codebase reduces the possibilities of such misunderstandings in the long run. Indeed, a

---

<sup>2</sup> Legend has it that my friend & colleague, Dr. Daniel de Magalhães Chada, along with Linhares, did not consult and re-check with Kanerva’s book and only discovered the discrepancy in code and ideas a couple of years afterward.

high-quality codebase seems to have become a scientific community's form of unequivocally standing behind a consensus. For example, the journal *Nature* analyzed the top-100 cited papers in history, to find:

... some surprises, not least that it takes a staggering 12,119 citations to rank in the top 100 — and that many of the world's most famous papers do not make the cut. A few that do, such as the first observation of carbon nanotubes (number 36) are indeed classic discoveries. But the vast majority describe experimental methods or software that have become essential in their fields. [...] The list reveals just how powerfully research has been affected by computation and the analysis of large data sets.

— Van Noorden et al. [92], emphasis mine.

It is no coincidence that scientific journals such as *BMC Neuroscience*, or the *Journal of Machine Learning Research* have specific sections on open-source software. The journal *Neurocomputing* states, bluntly: "software is scientific method by machine".

Of course, for the skeptical reader who may consider software a less worthy pursuit, there is also new work here. The mathematics of the model has been shown to be correct numerically (with a single, small, anomaly); we have shown how to execute unsupervised learning with nothing besides operations original to the SDM; we have studied the generalized Murilo read; we have seen noise filtering; the death of neurons; how information-theory may be of use; and finally, we have reproduced numerous of the original propositions put forth by Kanerva. The emphasis might have been on the *breadth of topics*, in detriment of depth here or there. The work on, say, reinforcement learning, is most definitely not the last word we will see on the subject, but a challenge left for readers to contemplate. But this is due to our research group's enthusiasm for the topic; we do indeed believe that SDM is — if not correct — extremely close to a full scientific understanding of human long-term memory. If so, it is such a monumental achievement that we want readers to be able to see all of what we see and imagine the vastness of possibilities.

Ralph Waldo Emerson once said: *do not go where the path may lead. Go, instead, where there is no path, and leave a trail.* Professor Pentti Kanerva has left the trail. It is my job to illuminate it and to pave it and to clear it; to try to deliver an easier pathway for the next generation. Some essays completely shut the door close at the end; this one intends to leave it wide open. As the reader might have noticed, this final section does not read as an analysis of the work done; it reads, instead, as a *desideratum*, a prologue, a yearning for others to join me in imagining the shape of things to come.



# 15

## APPENDIX

---



## LIST OF JUPYTER NOTEBOOKS

---

1. Calculate critical distance.ipynb
2. Calculate radius for any SDM.ipynb
3. Classification Test 1.ipynb
4. Classification Test 2.ipynb
5. Classification Test 3-Copy1.ipynb
6. Classification Test 3.ipynb
7. Critical Distance - New.ipynb
8. Critical Distance.ipynb
9. Distance between bitstrings.ipynb
10. Distances of activated hard-locations.ipynb
11. Generates a new SDM.ipynb
12. Intersection of activated hard-locations.ipynb
13. Kanerva-Table-7 - Experiment.ipynb
14. Kanerva-Table-7.3 - Generic Read.ipynb
15. Kanerva-Table-7.3 - Multiple dimensions.ipynb
16. Kanerva-Table-7.3 - Weighted table write.ipynb
17. Kanerva-Table-7.3.ipynb
18. Kanerva's Figure 1.2.ipynb
19. Noise filter 2.ipynb
20. Noise filter A-Z 0-1 Generator.ipynb
21. Noise filter with labels.ipynb
22. Noise filter.ipynb
23. Number of activated hard-locations.ipynb
24. Performance test.ipynb
25. Reseting hard-locations.ipynb
26. Sequences (Kanerva Ch 8).ipynb

- 27. Sequences in one SDM (Kanerva Ch 8).ipynb
- 28. TicTacToe.ipynb
- 29. Weighted operations using information.ipynb

## BIBLIOGRAPHY

---

- [1] Sparse distributed memory, January 2018. URL [https://en.wikipedia.org/w/index.php?title=Sparse\\_distributed\\_memory&oldid=822493454](https://en.wikipedia.org/w/index.php?title=Sparse_distributed_memory&oldid=822493454). Page Version ID: 822493454.
- [2] M. A. Aguiar and R. M. S. Julia. SDM-Go: An Agent for Go with an Improved Search Process Based on Monte-Carlo Tree Search and Sparse Distributed Memory. In *2013 IEEE 16th International Conference on Computational Science and Engineering*, pages 424–431, December 2013. doi: 10.1109/CSE.2013.71.
- [3] Igor Aleksander, Thomas John Stonham, and BA Wilkie. Computer vision systems for industry. *Digital Systems for Industrial Automation*, 1(4):305–320, 1982.
- [4] Ashraf Anwar and Stan Franklin. Sparse distributed memory for ‘conscious’ software agents. *Cognitive Systems Research*, 4(4):339–354, December 2003. ISSN 13890417. doi: 10.1016/S1389-0417(03)00015-9. URL <http://linkinghub.elsevier.com/retrieve/pii/S1389041703000159>.
- [5] Martin Berchtold. Processing Sensor Data with the Common Sense Toolkit (CSTK). Technical report, March 2005. URL [https://www.researchgate.net/publication/241441844\\_Processing\\_Sensor\\_Data\\_with\\_the\\_Common\\_Sense\\_Toolkit\\_CSTK](https://www.researchgate.net/publication/241441844_Processing_Sensor_Data_with_the_Common_Sense_Toolkit_CSTK).
- [6] M. M. Bongard. *The recognition problem*. July 1968. URL <http://www.dtic.mil/docs/citations/AD0682462>.
- [7] M. S. Brogliato. Understanding the critical distance in sparse distributed memory. Master’s thesis, Escola Brasileira de Administração Pública e de Empresas - EBAPE, Fundação Getulio Vargas, 2011.
- [8] Marcelo Brogliato. SDM Framework Documentation. URL <http://sdm-framework.readthedocs.io/>.
- [9] Marcelo S Brogliato, Daniel M Chada, and Alexandre Linhares. Sparse distributed memory: understanding the speed and robustness of expert memory. *Frontiers in Human Neuroscience*, 8: 222, 2014.
- [10] Alan S Brown. A Review of the Tip-of-the-Tongue Experience. *Psychological Bulletin*, 109(2):204–223, 1991.

- [11] Roger Brown and David McNeill. The Tip of the Tongue phenomenon. *Journal of Verbal Learning and Verbal Behavior*, 5:325–337, 1966.
- [12] CCRG. CCRG - Cognitive Computing Research Group - Projects. URL <http://ccrg.cs.memphis.edu/projects.html>.
- [13] Daniel de Magalhães Chada. *Are you experienced? Contributions towards experience recognition, cognition, and decision making*. PhD thesis, 2016.
- [14] Timothy M Chan, Kasper Green Larsen, and Mihai Pătrașcu. Orthogonal range searching on the ram, revisited. In *Proceedings of the twenty-seventh annual symposium on Computational geometry*, pages 1–10. ACM, 2011.
- [15] Bernard Chazelle. A functional approach to data structures and its use in multidimensional searching. *SIAM Journal on Computing*, 17(3):427–462, 1988.
- [16] P. A. Chou. The capacity of the Kanerva associative memory. *IEEE Transactions on Information Theory*, 35(2):281–298, March 1989. ISSN 0018-9448. doi: [10.1109/18.32123](https://doi.org/10.1109/18.32123).
- [17] Philip A Chou. The Capacity of the Kanerva Associative Memory is Exponential. In *Neural information processing systems*, pages 184–191, 1988.
- [18] Thomas M Cover and Joy A Thomas. *Elements of information theory*. John Wiley & Sons, 2012.
- [19] N. Cowan. The magical number 4 in short-term memory: A reconsideration of mental storage capacity. *Behavioral and Brain Sciences*, 24:87–185, 2000.
- [20] The CSTK Developers. CSTK: The CommonSense ToolKit. URL <http://cstk.sourceforge.net/>.
- [21] Tomasz S. Czajkowski, Utku Aydonat, Dmitry Denisenko, John Freeman, Michael Kinsner, David Neto, Jason Wong, Peter Yianacouras, and Deshanand P. Singh. From OpenCL to high-performance hardware on FPGAS. In *22nd International Conference on Field Programmable Logic and Applications (FPL)*, pages 531–534. IEEE, August 2012. ISBN 978-1-4673-2256-0. doi: [10.1109/FPL.2012.6339272](https://doi.org/10.1109/FPL.2012.6339272). URL <http://ieeexplore.ieee.org/document/6339272/>.
- [22] Antônio de Pádua Braga and Igor Aleksander. Geometrical treatment and statistical modelling of the distribution of patterns in the n-dimensional boolean space. *Pattern Recognition Letters*, 16(5):507–515, 1995.

- [23] Li Deng. The mnist database of handwritten digit images for machine learning research [best of the web]. *IEEE Signal Processing Magazine*, 29(6):141–142, 2012.
- [24] Peter J. Denning. Sparse Distributed Memory. *American Scientist*, 77:333–335, July 1989. ISSN 0003-0996. URL <http://adsabs.harvard.edu/abs/1989AmSci..77..333D>.
- [25] Blerim Emruli, Fredrik Sandin, and Jerker Delsing. Vector space architecture for emergent interoperability of systems by learning from demonstration. *Biologically Inspired Cognitive Architectures*, 11:53–64, January 2015. ISSN 2212-683X. doi: 10.1016/j.bica.2014.11.015. URL <http://www.sciencedirect.com/science/article/pii/S2212683X14000784>.
- [26] Kuo-Chin Fan and Yuan-Kai Wang. A genetic sparse distributed memory approach to the application of handwritten character recognition. *Pattern Recognition*, 30(12):2015–2022, 1997.
- [27] Charles H. Ferguson and Charles R. Morris. *Computer Wars: The Post-IBM World*. Beard Books, September 2002. ISBN 978-1-58798-139-5. Google-Books-ID: hOdAStd3mR4C.
- [28] M J Flynn, P Kanerva, and N Bhadkamkar. Sparse Distributed Memory: Principles and Operation. Technical Report CSL-TR-89-400, NASA Ames Research Center, 1989.
- [29] S Foldes. A characterization of hypercubes. *Discrete Mathematics*, 17(1):155–159, 1977.
- [30] Harry E Foundalis. *PHAEACO: a cognitive architecture inspired by Bongard’s problems*. PhD thesis, Indiana University, 2006.
- [31] Stan Franklin, Tamas Madl, Sidney D’Mello, and Javier Snaider. LIDA: A Systems-level Architecture for Cognition, Emotion, and Learning. *IEEE Transactions on Autonomous Mental Development*, 6(1):19–41, March 2014. ISSN 1943-0604, 1943-0612. doi: 10.1109/TAMD.2013.2277589. URL <http://ieeexplore.ieee.org/document/6587077/>.
- [32] R. M. French. When coffee cups are like old elephants, or why representation modules dont make sense. In A. Riegler and M. Peschl, editors, *Proceedings of the 1997 International Conference on New Trends in Cognitive Science*, pages 158–163. Austrian Society for Cognitive Science, 1997.
- [33] Frank Harary, John P Hayes, and Horng-Jyh Wu. A survey of the theory of hypercube graphs. *Computers & Mathematics with Applications*, 15(4):277–289, 1988.

- [34] Tim A Hely, David J Willshaw, and Gillian M Hayes. A new approach to Kanerva's sparse distributed memory. *IEEE Transactions on Neural Networks*, 8(3):791–794, 1997.
- [35] Douglas Hofstadter. *Gödel, Escher, Bach: An eternal golden braid*. Basic Books, 1980.
- [36] Douglas R Hofstadter. On seeing A's and seeing As. *Stanford Humanities Review*, 4(2):109–121, 1995. URL <https://web.stanford.edu/group/SRG/4-2/text/hofstadter.html>.
- [37] Y.-S. Hong and S.-S. Chen. Character recognition in a sparse distributed memory. *IEEE Transactions on Systems, Man, and Cybernetics*, 21(3):674–678, June 1991. ISSN 00189472. doi: 10.1109/21.97459. URL <http://ieeexplore.ieee.org/document/97459/>.
- [38] IM/UFRJ. Programa de Pós-Graduação em Ensino de Matemática. URL [http://www.pg.im.ufrj.br/pemat/dout\\_publico.htm](http://www.pg.im.ufrj.br/pemat/dout_publico.htm).
- [39] S. Jockel, F. Lindner, and Jianwei Zhang. Sparse distributed memory for experience-based robot manipulation. In *Proceedings of the 2008 IEEE International Conference on Robotics and Biomimetics*, pages 1298–1303. IEEE, February 2009. ISBN 978-1-4244-2678-2. doi: 10.1109/ROBIO.2009.4913187. URL <http://ieeexplore.ieee.org/document/4913187/>.
- [40] Daniel Kahneman and Amos Tversky. Prospect theory: An analysis of decision under risk. In *Handbook of the fundamentals of financial decision making: Part I*, pages 99–127. World Scientific, 2013.
- [41] P. Kanerva. *Sparse Distributed Memory*. MIT Press, 1988.
- [42] P. Kanerva. Hyperdimensional computing: An introduction to computing in distributed representation with high-dimensional random vectors. *Cognitive Computation*, 1:139–159, 2009.
- [43] Pentti Kanerva. Parallel Structures in Human and Computer Memory. *Cognitiva*, 85, June 1985. URL [https://cseweb.ucsd.edu/~gary/PAPER-SUGGESTIONS/SDM\\_Kanerva.pdf](https://cseweb.ucsd.edu/~gary/PAPER-SUGGESTIONS/SDM_Kanerva.pdf).
- [44] Pentti Kanerva. Sparse Distributed Memory and Related Models. In *Associative Neural Memories: Theory and Implementation*, page 41. Oxford University Press, 1993.
- [45] Pentti Kanerva. The Spatter Code for Encoding Concepts at Many Levels. In Maria Marinaro and Pietro G. Morasso, editors, *ICANN '94*, pages 226–229. Springer London, London, 1994. ISBN 978-3-540-19887-1 978-1-4471-2097-1. doi: 10.1007/978-1-4471-2097-1\_52. URL [http://link.springer.com/10.1007/978-1-4471-2097-1\\_52](http://link.springer.com/10.1007/978-1-4471-2097-1_52).

- [46] Pentti Kanerva. Binary spatter-coding of ordered K-tuples. In Gerhard Goos, Juris Hartmanis, Jan Leeuwen, Christoph Malsburg, Werner Seelen, Jan C. Vorbrüggen, and Bernhard Sendhoff, editors, *Artificial Neural Networks — ICANN 96*, volume 1112, pages 869–873. Springer Berlin Heidelberg, Berlin, Heidelberg, 1996. ISBN 978-3-540-61510-1 978-3-540-68684-2. doi: 10.1007/3-540-61510-5\_146. URL [http://link.springer.com/10.1007/3-540-61510-5\\_146](http://link.springer.com/10.1007/3-540-61510-5_146).
- [47] Pentti Kanerva. Fully Distributed Representation. In *In Proceedings RWC Symposium*, pages 358–365, 1997.
- [48] Pentti Kanerva. Hyperdimensional computing: An introduction to computing in distributed representation with high-dimensional random vectors. *Cognitive Computation*, 1(2):139–159, 2009.
- [49] Mingu Kang. In-memory Computing Architectures for Sparse Distributed Memory. *IEEE Transactions on Biomedical Circuits and Systems*, 10:855–862, 2016.
- [50] Mingu Kang, Eric P. Kim, Min-sun Keel, and Naresh R. Shanbhag. Energy-efficient and high throughput sparse distributed memory architecture. In *2015 IEEE International Symposium on Circuits and Systems (ISCAS)*, pages 2505–2508. IEEE, May 2015. ISBN 978-1-4799-8391-9. doi: 10.1109/ISCAS.2015.7169194. URL <http://ieeexplore.ieee.org/document/7169194/>.
- [51] Roland Karlsson. A fast activation mechanism for the kanerva sdm memory. In *SICS Research Report R95:10, Swedish Institute of Computer Science*, pages 69–70, 1995. URL <http://citeseerx.ist.psu.edu/viewdoc/download?doi=10.1.1.44.5112&rep=rep1&type=pdf>.
- [52] James D. Keeler. Comparison between Kanerva’s SDM and Hopfield-type neural networks. *Cognitive Science*, 12(3):299–329, 1988.
- [53] Thomas Kluyver, Benjamin Ragan-Kelley, Fernando Pérez, Brian E Granger, Matthias Bussonnier, Jonathan Frederic, Kyle Kelley, Jessica B Hamrick, Jason Grout, Sylvain Corlay, et al. Jupyter notebooks-a publishing format for reproducible computational workflows. In *ELPUB*, pages 87–90, 2016.
- [54] Hee-Yong Kwon. ATM call admission control using sparse distributed memory. In *Neural Networks, 1997., International Conference on*, volume 2, pages 1321–1325. IEEE, 1997. ISBN 978-0-7803-4122-7. doi: 10.1109/ICNN.1997.616226. URL <http://ieeexplore.ieee.org/document/616226/>.

- [55] Hee-Yong Kwon, Dong-Keyu Kim, Seung-Jun Song, Je-U. Choi, In-Heang Lee, and Hee-Yeung Hwang. ATM call admission control using sparse distributed memory. II. In *Neural Networks Proceedings, 1998. IEEE World Congress on Computational Intelligence. The 1998 IEEE International Joint Conference on*, volume 3, pages 1799–1803. IEEE, 1998.
- [56] Jean-Marie Laborde and Surya Prakash Rao Hebbare. Another characterization of hypercubes. *Discrete Mathematics*, 39(2):161–166, January 1982. ISSN 0012-365X. doi: 10.1016/0012-365X(82)90139-X. URL <http://www.sciencedirect.com/science/article/pii/0012365X8290139X>.
- [57] Yann LeCun, Léon Bottou, Yoshua Bengio, and Patrick Haffner. Gradient-based learning applied to document recognition. *Proceedings of the IEEE*, 86(11):2278–2324, 1998.
- [58] Owain Lewis. Awesome-Artificial-Intelligence: a curated list of Artificial Intelligence (AI) courses, books, video lectures and papers, April 2018. URL <https://github.com/owainlewis/awesome-artificial-intelligence>. original-date: 2015-01-27T09:27:48Z.
- [59] Haitong Li, Tony F. Wu, Abbas Rahimi, Kai-Shin Li, Miles Rusch, Chang-Hsien Lin, Juo-Luen Hsu, Mohamed M. Sabry, S. Burc Eryilmaz, Joon Sohn, Wen-Cheng Chiu, Min-Cheng Chen, Tsung-Ta Wu, Jia-Min Shieh, Wen-Kuan Yeh, Jan M. Rabaey, Subhashish Mitra, and H.-S. Philip Wong. Hyperdimensional computing with 3d VRRAM in-memory kernels: Device-architecture co-design for energy-efficient, error-resilient language recognition. In *2016 IEEE International Electron Devices Meeting (IEDM)*, pages 16.1.1–16.1.4. IEEE, December 2016. ISBN 978-1-5090-3902-9. doi: 10.1109/IEDM.2016.7838428. URL <http://ieeexplore.ieee.org/document/7838428/>.
- [60] Alexandre Linhares. A glimpse at the metaphysics of bongard problems. *Artificial Intelligence*, 121:251–270, 2000. URL <https://www.sciencedirect.com/science/article/pii/S0004370200000424>.
- [61] Alexandre Linhares and Marcelo Salhab Brogliato. Sparse Distributed Memory Framework Documentation. Technical report, February 2018. URL <https://media.readthedocs.org/pdf/sdm-framework/stable/sdm-framework.pdf>.
- [62] Alexandre Linhares, Daniel M. Chada, and Christian N. Aranha. The emergence of Miller’s Magic Number on a Sparse Distributed Memory. *PLOS One*, 6(1):e15592, Jan 2011. doi: 10.1371/journal.pone.0015592.

- [63] Jim Marshall and Lisa Meeden. Technical Report: Learning with a Sparse Distributed Memory. Technical report, Indiana University, Bloomington, Bloomington, Indiana, May 1989.
- [64] Mateus Mendes, Manuel Crisóstomo, and A Paulo Coimbra. Robot navigation using a sparse distributed memory. In *Robotics and automation, 2008. ICRA 2008. IEEE international conference on*, pages 53–58. IEEE, 2008.
- [65] Meng et al. A modified sparse distributed memory model for extracting clean patterns from noisy inputs. *Proceedings of International Joint Conference on Neural Networks*, June 2009.
- [66] Hongying Meng, Kofi Appiah, Andrew Hunter, Shigang Yue, Mervyn Hobden, Nigel Priestley, Peter Hobden, and Cy Pettit. A modified sparse distributed memory model for extracting clean patterns from noisy inputs. In *Proceedings of International Joint Conference on Neural Networks*, pages 2084–2089. IEEE, June 2009. ISBN 978-1-4244-3548-7. doi: 10.1109/IJCNN.2009.5178873. URL <http://ieeexplore.ieee.org/document/5178873/>.
- [67] Antje Meyer and Kathryn Bock. The tip-of-the-tongue phenomenon: Blocking or partial activation? *Memory & Cognition*, 20(6):715–726, 1992.
- [68] G. A. Miller. The magical number seven, plus or minus two: Some limits on our capacity for processing information. *Psychological Review*, 63:81–97, 1955.
- [69] Joseph Misiti. Awesome-Machine-Learning: A curated list of awesome Machine Learning frameworks, libraries and software, April 2018. URL <https://github.com/josephmisiti/awesome-machine-learning>. original-date: 2014-07-15T19:11:19Z.
- [70] Fabio Montagna, Abbas Rahimi, Simone Benatti, Davide Rossi, and Luca Benini. PULP-HD: Accelerating Brain-Inspired High-Dimensional Computing on a Parallel Ultra-Low Power Platform. *arXiv:1804.09123 [eess]*, April 2018. URL <http://arxiv.org/abs/1804.09123>. arXiv: 1804.09123.
- [71] Aaftab Munshi. The OpenCL specification. In *Hot Chips 21 Symposium (HCS), 2009 IEEE*, pages 1–314. IEEE, 2009.
- [72] Kenneth A Norman and Randall C O’reilly. Modeling hippocampal and neocortical contributions to recognition memory: a complementary-learning-systems approach. *Psychological Review*, 110(4):611, 2003.
- [73] Mohammad Norouzi, Ali Punjani, and David J Fleet. Fast exact search in hamming space with multi-index hashing. *IEEE Trans-*

- actions on Pattern Analysis and Machine Intelligence*, 36(6):1107–1119, 2014.
- [74] Ram Pai, Badari Pulavarty, and Mingming Cao. Linux 2.6 performance improvement through readahead optimization. In *Proceedings of the Linux Symposium*, volume 2, pages 105–116, 2004.
- [75] Rajesh Rao and Olac Fuentes. Hierarchical learning of navigational behaviors in an autonomous robot using a predictive sparse distributed memory. *Autonomous Robots*, pages 297–316, 1998.
- [76] Rajesh PN Rao and Dana H Ballard. Natural basis functions and topographic memory for face recognition. In *Proceedings of the 14th International Joint Conference on Artificial Intelligence*, pages 10–19, 1995.
- [77] Frank Ruskey. *Combinatorial Generation*. University of Victoria, working version (1j-csc 425/520) edition, 2003. URL <http://www.math.ubc.ca/~csis/1stworks.com/ref/RuskeyCombGen.pdf>.
- [78] Magnus Sahlgren and Pentti Kanerva. Permutations as a Means to Encode Order in Word Space. page 6.
- [79] Sayeef Salahuddin. Energy Efficient Computing with Hyper-dimensional Vector Space Models. In *2017 International Conference on Simulation of Semiconductor Processes and Devices (SISPAD)*, pages 9–12, Kamakura, Japan. IEEE.
- [80] Helen Shen. Interactive notebooks: Sharing the code. *Nature News*, 515(7525):151, 2014.
- [81] Marcus Tadeu Pinheiro Silva, Antônio Pádua Braga, and Wilian Soares Lacerda. Reconfigurable co-processor for Kanerva’s sparse distributed memory. *Microprocessors and Microsystems*, 28(3):127–134, April 2004. ISSN 01419331. doi: 10.1016/j.micpro.2004.01.003. URL <http://linkinghub.elsevier.com/retrieve/pii/S0141933104000043>.
- [82] David Silver, Thomas Hubert, Julian Schrittwieser, Ioannis Antonoglou, Matthew Lai, Arthur Guez, Marc Lanctot, Laurent Sifre, Dharshan Kumaran, Thore Graepel, et al. Mastering chess and shogi by self-play with a general reinforcement learning algorithm. *arXiv preprint arXiv:1712.01815*, 2017.
- [83] David Silver, Julian Schrittwieser, Karen Simonyan, Ioannis Antonoglou, Aja Huang, Arthur Guez, Thomas Hubert, Lucas Baker, Matthew Lai, Adrian Bolton, et al. Mastering the game of go without human knowledge. *Nature*, 550(7676):354, 2017.

- [84] Gunnar Sjodin. Improving the Capacity of SDM. Technical Report R95:12, Swedish Institute of Computer Science.
- [85] Javier Snaider and Stan Franklin. Extended sparse distributed memory. Paper presented at the Biological Inspired Cognitive Architectures 2011, Washington D.C. USA.
- [86] Javier Snaider and Stan Franklin. Modular Composite Representation. *Cognitive Computation*, 6(3):510–527, September 2014. ISSN 1866-9956, 1866-9964. doi: 10.1007/s12559-013-9243-y. URL <http://link.springer.com/10.1007/s12559-013-9243-y>.
- [87] Javier Snaider, Stan Franklin, Steve Strain, and E. Olusegun George. Integer sparse distributed memory: Analysis and results. *Neural Networks*, 46:144–153, October 2013. ISSN 08936080. doi: 10.1016/j.neunet.2013.05.005. URL <http://linkinghub.elsevier.com/retrieve/pii/S0893608013001354>.
- [88] Alvin J. Surkan. WSDM: Weighted Sparse Distributed Memory Prototype Expressed in APL. In *Proceedings of the International Conference on APL*, APL ’92, pages 235–242, New York, NY, USA, 1992. ACM. ISBN 978-0-89791-477-2. doi: 10.1145/144045.144142. URL <http://doi.acm.org/10.1145/144045.144142>.
- [89] Richard S Sutton and Andrew G Barto. *Reinforcement learning: An introduction*, volume 1. MIT press Cambridge, 1998.
- [90] Andreas Turk and Gunther Gorz. Kanerva’s Sparse Distributed Memory: An Object-oriented Implementation on the Connection Machine. In *Proceedings of the 14th International Joint Conference on Artificial Intelligence - Volume 1*, IJCAI’95, pages 473–479, San Francisco, CA, USA, 1995. Morgan Kaufmann Publishers Inc. ISBN 978-1-55860-363-9. URL <http://dl.acm.org/citation.cfm?id=1625855.1625917>.
- [91] Yoshinori Uesaka, Pentti Kanerva, and Hideki Asoh, editors. *Foundations of real-world intelligence*. Number no. 125 in CSLI lecture notes. CSLI Publications, Stanford, Calif, 2001. ISBN 978-1-57586-339-9 978-1-57586-338-2.
- [92] Richard Van Noorden, Brendan Maher, and Regina Nuzzo. The top 100 papers. *Nature*, 514(7524):550, 2014.
- [93] A. Wagner and D. Corneil. Embedding Trees in a Hypercube is NP-Complete. *SIAM Journal on Computing*, 19(3):570–590, June 1990. ISSN 0097-5397. doi: 10.1137/0219038. URL <https://pubs.siam.org/doi/abs/10.1137/0219038>.
- [94] Hasitha Muthumala Waidyasooriya, Masanori Hariyama, and Kunio Uchiyama. *Design of FPGA-Based Computing Systems with OpenCL*. Springer, 2018.

- [95] Henry S Warren. *Hacker's delight*. Pearson Education, 2013.
- [96] Yan Wu, Greg Wayne, Alex Graves, and Timothy Lillicrap. The Kanerva Machine: A Generative Distributed Memory. *arXiv:1804.01756 [cs, stat]*, April 2018. URL <http://arxiv.org/abs/1804.01756>. arXiv: 1804.01756.